HEAT EXCHANGER FOULING OF SOME CANADIAN CRUDE OILS

by

Murugan Srinivasan

B.Tech., Regional Engineering College, Tiruchirapalli, India, 1989

A THESIS SUBMITTED IN PARTIAL FULFILLMENT OF

THE REQUIREMENTS FOR THE DEGREE OF

MASTER OF APPLIED SCIENCE

in

THE FACULTY OF GRADUATE STUDIES

(Chemical and Biological Engineering)

THE UNIVERSITY OF BRITISH COLUMBIA

(Vancouver)

August 2008

ABSTRACT

Fouling refers to deposition of any kind of extraneous material that appears on the surface of process equipment, such as heat exchangers and reactors. This is a major economic penalty to oil refineries and heavy residuum upgrading units, thus creating incentives for a better understanding of fouling mechanisms which underlie methods to mitigate or control fouling.

This research was focussed on a comparative study of the fouling tendencies of three sour crude oils supplied by Shell Canada Limited: Light Sour Blend (LSB), Midale (MDL), and Cold Lake (CLK). The experiments were carried out using a re-circulation fouling loop equipped with an HTRI-type annular electrical probe. Fluids were re-circulated for a 48 hour period from a feed tank, through the annular fouling probe, and back to the tank. The unit was operated at a constant heat flux with time, so that fouling could be tracked by the increase in surface temperature of the probe. Velocity was held constant at 0.75 m/s in most experiments. The unit was pressurized to 860-1240 kPa, depending on the oil used. Bulk temperatures were varied over the range 200-280°C, and surface temperatures covered the range 330-380°C. The decrease in overall heat transfer coefficient varied from 3% to 60%, with most results being in the range 10-32%, depending on conditions. Fouling resistances up to 0.3 m^2K/kW were recorded.

The effects of various parameters, namely surface temperature, bulk temperature, film temperatures, and annular velocities, on fouling rates were studied for Light Sour blend in detail.

When correlating temperature effects on fouling rates, some authors use the surface temperature, while others use the average film temperature, $T_f = 0.5\ (T_s + T_b)$. In this study both were examined. A slightly modified film temperature, which gave more weight to the surface temperature, was found to be the best.

Deposits carefully recovered from the HTRI probe, after each experiment, were analyzed using energy dispersive x-ray, giving point analyses on the deposit surface, and by micro-elemental analysis for bulk content of C, H, S and N. Thermogravimetry was used to determine bulk ash content.

TABLE OF CONTENTS

LIST OF TABLES

LIST OF FIGURES

ABBREVIATIONS

AFT	Automated Flocculation Test
API	American Petroleum Institute
CAPP	Canadian Association of Petroleum Producers
CDU	Crude Distillation Unit
CII	Colloidal Instability Index
CLK	Cold Lake Crude Oil
DAS-8	Data Acquisition System (8 ports)
EDX	Energy Dispersion X-ray
EDX	Energy Dispersive X-Ray
HPLC	High Performance Liquid Chromotograph
HTRI	Heat Transfer Research Institute
LSB	Light Sour Blend Crude Oil
MDL	Midale Crude Oil
PFRU	Portable Fouling Research Unit
RVP	Reid Vapor Pressure
SAGD	Steam Assisted Gravity Draining
SEM	Scanning Electron Microscopy
SCO	Synthetic Crude Oil
SS	Stainless Steel
TAN	Total Acid Number
TEMA	Tubular Exchanger Manufacturers Association
TGA	Thermo Gravimetric Analyzer
UBC	University of British Columbia
WCSB	Western Canadian Sedimentary Basin

NOMENCLATURE

A	Surface Area for Heat Transfer (m^2)
A_o	Preexponential Constant (m^2K/kJ)
C	Concentration (g/L)
D_{eq}	Equivalent Diameter
E_f	Fouling Activation Energy (kJ/mol)
FR	Flocculation Ratio
I_N	Insolubility Number
P	State of Peptization of The Crude Oil
Pa	Peptizability of Asphaltenes
Po	Peptizability Power of Maltenes
Q	Heat Flow (W)
q	Heat Flux (kW/m^2)
R	Universal Gas Constant
Re	Reynolds Number Based on Equivalent Diameter and Film Temperature
Re_b	Reynolds Number
R_f	Fouling Resistance (m^2K/kW)
S_{BN}	Solubility Blending Number
T	Transmittance
T_b	Average Bulk Fluid Temperature (°C or K)
T_f'	Modified Film Temperature (°C or K)
t_f	Flocculation Time (s)
T_f, T_{film}	Conventional Film Temperature (°C or K)
T_s	Surface Temperature (°C or K)
$T_{s,o}$	Initial Surface Temperature (°C or K)
U	Heat Transfer Coefficient (kW/m^2K)
U_o	Clean Heat Transfer Coefficient (kW/m^2K)
V	Annular Velocity (m/s)

V_S	Volume of Solvent
V_T	Volume of Titrant
W_A	Weight of Crude Oil Sample
W_S	Weight of Solvent

SYMBOLS

α	Constant
β	Constant
τ	Shear Stress (Pa)
Δ	Differential
δ_f	Flocculation Solubility Parameter
δ_H	Solubility Parameter of N-Heptane
δ_{oil}	Solubility Parameter of The Crude Oil
δ_T	Solubility Parameter of Toluene
μ	Viscosity(Pa.s)
ν	Kinematic Viscosity (m^2/s)
ρ	Density (kg/m^3)

ACKNOWLEDGEMENTS

I wish to express my sincere thanks to Dr. A.P. Watkinson, my supervisor, for his beneficial guidance, utmost patience and support throughout the duration of this work.

I am thankful to the mechanical and electrical workshop staff for their technical support. Special thanks are also due to Mr. Horace Lam of Stores Department, for his help and support beyond his regular routine. I am also grateful to my friends and faculty in the department for their support.

Financial support provided by Shell Canada Limited, Syncrude Canada Limited and NSERC is gratefully acknowledged.

DEDICATION

To my dear wife Santhi, my loving kids Shyam Kumar and Vignesh Sharan.

INTRODUCTION

Fouling is a serious chronic problem for refiners and upgraders during petroleum processing, starting from storage of feedstock, refining itself, and then during storage of finished products. The main driving force in major oil companies is profitability and consequently process efficiency is of prime importance. Minimizing cost/barrel of crude oil is the current operating trend for most of the major oil processing units in the world, in order to survive with marginal profits.

The gradual depletion of conventional crude oils (Figures 1.1 & 1.2) will force the industries to look for more viable and economical production methods and alternative fuel sources. Oil sands are a potential candidate as fuel source, especially in Canada. Oil sands production has grown four fold since 1990 and exceeded 1 million barrels per day in 2004. A recent Canadian Association of Petroleum Producers (CAPP) forecast predicts that oil sands production will more than double by 2015, to reach 2.7 million barrels per day. As the conventional oil reserves continue to deplete in Western Canada, the share of production from oil sands will be of growing significance. Today, oil sands production accounts for one out of every two barrels of supply in Western Canada. By 2015, the oil sands share of production will rise to three out of every four barrels.

Alberta's reserves are estimated at 175 billion barrels deemed economically recoverable with today's technology. Those reserves place Canada second behind Saudi Arabia in the world ranking of crude oil reserves by country (Figure 1.3). At current production levels, reserves will sustain production of 2.5 million barrels per day for over 200 years.

Oil sands supply costs (Figure 1.4) vary with the type of production process. In the late 1980s and early 1990s, companies rationalized their production processes in response to lower world oil prices of the 1980s. Oil sands production costs are competitive with rival sources of supply, such as deep-water offshore developments. However, fouling and other corrosion/erosion issues associated with processing oil sands bitumen is many fold greater compared to the conventional crude oil processing. This in turn causes the

Figure 1.1

Figure 1.1 has been removed because of copyright restrictions.
Figure 1.1 is a plot of Canada Conventional versus Oil Sands Resources in Billions of Barrels. According to this plot, Oil Sands have been estimated to have 315 Billion Barrels recoverable, with 175 Billion Barrels recoverable under current economics.
Figure 1.1 was taken from the website: www.capp.ca/raw

Figure 1.2

Figure 1.2 has been removed because of copyright restrictions.
Figure 1.2 is a plot of Canadian Oil Production (WSCB Conventional Oil, Oil Sands and Offshore) Actual and Forecast in Thousands of Barrels per day from 1980-2015.
Figure 1.2 was taken from the website: www.capp.ca/raw

Figure 1.3

Figure 1.3 has been removed because of copyright restrictions.
Figure 1.3 is a plot of Global Crude Oil Reserves by Country. According to this plot Canada's Oil Sands reserves ranks 2nd only to Saudi Arabia.
Figure 1.3 was taken from the website: www.capp.ca/raw

Figure 1.4

Figure 1.4 has been removed because of copyright restrictions.
Figure 1.4 is a plot of Oil Sands Supply Costs by Recovery Type (Cold Production, Mining, SAGD (Steam Assisted Gravity Draining), Cyclic Stream and Integrated SCO (Synthetic Crude Oil)
Figure 1.4 was taken from the website: www.capp.ca/raw

upgrading operators to frequently shut down the exchangers and other furnaces for cleaning. Here the problems dealt with are not only the fouling associated in non-coking regime but also those associated with the coking regime, which further complicates the cleaning cycle (commonly called pigging). Pigging of furnace tubes is an extensive and elaborate procedure in which the mechanical integrity of the furnace tubes gradually deteriorates and which require periodic replacing.

These shutdown and or maintenance periods result in major cost penalties for the refiners and for the heavy oil upgraders. The cost associated with energy used for pre-heating and heating crude oils has been a driving force, which has lead to the development of highly complex heat integration in the processing units.

There is an immense potential for highly active research in the areas of petroleum fouling to either attempt to mitigate the fouling issues or at least elucidate the mechanism of fouling. This is helpful to the industry to improve the reliability and mechanical integrity of the giant processing units, which are not always but could be potential safety risks to the operating personnel due to the nature and severity of the operating conditions.

A number of recent advances in oil sands technology through operating experiences and ongoing research are expected to further reduce costs as development matures.

In this study, three crude oils (two of which were conventional crude oils) were subjected to high temperature fouling studies in the non-coking regime. Time, technical considerations, sample availability, and other factors limited the scope of the study to some extent.

Post-fouling studies such as deposit characterization, physical property changes of the test fluid, filtration for detection of suspended solids, and other studies were carried out. A major handicap in these pilot plant studies is that the infrastructure, in terms of equipment capability and resources for complete oil and deposit characterization, limits the scope of this research.

Also, the outcomes of small scale or pilot plant studies cannot be directly applied to industry, the main reason being the necessity for recirculation of the fluid being tested in the laboratory scale versus once-through processing as done in industry. Also, due to the reasons mentioned above, to simulate or create identical test conditions (with reference to the industrial processing unit) would require equipment of improved capability and resources. Hence, these studies are more effective to the refiners and upgraders as a comparative or inferential tool rather than an "off the shelf remedy", which is what is often expected.

LITERATURE REVIEW

"Fouling" in general refers to deposition of any kind of extraneous material that appears on the heat transfer surface during the lifetime of exchanger. Whatever the cause or the exact nature of the deposit, other than in exceptional circumstances an additional resistance to heat transfer is introduced, which reduce the operational capacity and overall performance of the heat exchanger. In many cases the deposit is thick and rough enough to cause significant increase in pressure drop across the heat exchanger resulting in a hydraulic and thermal limitation thereby reducing the overall capacity utilization in the process.

Fouling of heat exchangers is a chronic serious operating issue the results of which have economic and environmental penalties. The economic aspects include under capacity utilization due to increased pressure drops and increased maintenance costs with significant downtime. The environmental aspect will be additional energy consumption and subsequent pollutant generation, to overcome or mitigate the economic impacts.

Figure 2.1 represents a general refinery schematic. Most of the financial penalty due to fouling in an oil refinery is attributable to the crude distillation unit in which all of the crude fed to the unit is heated from ambient temperature to elevated temperatures in a network of shell and tube heat exchangers and furnaces. Depending on the refinery age and any design modifications, the number of heat exchangers in the pre-heat train can vary from 16 to 60 for crude units with distillation capacities of about 100, 000 bbl/day. They are grouped as heat exchanger trains and normally have two or more trains to accommodate cleaning fouled exchangers without shutting down the rest of the unit operation, downstream. The recovery of thermal energy in preheat train is critical. Panchal et al. (2000) reports that a loss of 1°C in the crude oil temperature entering the process heater equates to about 2 trillion Btu/year (2.1×10^3 teraJ/year) for U.S refineries and an energy cost of $4 million/year. Many heat exchangers foul under operating conditions for which they have been designed or under conditions widely different from the design. For many fluids, fouling increases with the increase in the tube surface

temperature and decreases with increase in the fluid velocity in the tube. Experimental data can be used to determine the threshold condition(s), at which fouling is minimal and

Figure 2.1 General Refinery Schematic

Figure 2.1 has been removed because of copyright restrictions.
Figure 2.1 shows a General Refinery Schematic.
Figure 2.1 was taken from the website: www.en.wikipedia.org/wiki/Oil_refinery.

tolerable in an operating heat exchanger. The fouling characteristics of a fluid may be determined in the laboratory or in-plant monitoring, using techniques by which the thermal hydraulics (velocity, bulk temperature and tube surface temperature) of a given heat exchanger are simulated. Figure 2.2 illustrates the crude pre-heat train configuration

Figure 2.2 Crude Pre-Heat Train Configuration

Figure 2.2 has been removed because of copyright restrictions.
Figure 2.2 shows the Crude Pre-Heat Train Configuration.
Figure 2.2 was taken from the website: www.en.wikipedia.org/wiki/Oil_refinery.

in a refinery. The complex and effective heat exchanger network is to optimize the energy costs and environmental issues related. Generally, the rate of fouling from the crude oil increases as the crude oil is heated along the train. Figure 2.3 shows a cross-sectional view of a heat exchanger tube which is fouled from the inside as well as the outside (tube side and shell side fouling). These foulants offer from moderate to severe heat transfer resistance based on the thickness of the foulant and the thermal conductivity of the deposits.

Figure 2.4 and Figure 2.5 indicate the decrease in heat transfer coefficient and increase in fouling resistance with time respectively. Figure 2.6 shows the increase in the system (exchanger) pressure drop with time. In case of soft deposits, the deposit can be easily damaged and might be partially carried away into the bulk of the liquid and or may start to accumulate in regimes of low turbulence (comparatively). This gradual build of foulants in the bulk of the liquid may go unnoticed until finally forcing a shutdown due to

Figure 2.3 Fouling layers – Inside and Outside of Heat Exchanger Tube

Figure 2.3 has been removed because of copyright restrictions.
Figure 2.3 shows the Fouling layers - Inside and Outside of a Heat Exchanger Tube.
Figure 2.3 was taken from the website: www.wlv.com/products/databook/

Figure 2.4 Heat Transfer Coefficient Declining with Time

Figure 2.4 has been removed because of copyright restrictions.
Figure 2.4 shows the Decline of Heat Transfer Coefficient with Time, in a heat exchanger (fouling conditions)
Figure 2.4 was taken from the website: www.wlv.com/products/databook/

Figure 2.5 Fouling Resistance Increasing with Time

Figure 2.5 has been removed because of copyright restrictions.
Figure 2.5 shows the Increase in the Fouling Resistance with time, in a heat exchanger.
Figure 2.5 was taken from the website: www.wlv.com/products/databook/

Figure 2.6 Pressure Drop Increasing with Time

Figure 2.6 has been removed because of copyright restrictions.
Figure 2.6 shows the Increase in Pressure Drop with Time, in a heat exchanger. (fouling conditions)
Figure 2.6 was taken from the website: www.wlv.com/products/databook/

high pressure drops in the system. About half of the financial penalties due to fouling in an oil refinery is attributable to the crude distillation unit (CDU) in which all the incoming crude oil is heated from ambient to elevated temperature in a network of shell and tube heat exchangers and furnaces. The fouling mechanism is undoubtedly complex involving crystallization of inorganics, corrosion, chemical reactions of organics and deposition of particulates. To make matters worse, the controlling mechanism(s) may well vary from exchanger to exchanger in the preheat train. An additional problem arises when the mechanism is not well understood, since it is clearly not easy to predict how much extra surface area should be provided in a new exchanger in order to cope up with the problem. The huge costs associated with fouling in crude pre-heat exchangers mentioned above are categorized as follows:

Energy costs and environmental impact: This corresponds to the additional fuel required for the furnace due to the reduced heat recovery in the pre-heat train as exchangers foul. Energy losses due to increased pressure drop (pumping power) may also be significant. The use of more fuel leads to additional production of CO_2 with the associated environmental impact along with economic impact as greenhouse gas emissions are penalized.

Production loss during shutdowns due to fouling: If the pre-heat train throughput is furnace-limited, a typical 10 per cent loss of production due to taking a heat exchanger out of service in a 100,000 barrel/day plant would cost $20,000 per day (assuming $2 per barrel of marginal lost production). The average cost to clean a heat exchanger would be $20,000 to $30,000. After shutdown, there is an additional cost due to out-of-specification production after production is restarted.

Capital expenditure: This includes excess surface area, costs for stronger foundations, provisions for extra space, increased transport and installation costs, costs of anti-fouling equipment, costs of installation of on-line cleaning devices and treatment plants, increased cost of disposal of the (larger) replaced bundles and, finally, the (larger) heat exchangers.

Table 2.1 Values for Proposed Design Resistances of Relevance to Crude Distillation Units Selected from Chenoweth (1990)*

Fluid	Temperature (°C)	Velocity m/s	Design R_f m^2K/kW	Comment
Crude Oil	120	>1.22	0.35-0.70	Desalted at ~ 120°C
Crude Oil	120-177	>1.22	0.53-0.70	Desalted at ~ 120°C
Crude Oil	177-232	>1.22	0.70-0.88	Desalted at ~ 120°C
Crude Oil	>232	>1.22	0.88-1.06	Desalted at ~ 120°C
Gasoline			0.35	
Light distillate/ Naphtha			0.35-0.53	
Kerosene			0.35-0.53	
Light Gas Oil			0.35-0.53	
Heavy Gas Oil			0.53-0.88	
Heavy Fuel Oil			0.88-1.23	
Atmospheric Tower Bottoms			1.23	

* Adapted from Crittenden et al. (1992)

Maintenance costs: This includes staff and other costs for removing fouling deposits and the cost of chemicals or other operating costs of anti-fouling devices. There are also economic and environmental penalties associated with disposal of cleaning chemicals after cleaning. It is clear that there are strong incentives for understanding the fouling mechanism and exploring effective strategies to mitigate fouling deposition in heat transfer equipment.

Chenoweth (1990) has published information on the final report of HTRI/TEMA Joint Committee to review the fouling section of the TEMA Standards. Table 2.1 gives values

for proposed design resistances of relevance to Crude Distillation Units selected from Chenoweth (1990).

2.1 Types of Fouling:

The types of fouling have been classified by Epstein (1983) as given below:

1. Crystallization Fouling – a broad class that is subdivided into: (a) Precipitation fouling (crystallization from solution of dissolved substances onto the heat transfer surface, sometimes called scaling) and (b) Solidification fouling (freezing of a pure liquid or the higher melting constituents of a multi-component solution onto a sub-cooled surface)

2. Particulate Fouling – accumulation of finely divided solids suspended in the process fluid onto the heat transfer surface. When settling by gravity prevails, the process may be referred to as sedimentation fouling.

3. Chemical Reaction Fouling – deposit formation at the heat transfer surface by chemical reactions in which the surface material itself is not a reactant.

4. Corrosion Fouling – accumulation of indigenous corrosion products on the heat transfer surface.

5. Biological Fouling – attachment of macro-organisms and or micro-organisms to a heat transfer surface along with the adherent slimes often generated by the latter.

For all the above categories of fouling, Epstein (1983) suggests the following five steps as the sequential events in fouling:

1. Initiation (delay, nucleation, induction, incubation, surface conditioning).
2. Transport (mass transfer).
3. Attachment (surface integration, sticking, adhesion, bonding).

4. Removal (release, re-entrainment, detachment, scouring, erosion, spalling, sloughing off, shedding).
5. Aging

Figure 2.7 5 X5 Fouling Matrix*

Figure 2.7 has been removed because of copyright restrictions.
Figure 2.7 shows the 5X5 Fouling Matrix developed by Epstein, in which the columns represent the primary categories of fouling and rows the sequential steps in fouling.
Figure 2.7 was taken from Epstein (1983).

Figure 2.7 illustrates the 5X5 Fouling Matrix for heat exchanger fouling developed by Epstein (1983), wherein the columns represent the primary categories of fouling and the rows represent the sequential events mentioned above.

Figure 2.8 Characteristic Fouling Curves*

Figure 2.8 has been removed because of copyright restrictions.
Figure 2.8 shows the Characteristic Fouling Curves (linear, falling rate and asymptotic) developed by Epstein.
Figure 2.8 was taken from Epstein (1983).

Epstein (1983) describes the characteristics of the fouling curves in the above Figure 2.8, in which initiation is associated with the delay period θ_D so often (but certainly not always) observed before any appreciable fouling is recorded after starting an experiment or process with a clean heat transfer surface. For chemical reaction fouling θ_D appears to decrease as the surface temperature is increased, presumably due to speeding up of the induction reactions. For all fouling modes, many investigators have reported that θ_D decreases as the surface roughness increases.

2.2 Chemical Reaction Fouling

Chemical reaction fouling results when chemical reactions occur in the fluid adjacent to the heated tube wall and the products of the reaction for a deposit. This type of fouling is important for organic fluids such as petroleum oils. For many fluids, the chemical reaction fouling process is strongly affected by the tube surface temperature and the velocity of the fluid flowing past the heated surface. Frequently the foulant or its precursor is generated in the equipment preceding the heat exchanger.

Figure 2.9 Overview of Chemical Reaction Fouling*

Figure 2.9 has been removed because of copyright restrictions.
Figure 2.9 shows the Overview of Chemical Reaction Fouling.
Figure 2.9 was taken from Crittenden et al. (1987).

The diversity of the hydrocarbon feedstocks and thermal environments encountered in the process industries makes it difficult to generalize about the chemical mechanisms by

which the deposits are formed. Crittenden et al. (1987) summarize the overview of chemical reaction fouling shown in Figure 2.9 as follows: When material of increasing molecular weight and structural complexity exceeds its solubility in the fluid, it forms a deposit which initially may not be rigid. This process occurs not necessarily at the heat transfer surface, but rather in a reaction zone where the local conditions are favorable. The foulant may have to be transported, perhaps in colloidal form, to be adsorbed on, or otherwise attached to, the surface. Reactants must be transferred by convective mechanisms to the reaction zone. Likewise reaction products, including the foulant if still mobile, may be transferred back to the fluid bulk to take part in further fouling reactions or to be deposited on cooler surfaces in downstream units. The possibility also exists for wholesale removal of deposits by turbulent action of the fluid. They also suggest that the individual chemical reactions are strongly dependent upon temperature, pressure, composition and the presence of catalysts, but the overall rate of chemical reaction fouling may, in addition be dependent upon other physicochemical mechanisms, such as mass transfer and surface phenomena. Thus, many parameters can affect, and in turn be affected by, the deposition process as shown in Figure 2.10.

Figure 2.10 Effect of Process Parameters on Chemical Reaction Fouling*

Figure 2.10 has been removed because of copyright restrictions.
Figure 2.10 shows the Effect of Process Parameters on Chemical Reaction Fouling.
Figure 2.10 was taken from Crittenden et al. (1987).

Watkinson (1988) attributes chemical reaction fouling of organic fluids to three general classes of reactions: autoxidation, polymerization, and thermal decomposition. In a literature review, Watkinson (1992) suggests that at moderate temperatures, hydrocarbon fouling appears to proceed via autoxidative polymerization, propagated by free radical chain reactions. Oxygen, sulfur, nitrogen and metal ions participate along with the unsaturated species. Reaction may take place in stages whereby the soluble gums form perhaps in the feed or storage system, then as temperatures are raised in the exchanger, polymerization occurs to yield insoluble product. If the temperature of the deposit is high enough the polymer will convert in time to a coke like material. The insoluble material may form on the hotwall or in the bulk and thus the deposition process may include particulate transfer.

The Figure 2.11 below shows a multi-step chemical reaction fouling mechanism proposed by Watkinson and Wilson (1997) that is explained as follows:

- The soluble Precursor A that enters with the incoming fluid may transport to the surface and undergo surface reaction to produce insoluble Deposit C on the wall
- Alternatively Precursors A may form insoluble Foulant B by reaction in the bulk liquid or in the thermal boundary layer and then Foulant B transport and adhere to the surface.
- Foulant B may undergo an ageing reaction on the surface to produce Deposit C.

Figure 2.11 Multi-Step Fouling Mechanism*

Figure 2.11 has been removed because of copyright restrictions.
Figure 2.11 shows the Multi-Step Fouling Mechanism.
Figure 2.11 was taken from Watkinson and Wilson (1997).

Based on the above plausible fouling mechanism, Watkinson and Wilson (1997) suggest that the analysis of chemical reaction fouling in a given system may entail:

1. Identification of the reactants and precursors
2. Determination of the kinetics of reactions that form the precursors and
3. Determination of whether the solid fouling phase is initially formed in the bulk, in the thermal boundary layer, or on the heated surface.

When these factors are known, available mathematical models can be used to describe the deposition process quantitatively.

2.3 Modeling of Chemical Reaction Fouling

Modeling of fouling is necessary to be able to predict the dependence of fouling resistances not only on time but on key design and operational parameters. An ability to carry out such modeling also aid in the determination of optimum cleaning cycles, the evaluation of anti-fouling treatments, and identification of process control strategies for networks of heat exchangers which are prone to foul, and thereby to affect the operability of downstream process units. Crittenden et al. (1988) summarize the chemical reaction fouling models as shown in Table 2.2.

Table 2.3 adapted from Watkinson (2005) summarizes the initial rate equations for a number of available fouling models, some of them being simplified for the sake of direct comparision. For complex case of crude oil fouling, the model parameters are not predictable, nevertheless, the effect of process parameters on fouling rate can be rationalized.

2.4 Crude Oil Sample Characterization for Fouling Studies

Crude oil is a very complex mixture of biological origin compounds that required millions of years to achieve equilibrium in the reservoir. As the crude oil travels through and leaves the reservoir it pick ups various minerals. As the crude oil travels through the pipelines, it suspends corrosion products, particularly iron oxides and iron sulfides. Time

Table 2.2 Chemical Reaction Fouling Models*

Authors	Application	Deposition Term	Removal Term	Remarks
Nelson (1934)[16]	Oil Refining	Rate is directly dependent upon thickness of thermal boundary layer.	None considered	Fouling rate can be reduced by increasing fluid velocity
Atkins (1962)[17]	Fired heaters in oil industry	Constant monthly increase in coke resistance for various refinery streams	None considered	Two layer concept – porous coke adjacent to fluid and hard coke adjacent to wall
Nijsing (1964)[18]	Organic coolant in nuclear reactors	Hydrodynamic boundary layer and diffusion partial differential equations (1) instantaneous first order reaction in zone close to wall (2) very rapid crystallization at hot surface	Product diffusion back to the fluid bulk is an integral part of the differential equations	(1) Solution with diffusion control fits plant data. Fouling rate predicted to increase with velocity (2) Extended to consider colloidal transfer to the hot surface
Watkinson and Epstein (1970)[19]	Liquid phase fouling from gas oils	Mass transfer and adhesion of suspended particles (1) sticking probability inversely proportional to exp (-E/RT) (2) sticking probability inversely proportional to hydrodynamic forces on particle as it reaches wall	First order Kern and Seaton[25] shear removal term	(1) Correct prediction of initial rate dependence on velocity (2) Incorrect prediction of asymptotic resistance on velocity
Jackman and Aris (1971)[20]	Vapour phase pyrolysis	Kinetics control – two reactions: (1) first order dissociation of A into products (2) zero order coke formation	None considered	(1) Quasi-steady state assumption (2) Untested
Fernandez-Baujin and Solomon (1976)[21]	Vapour phase pyrolysis	Kinetics and/ or mass transfer control with first order reaction	None considered	Solution with mass transfer control fits plant run-time data, i.e. fouling rate increases with velocity
Sundaram and Froment (1979)[22]	Vapour phase pyrolysis of ethane	Kinetics control (1) at surface temperature (2) first order in propylene concentration, a product of primary cracking reactions	None considered	(1) Quasi-steady state assumption (2) Good agreement between industrial and numerically simulated data
Crittenden and Kolaczkowski (1979)[21,24]	Hydrocarbons in general	Kinetics and/ or mass transfer control with first order reaction (later with other orders[5])	(1) Diffusion of foulant back into fluid bulk (2) First order Kern and Seaton[25] shear removal term	(1) Complex – many parameters (2) Limited testing with oils[24] (3) Tested with styrene polymerisation (4) Extended[24] to two layer concept proposed by Atkins[17]

* Adapted from Crittenden et al. (1988)

Table 2.3 Simplified Models for Initial Rate of Crude Oil Fouling*

Watkinson and Epstein (1970)	$dR_f/dt = a \exp(-E/RT_s) / V^n$
Epstein (1st Order Simplified) (1997)	$dR_f/dt = C_b / [a/V + bV^2 \exp(E/RT_s)]$
Ebert and Panchal (1997)	$dR_f/dt = a \exp(-E/RT_f) / Re^n - bV^2$
Yeap et al. (2004)	$dR_f/dt = 1 / [a/V\, T_s^{2/3} + bV^2 \exp(E/RT_s)] - cV^{0.8}$

* Adapted from Watkinson (2005)

spent in tankers and holding tanks results in variable oxygen dissolution. Clearly, all of these variables can have a profound impact on the fouling propensity of the crude oil. C.A.Bennett et al. (2006) provide a list of recommended crude oil characterization techniques (suggested by COFTF), the information obtained and the standards in Table 2.4. The Crude Oil Fouling Task Force (COFTF) is composed of heat transfer experts from many of the world's leading energy companies formed by Heat Transfer Research Incorporated (HTRI).

The principle endeavor of the COFTF is to ensure that crude oil fouling research is both standardized and industrially relevant. The COFTF-recommended characterization techniques cover all of the mechanisms known to contribute to crude oil fouling. The crude oil should be thoroughly mixed prior to the study so that particles are suspended uniformly. One should generally experiment with the whole crude oil. However, filtration (10 μm works well) facilitates mechanism isolation by eliminating sedimentation. Metal carbides, oxides and sulfides of V, Fe, and Ni are active catalysts for crude oil fouling reaction and could exist in the crude oil preheat train. Salts of alkali metal and alkaline earth metal elements result in crystallization fouling mechanism, especially the inverse solubility salts in the exchangers just prior to the desalter. The solubility is strongly influenced by polar forces, hence the utility of the acid number information. Crude oil chemistry is often characterized using SARA (Saturates, Aromatics, Resins and Asphaltenes) solubility fractions to simplify its overwhelming intricacy. A metric often correlated with crude oil fouling tendency is the colloidal instability index (CII) proposed

Table 2.4 Recommended Crude Oil Characterization Techniques*

Technique	Information Obtained	Standard
Transition metals (V, Fe, Ni) by ICP	Catalytic Mechanism	ASTM D-5708
Carbon Residue - Conradson	Coking propensity	ASTM D-189
Asphaltene flocculation propensity	Colloidal stability	ASTM D-7157
		ASTM D-7112
		ASTM D-7061
		ASTM D-7060
Asphaltene incompatibilty numbers	Colloidal stability	---
Asphaltene solubility versus temperature	Colloidal stability	---
Basic nitrogen	Colloidal stability	UOP - 269
Nitrogen by chemiluminescence	Colloidal stability	ASTM D-4629
SARA fractionation	Colloidal stability	---
Sulphur by oxidative microcoulometer	Corrosion, catalytic, and bacterial mechanisms	ASTM D-3120
Sulphur by x-ray fluorescence	Corrosion, catalytic, and bacterial mechanisms	ASTM D-4294
Acid number	Crystallization mechanisms	ASTM D-664
Elements (Na, K, Mg, Ca, Si, P) by ICP	Crystallization and sedimentation mechanisms	---
Total chloride	Crystallization mechanisms	ASTM D-4929
Nuclear magnetic resonance	Flocculate shape, size, and chemistry	---
Particle (photon or neutron) scattering	Flocculate shape, and size distribution	---
Induction period	Oxidation stability	ASTM D-525
Total oxygen content	Polymerization mechanisms	---
Sediment by extraction	Sedimentation mechanisms	ASTM D-473
Sediment particle size distribution	Sedimentation mechanisms	ASTM D-312
Kinematic viscosity	Used in calculations	ASTM D-445
Simulated distillation	Used in calculations	ASTM D-5307
Specific gravity	Used in calculations	ASTM D-5002
Watson K-factor	Used in calculations	UOP- 375

* Adapted from C.A.Bennett et al. (2006)

by Asomaning and Watkinson (2000), which is calculated with weight fractions as shown in Equation (2.1):

$$CII = \frac{\text{Saturates} + \text{Asphaltenes}}{\text{Aromatics} + \text{Resins}} \qquad 2.1$$

Of the SARA fractions, the heteroataoms (N,O and S) are primarily associated with the resins and asphaltenes. Heteroataoms have a profound impact on the fouling characteristics of a crude oil. Nitrogen was typically considered an antifouling component until recent disclosures by Van Den Berg et al. (2003) revealed that basic nitrogen contents in excess of 200 mg/kg usually indicate that the crude oil will not foul, that basic nitrogen contents below 100 mg/kg belong to rapid fouling crude oils and that crude oils with basic nitrogen contents of 100-200 mg/kg possess intermediate fouling potential.

Conversely, high sulfur contents might result in corrosion and heavy fouling. Oxygen accelerates fouling rates through polymerization mechanism and is particularly insidious in crude oil fouling research because variable storage conditions and durations can result in uncertain oxygen contents. The last of the heteroatoms recommended for tracking is phosphorous, a remnant of additives. Specific gravity and viscosity are necessary for multiple computations, such as flow rate and shear stress. Simulated distillation can be used to estimate boiling curves.

2.5 Organic Fouling in Crude Oil Processing

The most causes of organic fouling are:

1. Insoluble asphaltenes
    a. Self-Incompatible crude oils
    b. Adsorption from compatible, but nearly incompatible crude oils
    c. Cooling after a conversion unit
    d. Coke: Insoluble asphaltenes at thermal cracking temperatures
2. Polymerization of conjugated olefins

The phase behaviour of petroleum is complex because of the large mixture of diverse molecules and because petroleum has some properties of a colloidal dispersion and some properties of a solution. The largest, most aromatic molecules, the asphaltenes, are actually submicroscopic solids dispersed in the oil by the resins, the next largest, most aromatic group of molecules. This asphaltene-resin dispersion is dissolved into petroleum by small ring aromatics that are solvents but opposed by saturates that are non-solvents. Thus asphaltenes are held in petroleum in a delicate balance, and this balance can be easily upset by adding saturates or by removing resins or aromatics. Wiehe and Kennedy (2000) state that the blending of oils can greatly change the overall concentrations of these molecular types to upset this balance and precipitate asphaltenes.

Wiehe describes three modes of insoluble asphaltenes in the crude oils: asphaltenes may be insoluble in the crude oil (self-incompatible), the asphaltenes may precipitate when

crude oils are mixed (incompatible), and the asphaltenes may precipitate out of the crude oil onto metal surfaces (nearly incompatible).

Asomaning and Watkinson (2000) studied the petroleum stability effects on heat exchanger fouling using mixtures of heavy oils containing asphaltenes and carrier fluids consisting of a fuel oil cut with varying amounts of added aliphatics and aromatics. They concluded that at moderate bulk temperature and surface temperatures below 220°C, solubility phenomena affect the concentration of asphaltenes in suspension and consequently control fouling, and that fouling rate can be roughly correlated to the suspended asphaltenes measured by hot filtration, and with the colloidal instability index (CII) as defined by Equation (1).

2.6 Inorganic Fouling in Crude Oil Processing

The most causes of inorganic fouling are:

1. Sea Salts (Sodium, Calcium and Magnesium Chloride)
2. Iron Sulfide and Iron Oxide (Corrosion Products)
3. Ammonium Chloride after Conversion Unit
4. Ammonium Silicate (Clays or Catalyst Fines)

The inorganic deposition is caused mainly by poor crude oil desalting and or desalter upsets. Inorganic deposition is best treated by improving desalting. If sea salts are not removed in the desalter, they can deposit wherever the water gets evapourated. Since calcium and magnesium are not thermally stable, they can decompose in the presence of water in the resid conversion units, hydroconversion or coking, to form hydrogen chloride and react with ammonia released by the conversion to form the solid ammonium chloride.

Formation of iron sulfide is recognized as a key step in formation of fouling precursors in refinery operations. Iron may be naturally present in crude oils or generated by corrosion of pipelines and process equipment. In order to understand the reaction mechanisms of

iron and sulfur, their origins should be traced. Sulfur compounds naturally occur in crude oils in various amounts and forms depending up on the quality of crude: lower the API gravity of crude, higher the sulfur content. Sulfur compounds go through transformation during various refining processes, which may lead to increasing or decreasing reactivity of sulfur compounds in the downstream processes. Due to the low volatility of the metallic compounds, the distillation process concentrates iron compounds in heavy fractions such as resid and gas oil. The major source of iron is corrosion of process equipment and pipelines. Panchal et al. (1999), state that some of the heavy crude oils contain naphthenic acids in significant amounts of up to1%. They are known to produce corrosion products at temperatures typical of refining processes. Naphthenic acids, being volatile, are also found in the middle distillate, hence iron naphthenate can be found in various fractions. The refinery experiences suggest that iron salts of naphthenic acids cause an accelerated fouling.

Table 2.5 Test Conditions and Results for Fouling with Iron and Sulfur Compounds*

Test No.	Additives, ppm		Fluid Temperature °C	Surface Temperature °C	Velocity m/s	Fouling Rate
	Sulphur	Iron				
1	0	0	90	286-320	0.75	Low at 320°C
2	300	0	90	286-350	0.75	Low at 350°C
3	300	50	90	300, 330	0.75	High
4	300	100	90	296	0.75	High
5	300	100	90	280	0.75	High
6	300	50	88	280	0.75	Low
7	300	100	86	235-300	0.75	Low
8	300	100	93	280	1.12	High

* Adapted from Panchal et al. (1999)

The above Table 2.5 adapted from Panchal et al. (1999) summarizes the test conditions along with the results for their fouling studies on gas oil with iron and sulfur compounds. Sulfur was added as thiophenol. Iron was added in two different forms: For their test 3, ferric chloride was dissolved in cyclohexane carboxylic acid. The chemical analysis of the test fluid showed iron concentration of 19 ppm. Their tests 4 through 8 were conducted with addition of iron as acetate, which is soluble in gas oil. The chemical

analysis of the test fluid in test 4 showed iron concentration in the range of 33-42 ppm, which was lower than the calculated value in Table 2.5.

Figure 2.12 Fouling of Gas Oil without Additives (Test 1)*

Figure 2.12 has been removed because of copyright restrictions.
Figure 2.12 shows the Fouling of Gas Oil without Additives (Test 1)*.
Figure 2.12 was taken from Panchal et al. (1999)

Figure2.13 Effect of Iron Concentration on Fouling Rate (Tests 5, 6)*

Figure 2.13 has been removed because of copyright restrictions.
Figure 2.13 shows the Effect of Iron Concentration on Fouling Rate. (Tests 5, 6)*
Figure 2.13 was taken from Panchal et al. (1999)

Figure 2.12 shows their test for gas oil without additives. Gas oil alone did not produce significant fouling for surface temperatures up to 320°C and low fouling rate was observed for temperatures at 320°C. Figure 2.13 shows that the fouling rate for 100 ppm test was significantly greater than that for the 50 ppm test of added iron. The fouling rate started at a high value and continuously decreased with time reaching an asymptotic value. The authors believe that either iron and or sulfur compounds were consumed or stable compounds were formed during the test period.

Srinivasan and Watkinson (2005) report the deposit analysis of their fouling experiments conducted with sour crude oils namely Light Sour Blend (LSB), Midale (MDL) and Cold Lake Oil (CLK). The three crude oils had sulfur contents of 1.3%, 2.5% and 3.7% respectively. Deposits were analyzed using energy dispersive x-ray, giving point analyses on the deposit surface and a micro-elemental analysis for the bulk content of C, H, S and N. Results are shown in Table 2.6. Both inorganic matter and sulfur content in the

deposits were high. Sulfur can be present in either organic or inorganic forms, and hence a portion of the sulfur content appears in the ash analysis. Sulfur content averaged 18.4% and appeared from the EDX data to be linked to iron content. On average for LSB deposits, Fe/S mass ratios were 2.2-2.5, which is significantly higher than the Fe/S mass ratio of 1.745 for pure FeS. For CLK deposits, the S content ranged from 6-18%. Fe/S by EDX was 1.97-2.0. For MDL, the Fe/S, mass ratio was 1.6-1.8 and consistent with FeS.

Table 2.6 Analysis of Deposits from the Three Crude Oils Tested*

Oil	% Ash	% C	% H	% N	% S	% Fe* (C-f)	% S* (C-f)	Fe/S* (wt/wt)
LSB	71.6	17.0	1.2	0.34	17.8	56.5	25.3	2.2
LSB	84.3	4.5	0.7	0.30	22.1	N/A	N/A	N/A
LSB	57.2	35.2	1.5	0.53	12.6	66.2	26.0	2.5
MDL	44.4	22.8	1.2	1.80	24.3	58.5	37.3	1.6
MDL	80.9	9.4	0.9	0.30	23.6	65.2	32.1	2.0
CLK	25.7	66.4	3.1	1.32	7.1	51.6	26.1	2.0
CLK	61.5	26.0	2.4	0.31	17.2	58.5	29.3	2.0

* EDX surface analysis; carbon free basis

* Adapted from Srinivasan and Watkinson (2005)

2.7 Significance of Activation Energy for Hydrocarbon Fouling

Table 2.7 below, summarizes the work of researchers with an estimate for the activation energy for fouling. Temperature effects on fouling rates are commonly plotted in the "fouling Arrhenius" form as shown in Figure 2.14, where the logarithm of the initial fouling rate is plotted versus the inverse of the absolute surface or film temperature. The film temperature, determined from averaging the bulk and surface temperature, reflects the temperature in the thermal boundary region near the surface where reaction and adhesion processes may occur. The slope is equal to the negative activation energy divided by the universal gas constant. Although widely used, according to Watkinson (2005), it is not necessarily the best parameter to correlate fouling rates in all situations described as follows: For asphaltenes, the solubility increases with temperature. Hence the suspended asphaltene concentration, decreases with increasing bulk temperature. This

leads to a decrease in fouling rate with bulk fluid temperature at a given surface temperature. Thus, raising the film temperature by increasing bulk temperature will decrease fouling rates under this condition. By contrast, for particulate fouling due to other suspended impurities such as corrosion products or gum particles, the solubility of

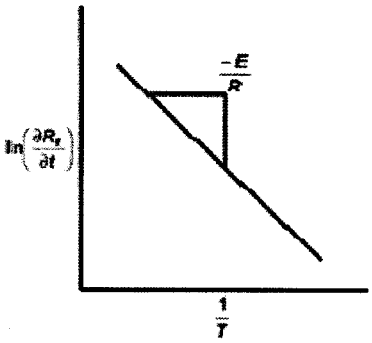

Figure 2.14 Determination of Activation Energy in Crude Oil Fouling

the foulant does not change markedly with bulk temperature, and fouling rates will increase with bulk temperature at a given surface temperature. For this latter situation the film temperature provides a good average value with which to correlate fouling rates. Fouling activation energies require care in interpretation, since they reflect the overall multi-step fouling process (Figure 2.11), and are influenced in magnitude by whether they are based on film or surface temperature, and possibly by flow effects. From Table 2.7, for the data from Watkinson (2005), the weakest temperature dependence of the fouling rate (20-42 kJ/mol) occurred for the lighter crudes and the foulant appeared to be suspended particulates. For medium oils, fouling activation energies were somewhat higher (59-84 kJ/mol). For blends which contained heavy oils, fouling was due to asphaltene or asphaltene plus oils and the fouling activation energies were high (81-184 kJ/mol).

It appears that whenever particulates already present in the oil stream cause fouling, the temperature dependence will be relatively low, reflecting an adhesion process, such as with the light crude oils. Where temperature dependent reactions or precipitation

processes generate insolubles or deposits, temperature dependence is higher, and rates can become much greater, as for the medium and heavy blends.

Table 2.7 Activation Energies for Hydrocarbon Fouling*

Fluid	Activation Energy kJ/mol	Surface Temperature Range, °C	Reference
Sour Gas Oils	120	146-204	Watkinson et al.(1969)
Styrene Polymerisation	39	22-98	Crittenden et al.(1987)
Pure n-paraffins	40	93-260	Taylor (1969)
Crude Oil	48		Asomaning et al. (2000)
Light Crude Oils	33	160-280	Crittenden et al.(1992)
Heavy Crude Oils	21	160-280	Crittenden et al.(1992)
Light Crude Oils	20-42	260-270	Watkinson (2005)
Medium Crude Oils	59-84	260-370	Watkinson (2005)
Heavy Blend Oil	81-184	220-290	Watkinson (2005)

* These fouling experiments were carried out under nitrogen blanketing

2.8 The Concept of Fouling Threshold

A number of detailed models for chemical fouling have been developed and predictive methods proposed. Several models incorporate a competition between deposition terms, and removal or hindrance terms which mitigate fouling (Table 2.2). A common feature of deposition mechanisms is the inclusion of reaction terms such that a high temperature at the wall, and within the sub-layer close to it, increases the rate of generation of foulant material. Mitigation mechanisms include diffusion of foulant material away from the wall, turbulent bursts "sweeping" surfaces clean, and surface shear forces either inhibiting the attachment of the foulant or removing deposited material before it has time

to become established. Temperature is generally associated with the promotion of fouling, whereas the effect of velocity is complex. In crude oil fouling studies, however, velocity is frequently associated with the mitigation of fouling via the effects of wall shear stress. Where competing mechanisms exist, it follows that no fouling will occur if the mitigating mechanism is more rapid than the deposition mechanism. Ebert and Panchal (1997), subsequently Panchal et al. (1999), and Knudsen et al. (1999), have used the competition concept to correlate the fouling data from field studies and laboratory trials. The latter data were obtained by passing the crude oil samples through tubular or annular sections under known flow and temperature conditions; the former were correlated on the basis of averaged parameter values. Their model expresses the average (linear) fouling rate under given conditions as a competition between a deposition term and a mitigation term:

$$R_f' = \alpha \mathrm{Re}^{\beta} \mathrm{Pr}^{\delta} EXP(-E/RT_f) - \gamma \tau_{wall} \qquad 2.2$$

Fouling rate = (deposition term - anti-deposition term)

where α ,β, γ, δ and E were parameters determined by regression, τ_{wall} is the shear stress at the tube wall, and T_f is the crude oil film temperature (average of the local bulk crude oil and the local wall temperatures).

The form of Equation (2.2) suggests that for some crude oils, it may be possible to identify combinations of temperature and velocity below which the fouling rate will be negligible. Ebert and Panchal described this locus as the "threshold condition" and, together with co-workers, have subsequently shown that several crude oils exhibited behavior which could be reasonably interpreted in terms of Equation (2.2).

The "fouling threshold" concept, proposed by Ebert and Panchal (1995) has been verified by field and laboratory observations (Knudsen et al. (1997); Panchal et al. (1997)). This concept suggests that chemical reaction fouling in crude oil heat exchangers is the result of two opposing mechanisms: formation and removal. The formation rate depends on the temperature of the heat transfer surface. Foulants are formed by chemical reaction of

crude oil near heat transfer surfaces. The removal mechanism is related to the transport of foulants away from the surface before deposition occurs. The removal rate depends on fluid velocity. When the rate of formation is higher than the removal rate, significant fouling may be expected. On the other hand, if the removal mechanism dominates, fouling deposition is negligible. The onset of the fouling process, or "fouling threshold", takes place when both the mechanisms are in balance. The original model presented by Ebert and Panchal (1995), along with some subsequently proposed modifications, is presented in Table 2.8.

Table 2.8 Fouling Threshold Models

Model	Authors
$R_f' = \alpha \mathrm{Re}^{\beta} \mathrm{Pr}^{\delta} EXP(-E/RT_f) - \gamma\tau$	Ebert and Panchal (1995)
$R_f' = \alpha \mathrm{Re}^{\beta} \mathrm{Pr}^{-0.33} EXP(-E/RT_f) - \gamma\tau$	Panchal et al.(1997)
$R_f' = \alpha \mathrm{Re}^{-0.8} \mathrm{Pr}^{-0.33} EXP(-E/RT_w) - \gamma \mathrm{Re}^{0.8}$	Polley et al. (2002a)

The fouling threshold may be considered as the maximum wall temperature, for a given flow velocity, below which significant deposition does not take place. The locus of the fouling threshold conditions divides the operating space in two regions. Above the threshold line significant fouling may be expected, and the severity of the deposition increases as the conditions move away from the threshold.

The importance of this model is that it demonstrates that fouling can be avoided or minimized by the appropriate selection of operating conditions. Fouling deposition can be kept at negligible level by designing and operating heat transfer equipment so that it operates inside the region of favorable conditions. The interest in and acceptance of the threshold modeling approach is expected to increase once examples of successful implementation of the methodology are publicized.

Polley et al. (2005) state that an integrated form of the Ebert-Panchal type of threshold fouling model has been developed to describe exchangers that operate with large temperature differences, both for data reconciliation purposes and for simulation of

Figure 2.15 Threshold Film Temperature As a Function of Flow Velocity

Figure 2.15 has been removed because of copyright restrictions.
Figure 2.15 shows the Threshold Film Temperature As a Function of Flow Velocity.
Figure 2.15 was taken from Rodriguez and Smith (2007)

exchanger's performance. The short-cut model (EXPRESS^{TM}) has been used to determine fouling model parameters for an operational pre-heat train. The results were very encouraging and the unmodified Ebert-Panchal model (Equation 2.3) provided a good fit to the measured data.

$$R_f' = \alpha \,\mathrm{Re}^{-0.66}\,\mathrm{Pr}^{-0.33}\, EXP(-E/RT_f) - \gamma\tau \qquad 2.3$$

2.9 Correlating Field and Laboratory Data for Crude Oil Fouling

Fouling mechanisms are essential to the development of mitigation techniques. The applicability of mechanisms deduced from laboratory tests to field situations is therefore an important issue. Asomaning et al. (2000) express concerns in the practice of simply extrapolating laboratory data to field fouling situations that has several shortcomings and raises several issues about its validity. In their views, the issues of significance, when

assessing the appropriateness of extrapolating laboratory fouling data to the field data include:

- Effect of fluid composition
- Effect of fluid recirculation in the laboratory on fouling data
- The nature of fouling mechanisms in the field and in the laboratory
- The fluid dynamics of heat exchangers in the field and fouling units in the laboratory
- Pressure effects and predominance of sub-cooled boiling in laboratory units
- The fact that laboratory experiments are done under carefully controlled conditions while field processes are subjected to vagaries of the process

If the mechanisms in the field and laboratory are not identical, the data from the two situations will not be comparable. Recirculation of test fluid, which results in long periods of heating, may alter its composition and result in differences between the fouling results obtained in the laboratory and field. If the crude oil is heated for a long time with recirculation, the state of aggregation and the solubility behaviour of asphaltenes can change and the fouling data obtained will differ from that obtained with the once-through flow conditions. Laboratory fouling tests are usually performed under severe and accelerated conditions, resulting in asymptotic fouling curves. On the other hand, conditions in the field may give rise to linear curves with the same fluid. Given the accelerated nature of laboratory tests, fouling rates, induction periods, and fouling resistances may not be comparable to those in field. Also, accelerated fouling conditions in the laboratory, may give rise to rapid aging of the deposits, and this aging could result in weakening of the deposit strength due to rapid thermal degradation. This will facilitate removal and thereby result in asymptotic fouling curves. Aging could also result in strengthening of the deposit due to further polymerization. This could favor linear fouling curves. Whether both of these processes occur in the laboratory and field experiments to the same degree is not known.

2.10 Effects of Fluid Velocity on Crude Oil Fouling

Figure 2.16 taken from Ebert and Panchal (1997) shows the data and predicted rates of fouling. For a given velocity, the fouling rate remains negligible until a threshold temperature is reached above which it rapidly increases with temperature. The threshold temperatures for the fluid velocities of 1.2, 2.5, 3.8 and 5.2 m/s were about 255, 331, 410 and 466°C, respectively. The results show that fouling deposition would be negligibly small, if the film temperature is maintained below the threshold value for a corresponding fluid velocity. The threshold-film temperature increases sharply with velocity.

Srinivasan and Watkinson (2005) report that their fouling study on Light Sour Blend (LSB) crude oil, exhibited fouling rates which varied with velocity to the -0.35 power. The values of the calculated film Reynolds numbers for their experiments, based on extrapolated viscosity data, were within the range of 1100-5600 (Re_b = 1000-5000). They attribute the low velocity exponent in their work to the influence of the flow regime. Panchal et al (1999) report a velocity dependence of -0.66 for the threshold model for flow conditions that were turbulent.

Figure 2.16 Comparision of Experimental and Predicted Fouling Rates*

Figure 2.16 has been removed because of copyright restrictions.
Figure 2.16 shows the Comparision of Experimental and Predicted Fouling Rates.
Figure 2.16 was taken from Ebert and Panchal (1997).

The Figures 2.17 and 2.18, from Watkinson (2005), show that for all six oils tested, the initial fouling rate decreased with increasing velocity at a fixed surface temperature. This included light and medium oils where fouling was caused by particulates, including solids initially present in the oil (GPS,CSK,BHO) and extra solids generated by autooxidation (SSB), as well heavy oil blends with suspended asphaltenes (HOP).

Figure 2.17 **Velocity Effects on Fouling Rates of Cossak, Gippsland and Light Sour Blend***

Figure 2.17 has been removed because of copyright restrictions.
Figure 2.17 shows the Velocity Effects on Fouling Rates of Cossak, Gippsland and Light Sour Blend.
Figure 2.17 was taken from Watkinson (2005).

Figure 2.18 **Velocity Effects on Fouling Rates of Sweet Blend, Bach Ho and Heavy Oil- Paraflex Blend***

Figure 2.18 has been removed because of copyright restrictions.
Figure 2.18 shows the Velocity Effects on Fouling Rates of Sweet Blend, Bach Ho and Heavy Oil- Paraflex Blend.
Figure 2.18 was taken from Watkinson (2005).

A similar trend was also found for medium sour oil (LSB) where corrosion played a role. Although the velocity range was limited, and the Reynolds numbers often include some values in the transition region, the decline in the rate with increasing velocity suggests that the transport step does not control fouling rates for this particular case.

2.11 Effects of Suspended Impurity in Crude Oil Fouling

Watkinson (2005) reports the effect of fine inorganic particulates and or suspended solids in Crude Oil. Figure 2.19 is a plot of fouling resistance versus time for Syncrude Sweet Blend (SSB). The SSB oil samples were prepared to result in 250 ppmw iron oxide and 250 ppmw aluminium oxide suspensions, respectively.

Figure 2.19 **Fouling Resistance versus Time with SSB Oil and Particulate Additions*** (T_b = 155°C, $T_{s,o}$ =290°C, V=0.44m/s)

Figure 2.19 has been removed because of copyright restrictions.
Figure 2.19 shows the Fouling Resistance versus Time with SSB Oil and Particulate Additions* (T_b = 155°C, $T_{s,o}$ =290°C, V=0.44m/s)
Figure 2.19 was taken from Watkinson (2005).

Both iron and aluminium oxides added yielded an order of magnitude increase in the fouling rate with a similar increase in suspended solids content. Figure 2.20 is a plot of fouling resistance versus time for Crude Oil- Bach Ho (BHO). A sample of crude oil which initially contained about 0.5 wt% gum-like solids, was filtered through a 1-micron filter, and fouling rate of the fluid compared with and without filtration (Saleh, 2006).

Results indicate that near elimination of suspended solids can reduce extent of fouling to close to detection levels.

Figure 2.20 **Effect of Removal of Suspended Solids by Pre-filtration on Fouling of BHO Oil*** (T_b = 80°C, $T_{s,o}$ =240°C, V=0.25m/s, P=379kPa)

Figure 2.20 has been removed because of copyright restrictions.
Figure 2.20 shows the Effect of Removal of Suspended Solids by Pre-filtration on Fouling of BHO Oil* (T_b = 80°C, $T_{s,o}$ =240°C, V=0.25m/s, P=379kPa)
Figure 2.20 was taken from Watkinson (2005).

2.12 Effect of Oxygen on Hydrocarbon Fouling

Watkinson et al. (2000) report that the fouling rate over 16 h of operation in the presence of pure air is about 10 times that under nitrogen. In practice, oxygen is believed to enter the system in trace amounts through improper storage conditions, and hence would be present at much lower concentrations than those in Figure 2.21. The solubility of oxygen in oil was therefore determined over the temperature range 25-90°C, using a GC-MS method. Eaton and Lux (1984) report that the effect of air on the fouling rate is greatly dependent on the type of hydrocarbon feed stock. For a hydrodesulfurizer feedstock originating from a delayed coker, air caused the fouling to increase from a totally non-fouling condition to a very high fouling mode, depending on the partial pressure of air. The amount of air was varied by pressurizing with nitrogen at various air ratios. For 100% nitrogen, no fouling was observed in their study. The effect of dissolved oxygen content on the initial fouling rate is shown in Figure 2.22. At low concentrations, the fouling rate was dependent almost linearly on dissolved oxygen content.

Figure 2.21 **Fouling Resistance versus Time for SSB Oil with 100% Nitrogen and Air Saturation** (T_b = 155°C, $T_{s,o}$ =290°C, V=0.44m/s)

Figure 2.21 has been removed because of copyright restrictions.
Figure 2.21 shows the Fouling Resistance versus Time for SSB Oil with 100% Nitrogen and Air Saturation (T_b = 155°C, $T_{s,o}$ =290°C, V=0.44m/s).
Figure 2.21 was taken from Watkinson et al. (2000).

Figure 2.22 **Effect of Dissolved Oxygen Content on Fouling Rate for SSB Crude Oil*** (T_b = 75°C, $T_{s,o}$ =290°C, V=0.44m/s)

Figure 2.22 has been removed because of copyright restrictions.
Figure 2.22 shows the Effect of Dissolved Oxygen Content on Fouling Rate for SSB Crude Oil* (T_b = 75°C, $T_{s,o}$ =290°C, V=0.44m/s).
Figure 2.22 was taken from Watkinson et al. (2000).

At concentrations above about 10 ppmw the curve flattens out into an oxygen-independent region. Under the highest dissolved oxygen concentration in their study, the

sparge gas contained 15% air and 85% nitrogen, the fouling rate was about 2.7 times that under nitrogen blanketing.

2.13 Deposit Analysis

Foulant deposits contain a wealth of information about the fouling process. Characteristics of the deposits formed on the heat exchanger metal surface provide information about the mechanisms forming those deposits. C.A.Bennett et al. (2006) mention the problem inherent to laboratory and pilot scale crude oil fouling research, which is the paucity of fouling deposit available for analysis. As a result, characterization techniques must be selected prudently, and Table 2.9 provides a list of prioritized fouling deposit characterization techniques.

Table 2.9 Prioritized Fouling Deposit Characterization Techniques*

Priority	Minimum Sample	Technique	Information Obtained
1	~ 10 mg	Thermogravimetric analysis	Volatile compound, fixed carbon, and ash contents
2	~ 1 mg	Fourier transform infrared spectroscopy	Functional group identification
3	~ 1 mg	Scanning electron microscopy/	Deposit morphology/surface elemental mapping
		energy dispersion spectroscopy	
4	~ 20/100 mg	Combustion analysis	Bulk nonmetal (CHN/OS) contents
5	~ 20 mg	X-ray fluorescence	Bulk elemental analysis
6	~ 30 mg	X-ray diffraction	Crystalline compound identification
7	~ 2 mg	X-ray photoelectron spectroscopy	Surface elemental and chemical analysis
8	~ 100 mg	Nuclear magnetic resonance	Functional group identification using both ^{1}H and ^{13}C

* Adapted from C.A Bennett et al. (2006)

The COFTF suggests that every effort should be made to avoid contamination and ambiguity in the sampling techniques for deposit characterization. COFTF advocates removing the deposits from the fouling rod with a high purity aluminium tool because it leaves a distinctive elemental fingerprint and does not harm the rod. Thermogravimetric analysis (TGA) is considered as the most valuable of the fouling analyses. Fourier transform infrared spectroscopy (FT-IR) is a very valuable characterization technique because it provides functional group information with minimal sample and preparation requirements. Scanning electron microscopy (SEM) and energy dispersion spectroscopy (EDS), also known as energy dispersive x-ray analysis (EDX or EDXA), are typically

performed in tandem because both use electron beams. SEM yields information about morphology of the sample up to a magnification of two million times. Morphology can indicate the mechanism of deposit formation – uniformly layered growth versus particle entrapment, for example. EDS complements SEM by focusing the electron beam on a small area, detecting the quantized x-rays emitted from the near-surface region and assigning an elemental analysis. Mapping regions strategically provides invaluable information about deposit formation and constitution. Burning a combustible sample in pure oxygen at 1000°C (1832°F), fully oxidizing the products with catalysts, and using chromatography to separate the gases render valuable data on bulk nonmetal content. Pyrolysis is used to measure bulk oxygen content. Nonmetal contents suggest which organic molecules contributed to the deposit. For example, H/C ratios indicate if the organic components of the deposit are waxy, asphaltenic, or coke. Nitrogen and sulfur constituents might be related to resins and asphaltenes, but researchers must recognize that there can be other sources of these elements (e.g., Fe_xS_y). Oxygen content can be attributed to polymerization mechanisms, but deposits absorb oxygen from air. Thus, indisputable oxygen analysis requires glove box procedures.

The COFTF also sees value in the strategic application of X-ray photoelectron spectroscopy (XPS). An x-ray irradiated sample ejects quantized core electrons from atoms in the near surface region. The binding energies of these quantized electrons respond to the chemical environment, furnishing both elemental identification and an oxidation state. Thus, chemical species in the near surface region can be distinguished regardless of crystallinity.

Solid –state ^{1}H and ^{13}C nuclear magnetic resonance (NMR) might be a powerful tool for fouling deposit characterization. Although ^{13}C NMR requires more sample than the ^{1}H NMR, it produces similar spectra. NMR might be able to identify functional groups prone to foul.

2.14 Mitigation Techniques of Hydrocarbon Fouling and Industrial Practices

Fouling of heat transfer equipment is one of the most common operational problems confronted by the chemical processing industries, causing detrimental effects by affecting the thermal and hydraulic performance of the affected heat transfer equipment, due to accumulation of fouling deposits. The total cost associated with fouling deposit is significant. Fouling affects both the capital and the operating cost of heat transfer equipment. The traditional method to accommodate fouling is to assign an individual fouling resistance, or "fouling factor", to each stream. This fouling factor is the expected resistance due to fouling at the end of run of the heat exchanger cleaning cycle, based on user experience. The sum of the fouling, fluid and metal resistances provides a total design resistance to calculate the required surface area. The Tubular Exchanger Manufacturers Association (TEMA) publishes fouling factors by service. The use of large fouling factors can be a self-fulfilling prophecy. The fouling resistance for most mechanisms is inversely proportional to velocity. Large fouling factors or other design margins result in added surface area. A design with large surface area will always have lower fluid velocity than a design with less area at the same given pressure drop. As surface area is added, velocity decreases. As velocity decreases, fouling increases. Thus the prophecy is fulfilled. Also, the capital cost increases as a consequence of the large allowances usually specified in the design of heat transfer equipment. The increase in the operating cost stems from the increase in the energy consumption, extra maintenance and cleaning of equipment, use of antifouling additives and loss of production. It is clear that there are strong incentives for effective strategies to mitigate fouling deposition in heat transfer equipment.

Wilson et al. (2005) summarize the currently available mitigation techniques as follows:

a. Increased tube-side velocity
b. Switching the crude from the tube side to shell side, which benefits from the difference between inner and outer surface areas on standard exchanger tubes – the lower heat flux on the outer surface reduces the surface temperature noticeably

c. Use of inserts (e.g. HiTran, Spirelf, Turbotal), offering enhanced heat transfer and fouling resilience but with increased pressure drop for a similar flow rate.
d. Use of alternative baffle or tube type.
e. Accepting fouling but cleaning regularly. Few plants actually monitor fouling and use the information to optimize their cleaning actions.
f. Chemical additives

Numerous types of antifoulant additives have been described in literature. Watkinson and Wilson (1997) mention about antioxidants, metal deactivators (MDAs), dispersants, detergents, size limiters and coke suppressants for fouling mitigation. Antioxidants interrupt the formation of fouling precursors either by converting hydrogen peroxides into stable products or by scavenging peroxy radicals. Metal deactivators reduce the initiation property of metal ions, whereas detergents and dispersants prevent fouling precursors from generating permanent deposits.

Figure 2.23 Changing Operating Conditions to Mitigate Fouling*

Figure 2.23 has been removed because of copyright restrictions.
Figure 2.23 shows the effect of Changing Operating Conditions to Mitigate Fouling.
Figure 2.23 was taken from Rodriguez and Smith (2007).

The effect that some operating variables have on the rate of fouling deposition can be exploited as a fouling mitigation strategy. Operating conditions of heat exchanger networks prone to fouling deposition can be modified so that the severity of this problem

is reduced. Considering the chemical reaction fouling in crude oil heat exchangers and according to the fouling threshold model, for heat exchangers operating at conditions of velocity and temperature above the fouling threshold, severe fouling deposition can be expected. Fouling deposition in heat exchangers that operate above the fouling threshold can be mitigated by moving the operating conditions towards the threshold line, as indicated in Figure 2.23. The severity of the deposition will decrease as the operating conditions are moved closer to the threshold. In case that the operating conditions move below the threshold line, minimum or negligible fouling deposition can be expected. As observed in Figure 2.23, the changes required to move the operating point towards to the region of favourable conditions imply either increasing the velocity, decreasing the wall temperature or a combination of both. Rodriguez and Smith (2007) present a new approach that combines the optimization of operating conditions with the optimal management of cleaning actions in a comprehensive mitigation strategy. The proposed approach leads to higher energy savings, lower operational costs and fewer disturbances in the operation of the background process.

Nesta and Bennett (2005) report that fifteen crude oils which Heat Transfer Research Institute (HTRI) has studied thus far suggest that tube side velocities above 2 m/s and wall temperatures below 300°C are reasonable guidelines for designing fouling resistant heat exchangers via the method termed low-foul design. The low foul design method is applicable to medium through high boiling point liquid hydrocarbon mixtures with API gravity less than 45 (chosen from experience). The crux of the low-foul method is to provide velocity equal to, or greater than, a critical velocity that significantly mitigates fouling. Application of this field-proven design methodology will significantly lower capital costs and substantially increase run time between cleanings.

D.G.Klaren et al.(2007) report the striking advantages of the zero fouling self-cleaning design that require only one-third of the heat transfer surface of the conventional crude pre-heater and that much longer operating periods can be achieved between inspections or cleanings. The zero fouling mechanism described in their article does not attempt to reduce fouling by using chemicals. Neither does it increase turbulence, and as a

consequence, reduce wall temperatures for fouling mitigation. Instead, it is based on the concept of "let fouling happen", but it removes the fouling deposits as they are being formed. The design of the zero fouling shell and tube heat exchangers handling two severely fouling process streams (one in the tubes and one in the shell) is feasible by employing the self-cleaning heat exchange technology, which makes use of the circulation of cleaning particles and a sophisticated shell side design. This new zero fouling self-cleaning design has been compared with a conventional severely fouling crude oil pre-heater, and it has been shown that a reduction in the required heat transfer surface from 700 m^2 for the conventional exchanger to 229 m^2 for the newly designed heat exchanger can be achieved.

Although there may be cases where one or more fouling mechanisms may predominate in the crude exchanger fouling, asphaltene precipitation is of great significance. Asphaltenes are high molecular weight components of the crude oil and are typically insoluble in paraffinic hydrocarbons, such as heptane, but soluble in xylene and other aromatic solvents. Asphaltenes have a high average molecular weight and a very broad molecular weight distribution. The mere presence of asphaltenes does not necessarily mean a crude oil will foul. Asphaltenes that are incompatible with the crude oil chemistry and composition have a much greater tendency to precipitate and foul. The unique chemistry of a particular crude oil, and the types and quantities of asphaltenes present, determine the potential for the particular crude to foul.

2.15 Objectives of the Present Work

The specific objectives of this study include but are not limited to:

- Modifying and rebuilding the existing fouling unit at The University of British Columbia to be able to run high temperature fouling runs at moderate pressures under N_2 blanketing.
- Carrying out fouling runs for the three different crude oils provided by Shell Canada Limited at varying bulk and surface temperatures.

- Investigating the fouling mechanism in detail for a single crude oil.
- Studying the effects of velocity for a single crude oil.
- Investigating the oil compatibility for the three crude oils.
- Comparing the fouling tendency for the three crude oils with those in literature in terms of activation energy.

EXPERIMENTAL SETUP

3.1 Test Crude Oils

Petroleum Industry has used labels, and in some cases specifications, to group crude oil grades into light, medium, heavy and sour. Not all follow the same conventions on what constitutes light, medium and heavy. Some sub-groupings are present such as high Total Acid Number (TAN) variants of heavy sour crude oils. In general, the Western Canadian Sedimentary Basin (WCSB) grades could be described as follows:

1. Condensate
2. Synthetic Crude
3. Light Sweet Crude
4. Light Sour Crude
5. Medium Sweet Crude
6. Medium Sour Crude
7. Heavy Sour Crude

This research or study was undertaken to provide fouling information on a set of crude oils supplied by Shell Canada Limited. Three commercial crude oils were provided in quantities of 20-40 L: Light Sour Blend (LSB), Midale (MDL), and Cold Lake Crude (CLK).

The crude oils used in this study fall in the above classification as follows:

LSB	:	Light Sour Crude
MDL	:	Medium Sour Crude
CLK	:	Heavy Sour Crude

This research was carried out in two parts. A comparative study was carried out using the three crude oils in the first phase of the study. The second phase of the study focused on the detailed fouling behavior of a single crude oil - LSB.

Table 3.1 Comparison of Crude Oil Assays (averages) – LSB, MDL and CLK

COMPARISION OF CRUDE ASSAY (TYPICAL AVERAGES) - FOR LIGHT SOUR BLEND, MIDALE & COLD LAKE

Basic Analysis Information

Analysis	Unit	LSB	MDL	CLK
Relative Density		0.85	0.88	0.93
API Density		35.80	29.40	20.70
Absolute Density	kg/m3	845.10	878.70	928.60
Total Sulphur	wt%	1.23	2.39	3.55
MCR	wt%	2.90	5.90	10.70
SW	Vol%	-	0.40	-
Sediment	ppmw	532.00	378.00	176.00
TAN		0.13	0.18	0.90
Salt in crude	ptb	96.90	37.90	13.80
Iron	mg/L	-	-	-
Nickel	mg/L	5.40	15.80	60.80
Vanadium	mg/L	8.50	29.30	155.40
Molybdenum	mg/L	-	-	3.20

Light Ends

Component	Unit	LSB	MDL	CLK
Methane	Vol%	-	-	-
Ethane	Vol%	0.06	0.04	0.03
Propane	Vol%	0.61	0.48	0.04
isoButane	Vol%	0.39	0.32	0.15
nButane	Vol%	1.64	1.22	0.82
Total Butanes	Vol%	2.03	1.54	0.97
Total C4 minus	Vol%	2.70	2.06	1.04
isoPentane	Vol%	1.29	1.00	3.38
n-Pentane	Vol%	1.95	1.32	3.57
Hexanes	Vol%	5.67	4.21	4.88
C7 Paraffins	Vol%	1.25	1.05	0.84
C7 Napthenes	Vol%	2.62	2.13	1.34
C7 Aromatics	Vol%	0.99	1.01	0.51
nHeptane	Vol%	1.28	0.98	0.74
Total Heptanes	Vol%	6.14	5.12	3.56
C8 Paraffins	Vol%	1.94	1.59	0.80
C8 Napthenes	Vol%	2.09	1.86	0.60
C8 Aromatics	Vol%	1.56	1.23	0.50
nOctane	Vol%	1.20	0.93	0.44
Total Octanes	Vol%	6.79	5.48	2.57
C9 Paraffins	Vol%	1.17	1.01	0.35
C9 Napthenes	Vol%	1.15	0.96	0.34
C9 Aromatics	Vol%	2.12	1.63	0.54
nNonane	Vol%	0.92	0.76	0.25
Total Nonanes	Vol%	5.35	4.38	1.56
C10 Paraffins	Vol%	1.37	1.18	0.42
C10 Napthenes	Vol%	0.14	0.13	0.06
C10 Aromatics	Vol%	-	-	-
nDecane	Vol%	0.90	0.77	0.22
Total Decanes	Vol%	2.41	2.72	1.04

Distillation Information

% Distilled Off	Unit	LSB	MDL	CLK
IBP	°C	33.70	31.90	32.30
1%	°C	34.00	34.80	33.50
5%	°C	48.70	82.60	57.80
10%	°C	92.40	114.50	109.40
15%	°C	133.00	151.10	181.90
20%	°C	171.00	185.70	242.40
25%	°C	203.90	218.50	285.40
30%	°C	235.30	249.20	320.80
35%	°C	263.90	277.60	354.10
40%	°C	292.90	305.90	386.80
45%	°C	319.80	334.10	417.40
50%	°C	348.00	363.70	447.60
55%	°C	375.10	393.50	479.10
60%	°C	404.00	423.40	513.00
65%	°C	433.50	453.70	548.40
70%	°C	464.90	487.50	584.50
75%	°C	496.60	525.70	619.00
80%	°C	530.20	571.20	651.40
85%	°C	567.30	619.70	672.80
90%	°C	585.00	653.00	686.40
95%	°C	629.70	686.30	710.30
98%	°C	697.30	711.00	724.90
99%	°C	-	-	-
100%	°C	-	-	
FBP	°C	712.60	715.30	722.30
Residue	%	6.50	9.42	10.08

Yield on Crude

Component	Unit	LSB	MDL	CLK
C4 and lighter	Wt%	3	2	1
Naphtha (C5-190°C)	Vol%	20.8	18.7	14
Kerosene (190°C-277°C)	Vol%	16	15	9.9
Distillate (277°C-343°C)	Vol%	11	11	8.6
Gas Oil (343°C-565°C)	Vol%	30.3	33.3	34.5
Residue (565°C+)	Vol%	18.9	20	32

BTEX

Component	Unit	LSB	MDL	CLK
Benzene	Vol%	0.3	0.47	0.25
Toluene	Vol%	0.79	0.69	0.41
EthylBenzene	Vol%	0.48	0.46	0.05
Xylenes	Vol%	0.79	0.49	0.36

Light Sour Blend originates from Southeast Saskatchewan. It had sulfur content in the range of 1.25 - 2.0 (wt %). Typical benchmark values reported by Shell Canada Limited are 1.26 wt %. The average sulfur content for a period of 22 months was 1.58 (wt %).

Table 3.1 provides a comparative summary of the test crude oil assays (averages). This data was sourced and compiled from http://www.crudemonitor.ca. This website provides information pertaining to the quality of the Western Canadian Crude Oils. The data and information provided on this website are through the Canadian Association of Petroleum Producers (CAPP).

The quality of the test crude oils can be sorted based on the following key physical properties and or contaminants present in them. Table 3.1 and Table 3.2 were used to do the following quality comparison between the crude oils.

3.1.1 API Density

Based on the API gravity of the test crude oils, the crude oils can be ranked from heavy crude oil to light crude oil as follows:
CLK (20.7)> MDL (29.4)> LSB (35.8).

3.1.2 Total Sulfur Content

Based on the total sulfur content in the test crude oils, the crude oils can be ranked from highly sour crude to light sour crude as follows:
CLK (3.55 wt %)> MDL (2.39 wt %)> LSB (1.23 wt %).

3.1.3 Micro Carbon Residue (MCR)

Based on the MCR in the test crude oils, the crude oils can be ranked from high MCR content to low MCR content as follows:
CLK (10.7 wt %)> MDL (5.9 wt %)> LSB (2.9 wt %).

3.1.4 Sediments and Salt in Crude

Based on the sediments and salt in the test crude oils, the crude oils can be ranked from high salt and sediments content to low salts and sediment content as follows: CLK < MDL < LSB.

3.1.5 Metal Content (Nickel and Vanadium)

Based on the metals content (nickel and vanadium) in the test crude oils, the crude oils can be ranked from high metal content to low metal content as follows: CLK > MDL > LSB.

3.1.6 Asphaltene Content

Based on the asphaltenes content (C_5 asphaltenes –Shell Method) in the test crude oils, the crude oils can be ranked from highly asphaltenic crude oil to low asphaltenic crude oil as follows:
CLK (13.2 wt %) > MDL (6.44 wt %) > LSB (3.13 wt %).

3.1.7 Residue ($565^{o}C^{+}$)

Based on the residue ($565^{o}C^{+}$) content in the test crude oils, the crude oils can be ranked as follows:
CLK (32 vol %)> MDL (20 vol %) > LSB (2.03 vol %).

3.1.8 Viscosity

Based on the viscosity of the test crude oils at 25°C, the crude oils can be ranked from highly viscous crude oil to moderately or low viscous crude oil as follows: CLK (157.8 mPa-s)> MDL (27.3 mPa-s) > LSB (12.7 mPa-s).

Most of the analytical properties of the crude oil can correlate to its fouling tendency (Sections 2.4, 2.5 and 2.6). The significant parameters as discussed above include, sulphur content, MCR, metals content, solids content, asphaltene content, salt content etc., These components can be termed as "bad actors" influencing the fouling tendency or fouling potential of the crude oil. From the individual analytical property comparisons and based on their "content of overall bad actors" influence, the crude oils can be ranked as follows for their fouling propensity; CLK > MDL > LSB. This assumption is based on the available crude oil characterization. To characterize fouling of a given crude oil, one generally requires over nine experiments. Three levels of each of the following variables should be explored: velocity, surface temperature, and bulk or film temperature. In this project, due to experimental set-up limitations, velocity was generally held constant, and 3-5 experiments at different temperatures were done to characterize fouling of each of the crude oils.

Table 3.2 Benchmark Crude Analytical Data (as supplied by Shell Canada Limited)

S.No	Analysis	Units	CLK	MDL	LSB
1	Density @ 15 °C	(g/cc)	0.9582	0.8994	0.8534
2	Viscosity@ 25 °C	(mPa-s)	157.8	27.26	12.74
3	Viscosity@ 6 °C	(mPa-s)	566.2	113.5	161.7
4	"C_5 Asphaltenes Shell Method"	(wt %)	13.2	6.44	3.13
5	"C_7 Asphaltenes (ASTM D3279-97)"	(wt %)	8.58	5.05	2.05
6	Carbon Residues	(wt %)	10.6	6.49	3.56
7	Ash	(wt %)	0.036	0.003	0.003
8	Toluene Insolubles	(%)	0.09	0.06	0.06
9	"Hot Filtration (ASTM D4870)"	(%)	0.03	0.02	< 0.01
10	Organic Sulfur	(ppm)	36750	24580	12600
11	Nickel	(ppm)	66	18	7
12	Vanadium	(ppm)	157	30	10
13	Calcium	(mEq/L)	2	< 1	< 1
14	Sodium	(mEq/L)	15	1	< 1
15	Iron	(ppm)	4	< 1	< 1
16	Aluminium	(ppm)	< 5	< 5	< 5
17	Zinc	(ppm)	< 1	< 1	< 1
18	Copper	(ppm)	< 1	< 1	< 1
19	Filterable Solids)	(wt %)	0.07	0.15	0.05
20	Centrifugal Solids (BS from BS&W	(v %)	0.35	0.1	< 0.025
21	API Gravity 15 °C		16.17	25.83	34.31

3.2 Experimental Apparatus

Figure 3.1, shows a schematic diagram of the flow loop, which consists of a feed vessel, pulsation dampener, orifice plate flow-meter, annular fouling test section, and associated heaters, controls, and data logging system. Photographs are shown as Figures 3.2.a, b, c and d.

3.2.1 Feed Vessel

The stainless steel supply vessel holds up to 7.5-liters of an oil sample. It has been fabricated to withstand a maximum hydro-test pressure of 2070 kPa. The vessel has a 9.55-mm SS316 internal cooling coil to control the bulk temperature. The vessel was fabricated with a 40-schedule 8" SS316 pipe with a 10mm bottom plate and a 250-pound rated flange with 125-Ra inner serration on the top. A 250 pound rated blind flange was used and ports for external and internal connections for the vessel were drilled. SS-316 half couplings with female threads were welded to the ports. One inch SS-316 coupling with female thread was welded to the bottom plate with a drilled outlet port. The welds were carried out with qualified welder and quality assurance carried out on the welds using dye penetrant test. SS-316 gasket with graph-oil inner ring was used to mate the flanges of the vessel. The pictures of the vessel and inner cooling coil post-fabrication and pre-assembly are shown in Figure 3.2.e. The feed vessel design and construction was a very crucial component in the development of the fouling apparatus due to the severity of the test conditions and associated potential hazards.

3.2.2 Pump and Flow Measurement

The pump is a roto-gear- positive displacement pump with a maximum capacity of 15 liters per minute @ 140 kPa. The original mechanical seal configuration was modified to the conventional packing configuration due to frequent failures of the mechanical seal which is due to several factors not considered during the initial stages of

the fouling loop design and implementation. Recommendations to improve the existing system are elaborated in Chapter VI.

The driver was an induction motor with intrinsic safety, overload protection and other inherent safety features like the high bearing and high winding temperature protections/trips. A V-belt was used to connect the pulley mounted on the driver shaft to the pulley mounted on to the pump shaft. The ratio of the pump shaft pulley to the motor shaft pulley was approximately one for maximum capacity utilization of the pump within the vendor specified limits of the pump characteristics. At higher r.p.m's there would be excessive slippage of the roto-gear assembly causing flow reduction and excessive pulsation in the flow. The pump and the motor assembly were firmly mounted on a common self-supporting base plate. The base plate was not mounted on a pedestal nor firmly grouted to the ground. It was left floating with the support from the suction and discharge piping/tubing and was one of the important reasons for frequent mechanical seal failure due to the excessive vibrations given the severity of the operating conditions.

The stuffing box was packed with 8 sets of graph-oil packings that can stand high temperatures and are self-lubricating with a very minimal leakage rate for cooling and avoiding shaft seizure. Also, the leakage rate through the packing is dictated by the motor bearing temperature that has a trip setting on high bearing temperature (140°C).

During wear out of the packing, the leak rate was adjusted using the gland guide bolts. After an average of four runs the wear out on the packing would be excessive necessitating complete overhaul and re-packing of the stuffing box with new sets of graph-oil packing material. Pressure in the system is limited to 1240 kPa, because of the packing and potential risk of fire hazard due to the reliability issues with the packing. One another major disadvantage with the packing configuration was the wear out on the shaft leading to the shaft replacement every ten to twelve runs.

The flow is measured using an orifice plate assembly equipped with a differential pressure transducer. The output was recorded through the data acquisition system.

3.2.3 Test Loop

The suction part of the loop consists of 2.54 cm Outside Diameter (OD) SS 316 tubing. There was no isolation valve in the suction line. The remainder of the loop was generally fabricated from 1.27 cm OD SS 316 tubing. Swage-lock tube fittings were used to ensure safety. A ball valve was placed between the test section and the feed vessel for isolating purposes. The pump discharge was routed through a pulsation dampener which had a 1 kW electrical heater connected to a feedback control circuit to control the bulk temperature. The flow rate to the test section was adjusted using a 1.3-cm needle valve, bypassing the excess flow to the feed vessel.

The piping was completely insulated to minimize heat losses from the system and due to the limitations on the heat duty available as well for the temperature range of this study.

3.2.4 Heat Tracing

The suction line was completely wrapped with a coil of 6.35 mm copper tubing, which was connected to steam @ 414 kPa. Steam was only used during startups to ensure proper suction of highly viscous test oils, and during shut down to prevent freezing in the suction line

3.2.5 Annular Test Section and Fouling Probe

A new annular test section (Figure 3.2a & 3.2b) was built to accommodate the required velocity for this project. The material of construction was SS316 (pipe). The annular inside diameter was 1.5875 cm. The HTRI- probe (Figure 3.2d), supplied by Ashland Chemical-Drew Division was rated @ 1.92 kW and 240 V. Its outside diameter was 1.065 cm giving a cross-sectional area available for flow of 1.09cm^2 and an equivalent (hydraulic) diameter of 0.52cm. The heated length of the probe is 10.2 cm.

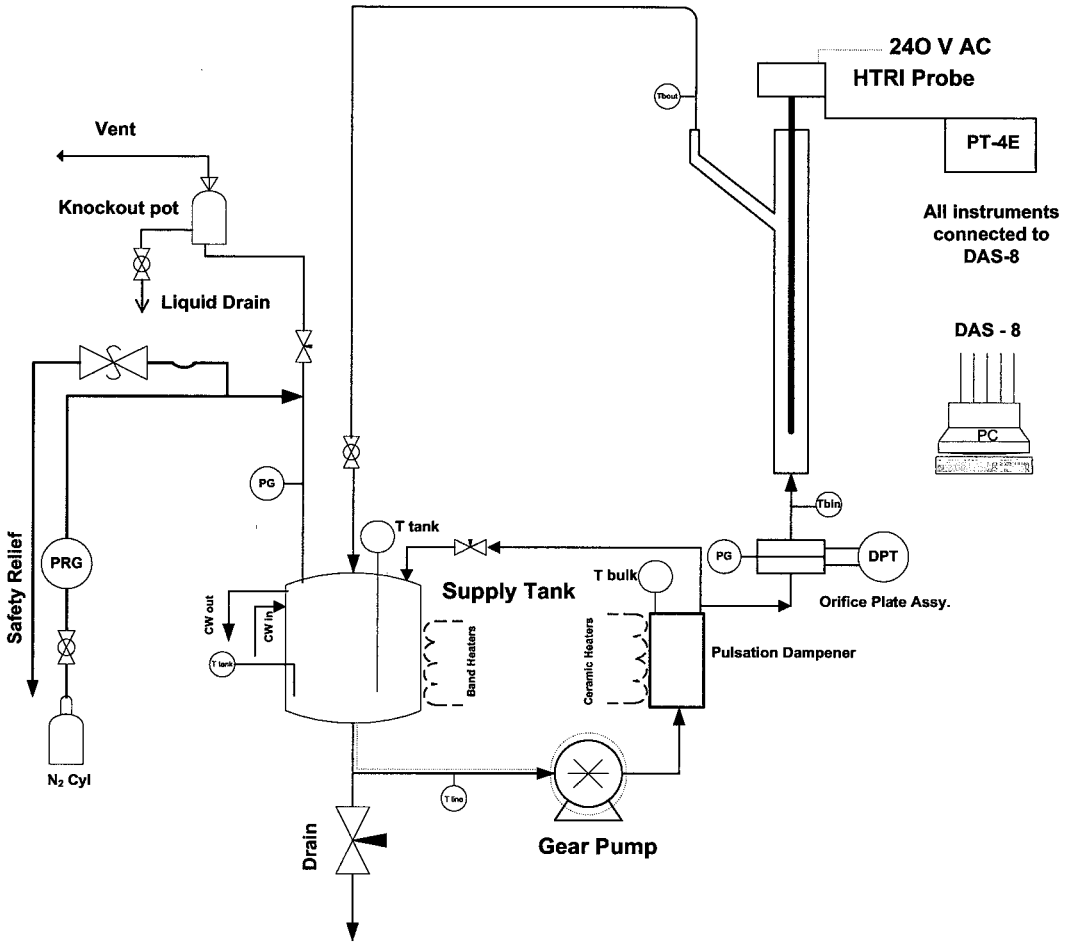

DPT	Differential Pressure Transmitter	**PRV**	Pressure Relief Valve
PG	Pressure Gauge	**Tb in**	Bulk Temperature In
PRG	Pressure Regulator	**Tb out**	Bulk Temperature Out
Cw in	Cooling Water In	**T line**	Line Temperature
Cw out	Cooling Water Out	**PT-4E**	Probe Thermocouples-4 No's
T vessel	Fluid Temperature (vessel)	**T bulk**	Bulk Temperature Controller
-------	Steam Tracing	**N_2 cyl**	Nitrogen Cylinder

Figure 3.1 Schematic of High Temperature Fouling Loop

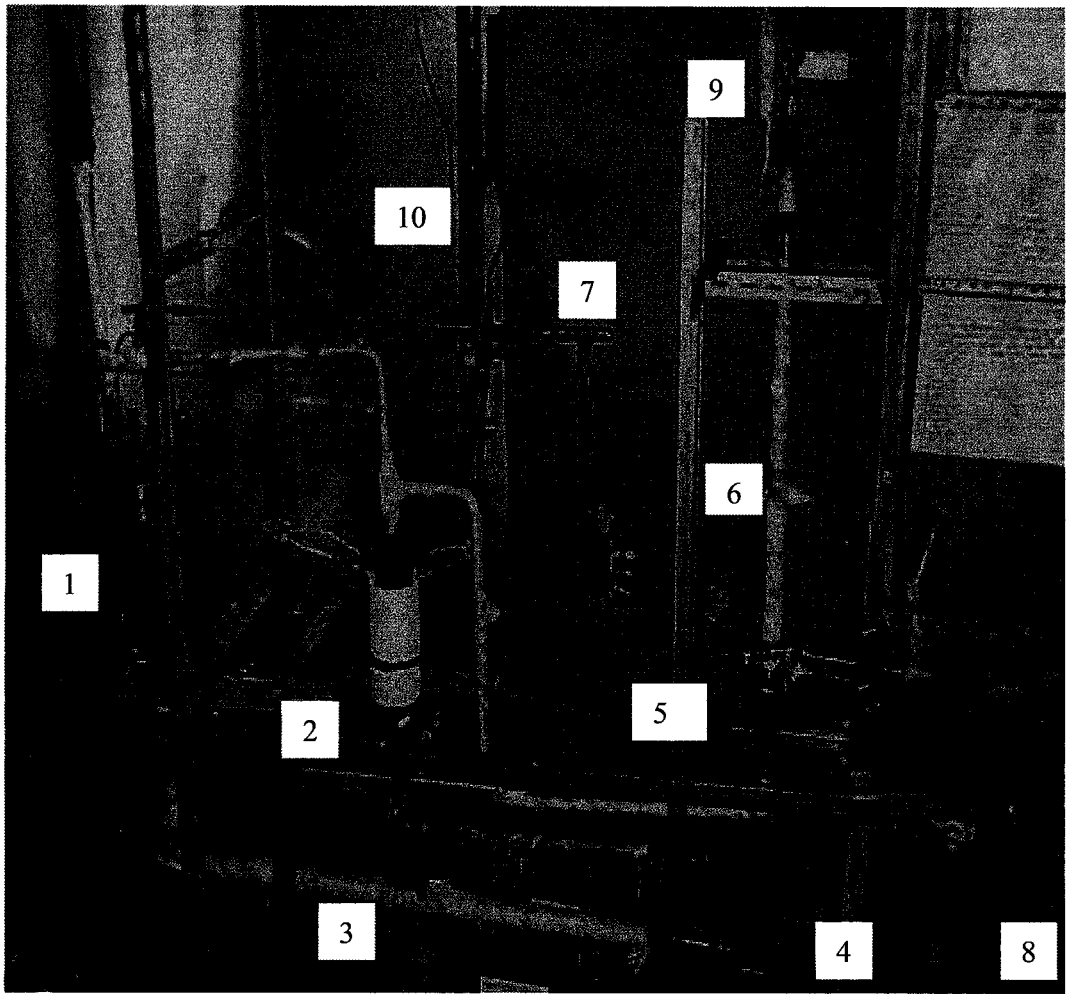

1.	Feed Vessel and Band Heater
2.	Pulsation Dampener and ceramic heater
3.	Suction Piping-pump
4.	Roto-gear pump
5.	Orifice Plate Assembly
6.	Insulated Test Section
7.	Safety Relief Valve
8.	Pump Drive-motor
9.	HTRI Probe
10.	Nitrogen supply from cylinder

Figure 3.2a Photograph of High Temperature Fouling Unit (Front View)

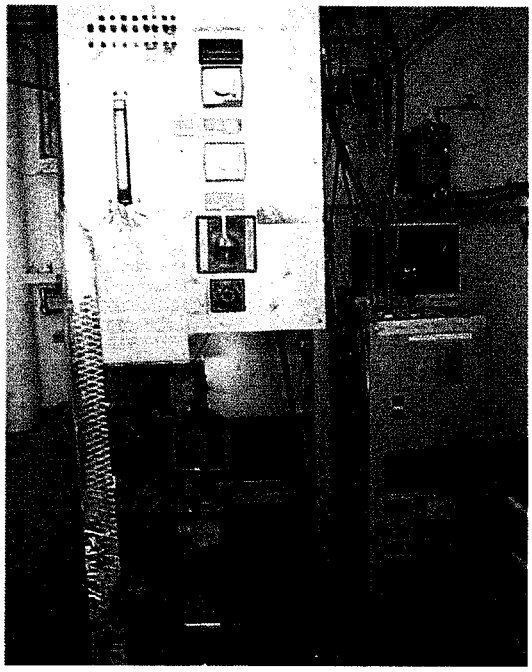

Figure 3.2b Fouling Unit – Side View with All Power Controls

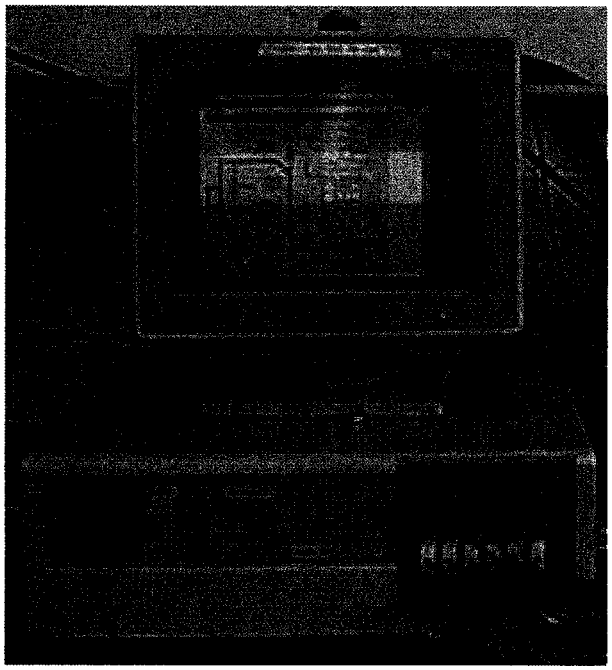

Figure 3.2c Fouling Unit Data Acquisition System

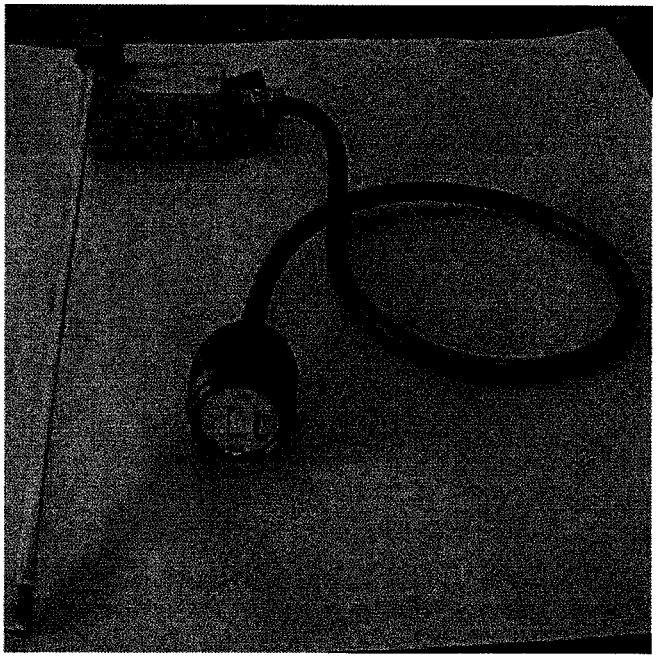

Figure 3.2d HTRI - Probe

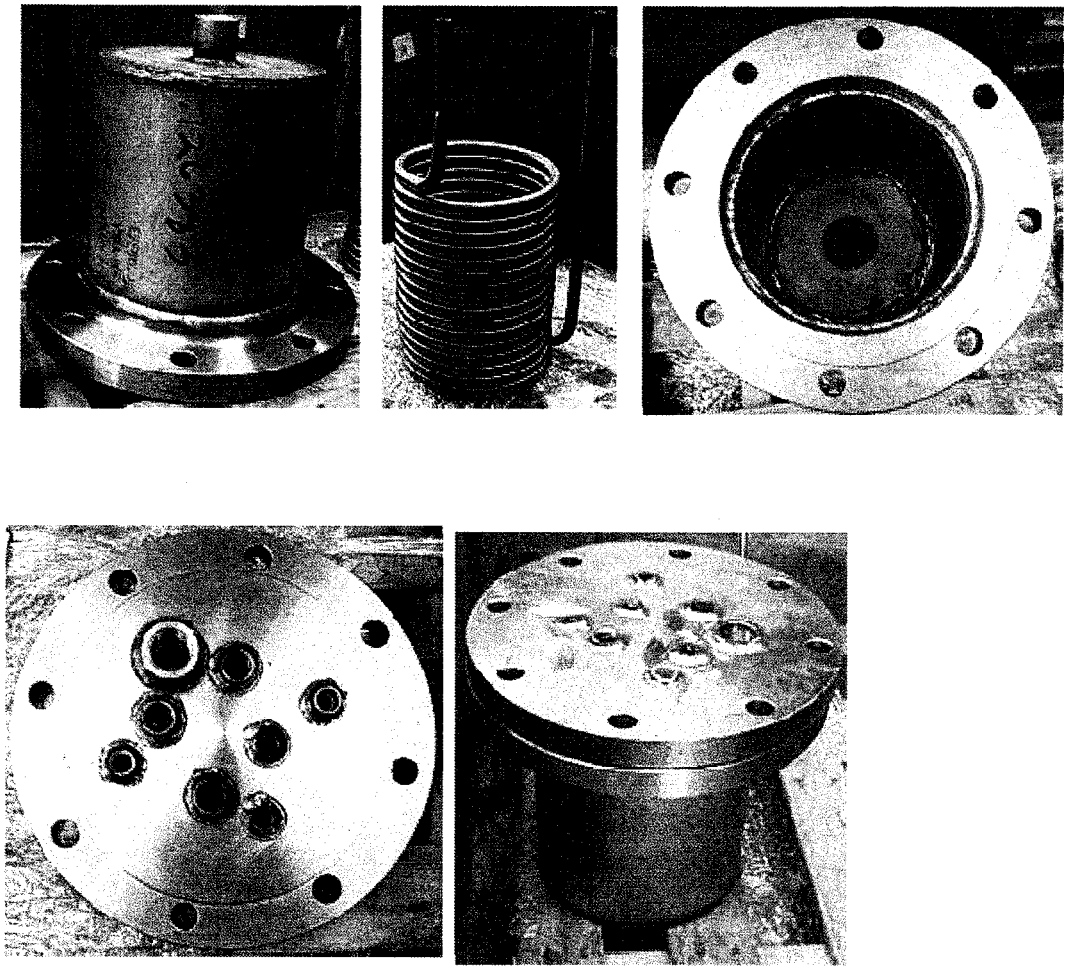

Figure 3.2e Pictures Showing the Pre-Assembly Components of the Feed Vessel with the Cooling Coils and Other Ports. (Post-Fabrication)

The maximum design surface temperature of the probe is 630°C. There are four thermocouples located beneath the metal skin of the probe at one axial position, (7.8 cm downstream of the start of the 10.2 cm heated length) and at four angular locations. One of the four thermocouples is used for a high temperature safety power cut-off alarm. The other three are averaged to give the surface temperature, using a correction for the decrease in temperature from the measured point under the stainless steel skin to the outside surface of the probe. The correction factor was supplied by the calibration from the manufacturer. The power control to the probe is electronically done

with feed-back control logic. Thus the heat flux is maintained constant with time (except for very occasional surges in the main incoming power).

3.2.6 Pressure Control

The system pressure was maintained manually using nitrogen. There is an excess flow check valve connected close to the point of entry of nitrogen to avoid backup of volatiles from the system. A vent line from the system enters a coil which is immersed in cold water to avoid venting of hot vapor. The cooled vent-gas is routed close to the hood suction line through a seal pot to capture any liquid. The loop has a pressure relief valve set at 1380 kPa. Further discussion of system pressurization and control is given under operating procedures.

3.2.7 Data Acquisition System

A DAS-8 used for the data acquisition system, is supported by in-house built software. The system is capable of saving real time data as well as averaged data for a specified interval of time. The data can be recorded as a text file and then later analyzed using an excel spreadsheet.

Also, a safety feature or software interlock is incorporated in the system to protect the probe from overheating. If the maximum safe surface temperature and current are reached (including spikes lasting for a minute), the system will shut down the power supply to the probe. The electrical system has been designed with many circuit breakers, fuses, relays and trips for enhanced safety

EXPERIMENTAL PROCEDURE

4.1 Sample Preparation:

An oil sample of 4.5 kg was weighed into a dedicated container using a digital balance. The sample was then loaded into the clean 7.5–liter feed tank. The feed tank was first pressurized with N_2 to 700 kPa and then depressurized. This procedure was repeated thrice to purge the air out of the system. The pump was then started and the fluid circulated under nitrogen (with partial purging/venting) for five minutes at the desired flow-rate as previously calibrated and indicated via the orifice plate differential pressure transmitter cell. This procedure was meticulously and consistently followed to ensure the system was oxygen free for all the runs.

4.2 Pre-Heat Up and System Pressurization

The bulk temperature during most of the experiments was in the range of 135°C – 275°C. After the purging was complete, the vent valve was closed, and the tank and pulsation dampener heaters were switched on. The bulk temperature control via the pulsation dampener heater had an accuracy of ± 2 %, which was reasonable for this system. The system was vented periodically (total time 2-3minutes) during this heat-up phase which normally took about 1.5 hours. When the fluid reached about 100°C, the system was pressurized with N_2 to the maximum regulator pressure of 930 kPa and heating was continued.

A pressure difference of 170 kPa was normally observed between the regulator pressure and the system pressure due to the presence of a check valve with a minimum inlet pressure of 170 kPa. There was no pressure control in the system. The regulator pressure was maintained constant for all the runs. Venting of the system was attempted only in cases when the system pressure exceeded 180 psig for safety reasons. Also, the tubing/ piping were arranged in a way that during venting, mostly N_2 was only bled-off the

system. Since the initial system pressure was held constant with nitrogen for all the runs, the pressure varied for different crude oils based on their Reid Vapor Pressures.

4.3 HTRI Probe Power-Up

When the bulk temperature was 75 to 100°C below the desired value, the power to the probe was switched on, and the set point values of the bulk and surface temperatures were input to the controller. The surface temperature and bulk temperature were reached in about 40 minutes. After this the probe was switched to an automated feedback controller, which maintained the current to the probe at the required set point. Thereafter the heat flux to the probe was maintained almost constant (a variation of ± 1.5–2 % of the heat flux from the set value is normal).

4.4 Fouling Runs and Saving of Data

Experiments were typically carried out for two to five days of continuous operation. There were two modes to save the data from the data acquisition system. One was the real time data and the other was the average data. For the average data mode, the time interval was specified. The data was averaged for that time span and the resulting data points were stored as a text file. Later this data was retrieved and analyzed using an excel spreadsheet. Calculation methods are given below.

4.5 Shutdown Procedure

When a fouling run was terminated, the heaters and the probe were switched off and the fluid was allowed to cool down to room temperature by continuing the circulation. The system was allowed to cool under nitrogen blanketing to avoid air entry into the system. Before stopping the pump the final sample was collected in 2 one-liter bottles for testing of the fluid properties.

The probe was removed from the annulus with extreme care to prevent any deposit from getting scraped off the surface in the case of very weak deposits. The deposit was then washed with n-hexane to remove oil. A picture of the probe deposit was taken using a digital camera with a certain amount of magnification and fine tuned using a photo-editor. The deposit was allowed to dry naturally for at least 1-2 hours, and then it was scraped off with a fine sharp blade and stored in a sample vial for subsequent analysis. In cases of very rigid and heavy deposition, the thickness of the deposit was measured using a caliper over the length of the heated section of the probe, and the average thickness of the deposit was estimated. The surface of the probe was cleaned, first with medium grit and then with fine grit (# 300)- emery paper. The surface was then polished with the fine grit emery paper. Before inserting the probe into the loop for the next run, the surface of the probe was cleaned with Varsol®.

4.6 Flushing the Loop

The oil sample from the system was completely drained, and the loop was purged with N_2. Then 4 liters of Varsol® was placed in the feed tank and the circulation was established at 75°C - 85 °C. The circulation was carried out for a minimum of 6 hours, then the system was cooled and the Varsol® was completely removed from the system by draining and then nitrogen purging to ensure that there were no pockets of the Varsol® present, which might affect the results. When the type of oil to be used is different from that of the previous run, the loop was also rinsed with a small amount of the new crude oil.

4.7 Experimental Calculation Methods

Heat flow to the oil, Q (W) was determined from voltage (v) and current (I) measurements, and the heat flux (kW/m^2) determined using Q, and A, the heated area of the probe. We define an overall heat transfer coefficient, U, as in equation (4.1) below:

$$Q = v * I = U A (T_s - T_b) \qquad 4.1$$

Here T_s is the surface temperature of the heated probe, and T_b the average bulk temperature of the fluid. Average values of T_s are evaluated from three thermocouples located at the same axial position, and different angular positions. The average bulk temperature of the fluid is determined from the average of the inlet and outlet fluid temperature measurements.

The overall heat transfer coefficient is calculated at approximately $¾^{th}$ of the heated section (from the start of the heated section) of the probe at any time from

$$U(t) = q\,(t) / (T_{s\,(t)} - T_{b\,(t)}) \qquad 4.2$$

Where the heat flux q, is given by

$$q = Q/A \qquad 4.3$$

Generally the unit is operated at constant q, and with constant T_b, with time, hence the decline in U due to fouling, is determined by the increase in T_s with time. There is a short period (2.5-3.5 hrs) of unsteady state heat transfer at the beginning of the runs and in some cases, an induction period before fouling begins.

The fouling resistance is determined from

$$R_f = 1/U\,(t) - 1/U\,(t=0) \qquad 4.4$$

The value of U (t=0) was calculated from ten data points from 2.5-3.5 hours.

Since 1/U (t=0) is a constant, the fouling rate can be determined from the slope of the curve 1/U (t) versus time, t.

$$\text{Fouling rate} \qquad d\,R_f / dt = d\,[1/U\,(t)] / dt \qquad 4.5$$

Rates were determined by curve fitting the linear part of the 1/U Vs t curve. The section of the curve, over which the rate was measured, was indicated, since the fouling rate changes with time in some cases.

RESULTS AND DISCUSSIONS

5.1 Crude Oil -Fouling Studies

Table 5.1 summarizes the operating conditions for all of the fouling experiments. In addition to operating conditions, the rates of fouling are reported, and some other derived numbers for plotting of results.

5.2 Fouling Results of a Typical Run

Figure 5.1 for Run 4 is a typical plot of the experimental results. In Figure 5.1, the heat flux, q remains constant over the full 46 hours of the experiment. There is a period of unsteady state behavior in the initial 3-4 hours, when surface and bulk temperatures rapidly increase.

The heat transfer coefficient, U, increases during this unsteady period, and then reaches a constant value for a couple of hours before fouling begins to show its effect in reducing the heat transfer coefficient with time. The fouling process is indicated by the slow steady increase in surface temperature over the 43 remaining hours of the run, during which the bulk temperature remains constant. The final value of the heat transfer coefficient is roughly 30% below the initial value. Any fouling which causes less than about a 5% decline in U, is within the scatter of the data. The value of the overall coefficient for the clean surface is calculated from its values during the period 2.5-3.5 hours from the start. A reasonable average of the clean heat transfer coefficient is determined for each run. This value is used in the calculation of the fouling resistance R_f, shown plotted in Figure 5.2 R_f increases more rapidly during the first 21 hours, and then the fouling process appears to fall off. In Run 4, the fouling rate is highest at the beginning (roughly 8.3 E-07 m^2K/kJ), and over the duration of the run, averages slightly lower at 5.67E-07 m^2K/kJ. By contrast, in Run 5 (Figure 5.5), the increase in R_f is linear with time, and the fouling rate is constant. For consistency in this work, a linear increase in fouling resistance is assumed, and hours over which the rate is calculated are listed in

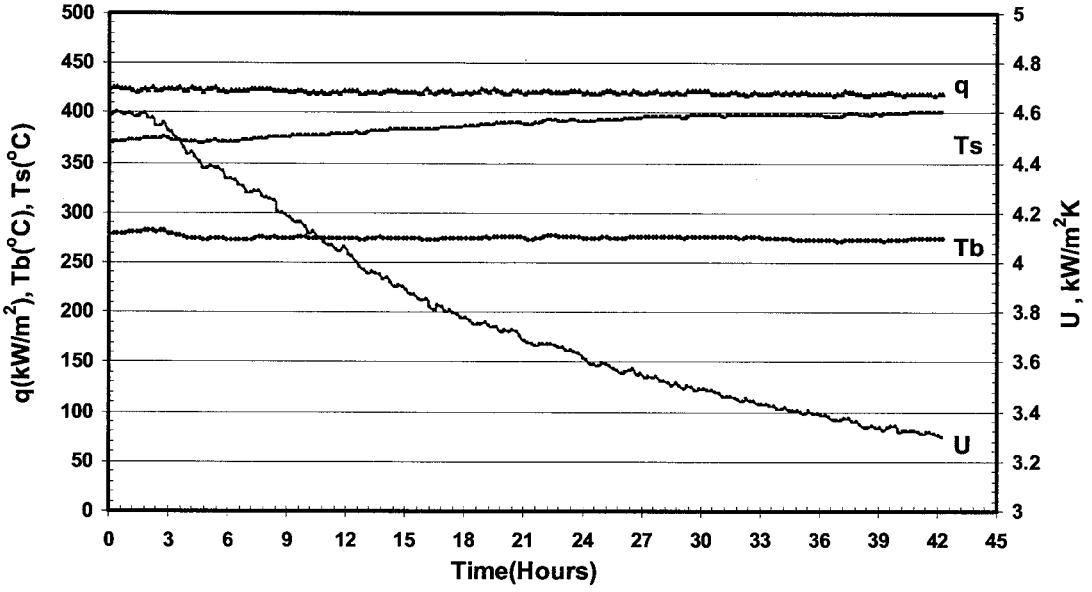

Figure 5.1 Overall Parameter Plot for LSB Crude Oil – Run 4

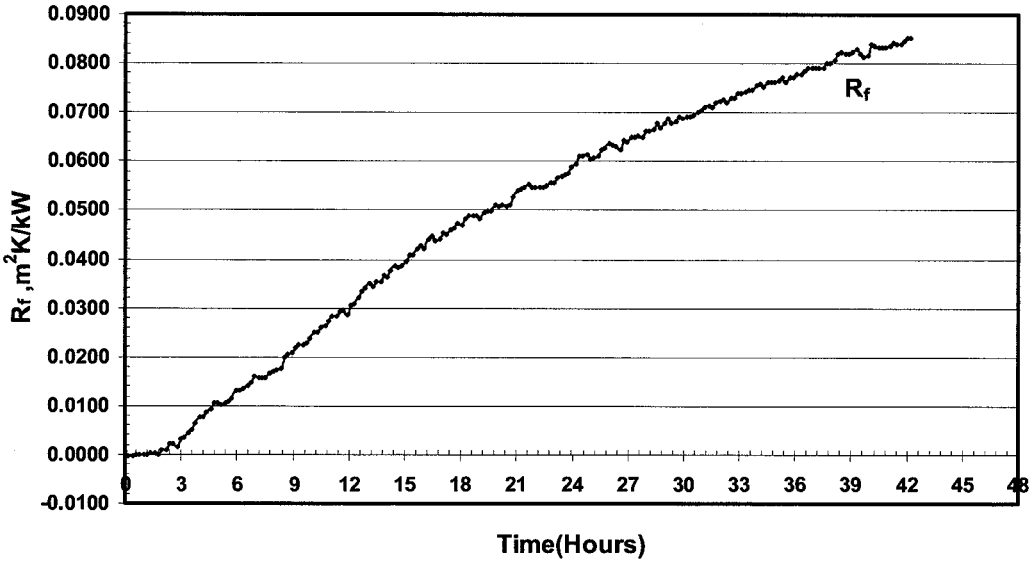

Figure 5.2 Fouling Resistance Vs Time Plot for LSB Crude Oil – Run 4

⇐ Flow Direction

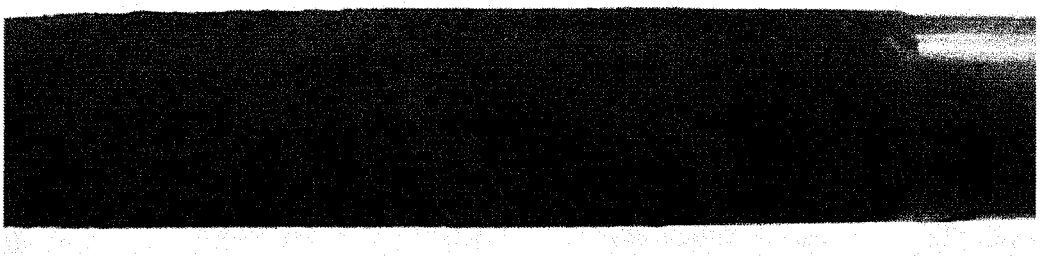

Figure 5.3 Picture of Fouled Probe for LSB Crude Oil – Run 4 (Flow Entry)

⇐ Flow Direction

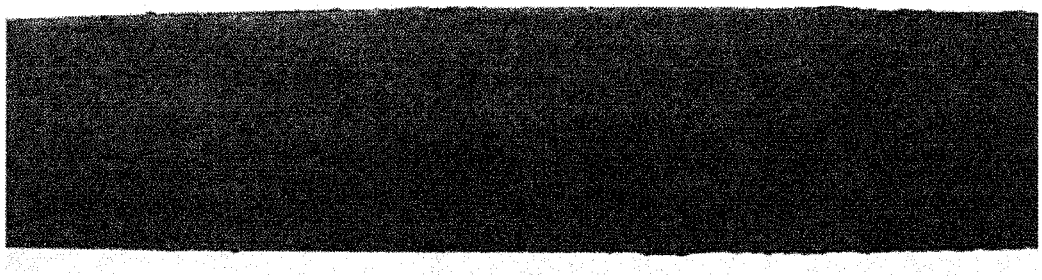

Figure 5.4 Picture of Fouled Probe for LSB Crude Oil – Run 4 (Mid-Section)

Table 5.1

Summary of Results

Crude	Batch Size (kg)	Run No.	P (PSIG)	Start time(hrs)	End time(hrs)	Vel (m/s)	Tb in °C	Tb out °C	Delta Tb °C	Tb avg °C	Ts @t=0,°C	Tfilm °C	q , kW/m²	U start, kW/m²K	U end, kW/m²K	% Decrease in U	Fouling Rate, 10^{-7} (m²K/kJ)	Time Period (Hours)	1000/Ts (K)	1000/Tf (K)
	4.5	1A	140	4.5	16.0	0.30	129.3	139.6	10.4	134.4	250.0	**192.2**	389.4	3.2350	3.1400	2.8	**3.46**	4.5-16.0	1.9120	2.1495
	4.5	3A	160	3.2	23.4	0.75	206.1	217.6	11.5	211.8	297.0	**254.4**	426.7	4.3785	4.1458	5.3	**1.29**	3.2-23.4	1.7544	1.8961
LSB	4.5	4	125	5.0	46.2	0.75	270.0	280.7	10.7	275.4	371.0	**323.2**	421.0	4.4869	3.3012	28.1	**5.67**	4.5-42.0	1.5528	1.6774
	4.5	5	125	3.0	47.8	0.75	251.0	262.1	11.0	256.5	350.5	**303.5**	423.3	4.5619	3.6287	20.4	**3.91**	9.7-47.8	1.6038	1.7346
	4.5	10	125	3.0	48.0	0.75	265.0	276.3	11.2	270.6	370.0	**320.3**	433.5	4.3926	3.0270	31.2	**6.69**	7.54-48.0	1.5552	1.6854
	3.5	15	125	4.4	37.3	0.75	277.0	288.4	11.4	282.7	375.5	**329.1**	436.6	4.6590	3.8529	17.3	**3.51**	7.7-37.3	1.5420	1.6608
	2.5	18	125	2.4	28.9	0.75	250.0	261.0	11.0	255.5	354.0	**304.8**	422.0	4.3122	3.3784	21.6	**10.27**	11.50-28.9	1.5949	1.7309
	4.5	19	125	3.4	47.6	0.75	251.0	262.0	11.0	256.5	355.0	**305.8**	422.2	4.3000	3.6400	15.4	**4.16**	17.3-47.6	1.5924	1.7279
	4.5	21	125	0.6	47.9	0.75	267.6	276.3	8.7	272.0	355.0	**313.5**	342.7	4.1969	3.1908	24.0	**4.16**	0.6-47.9	1.5924	1.7051
	4.5	23	125	12.9	51.8	0.75	270.9	277.1	6.2	274.0	335.0	**304.5**	251.5	4.1779	3.4906	16.5	**3.06**	12.9-51.8	1.6447	1.7316
	4.5	24	125	0.6	50.3	0.75	281.9	289.6	7.7	285.7	360.5	**323.1**	321.2	4.3412	3.3334	23.2	**4.90**	0-50.3	1.5785	1.6775
	4.5	25*	125	0.6	50.0	0.75	268.0	277.7	9.8	272.8	362.5	**317.7**	395.8	4.4837	2.7534	38.6	**20.00**	0-49.9	1.5735	1.6929
	4.5	27	125	12.3	48.2	0.75	240.4	254.6	14.2	247.5	357.0	**302.2**	484.4	4.4378	3.6502	17.8	**3.50**	12.3-48.2	1.5873	1.7384
	4.5	29	125	0.6	49.2	0.35	267.4	283.8	16.3	275.6	375.0	**325.3**	420.6	3.9960	2.8224	29.4	**6.98**	0.6-49.2	1.5432	1.6714
	4.5	30	125	7.5	43.6	0.15	263.1	289.5	26.4	276.3	375.0	**325.7**	353.8	3.5877	2.3498	34.5	**9.91**	7.5-43.6	1.5432	1.6704
	4.5	32	125	12.3	48.2	0.75	276.2	284.6	8.4	280.4	363.5	**321.9**	260.8	3.3454	1.9189	42.6	**6.75**	12.3-48.20	1.5711	1.6808
MIDALE	4.5	6A	125	5.0	38.7	0.75	141.0	150.8	9.7	145.9	250.0	**197.9**	342.2	3.1963	2.9228	8.5	**2.98**	9.7-38.7	1.9120	2.1234
	3.25	7	125	1.0	43.6	0.75	242.1	253.2	11.1	247.7	345.0	**296.3**	413.5	4.2134	4.1048	2.6	**0.43**	4.7-43.6	1.6181	1.7565
	4.5	11	125	2.0	50.9	0.75	254.3	265.0	10.7	259.7	352.5	**306.1**	423.0	4.5293	3.2994	27.2	**3.62**	4.6-50.9	1.5987	1.7269
	4.5	16	125	1.2	47.6	0.75	276.4	287.0	10.6	281.7	378.5	**330.1**	433.3	4.1603	3.3096	20.3	**4.18**	5.4-42.2	1.5349	1.6581
	4.5	12	125	2.0	51.0	0.75	260.8	271.6	10.8	266.2	382.0	**324.1**	420.6	3.6044	1.4680	59.2	**9.44**	4.2-48.6	1.5267	1.6748
	4.5	13	125		run aborted															
COLD LK	4.5	14	125	5.2	45.0	0.75	249.0	256.9	7.9	252.9	352.5	**302.7**	302.6	3.0493	2.5097	17.6	**6.84**	18.8-45.0	1.5987	1.7370
	4.5	17	125	2.8	19.8	0.75	230.3	238.3	8.0	234.3	335.5	**284.9**	302.2	2.9278	2.6014	11.2	**9.29**	8.3-19.8	1.6434	1.7924
	4.5	33	125	7.5	48.3	0.75	243.8	250.5	6.7	247.2	342.5	294.8	261.9	0.3769	2.7115	26.2	**8.78**	7.5-48.3	1.6247	1.7611

* - Contaminated sample (iron rust).

Table 5.1. The estimated Reynolds number at the film temperature of 310°C is given as 5600 in Appendix II. Figure 5.3 is a photo of the fouled probe at the end of the fouling process. Figure 3.2d shows the clean probe, prior to the fouling run. The deposit is seen to be black, and have some roughness to it. It is restricted to the heated section of the probe - no significant deposit is observed on the downstream-unheated portion of the probe.

Results for each run are not discussed individually. For cases where the decrease in U was less than 5%, or the fouling rate < 1E-07 m^2K/kJ, fouling is assumed to be below detection limits for the apparatus and procedures used.

5.3 Fouling Resistance versus Time Plots

Figures 5.5, 5.6, and 5.7 show fouling resistance values versus time for three oils tested namely LSB, MDL, and CLK respectively. For LSB, after 48 hours final R_f values were 0.055 to 0.10 m^2K/kW; for Midale, results were lower with values in the range, <0.07 m^2K/kW. For Cold Lake, fouling was more severe, yielding R_f values after 48 hours of 0.07-0.15 m^2/kW. At lower surface temperature, R_f reached 0.064 m^2K/kW. The fouling rates represent the slopes of the R_f versus time plots.

5.4 Fouling Rate versus Surface Temperature for Various Crude Oil Samples

A linear plot of fouling rate versus surface temperature is shown in Figure 5.8. The range of experiments covered is from surface temperatures of 296°C to 384°C. Note that the bulk temperature is also varying in these experiments. Based on the data shown fouling rate at a given surface temperature is highest for Cold Lake, followed by LSB and Midale.

Plotting these same results on a semi-log plot (Figure 5.9) shows of course the same order.

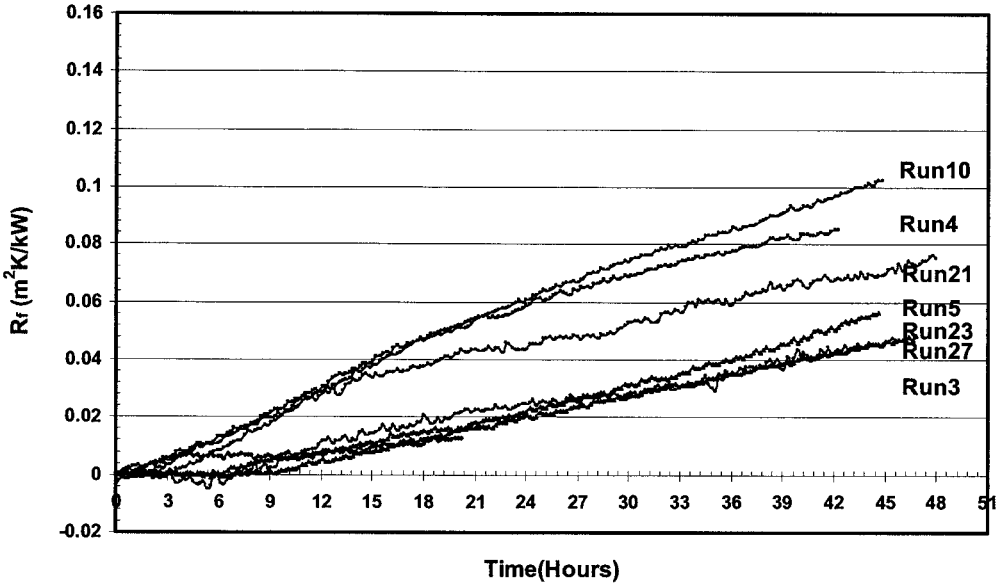

Figure 5.5 Fouling Resistance Vs Time Plot for LSB Crude Oil Runs

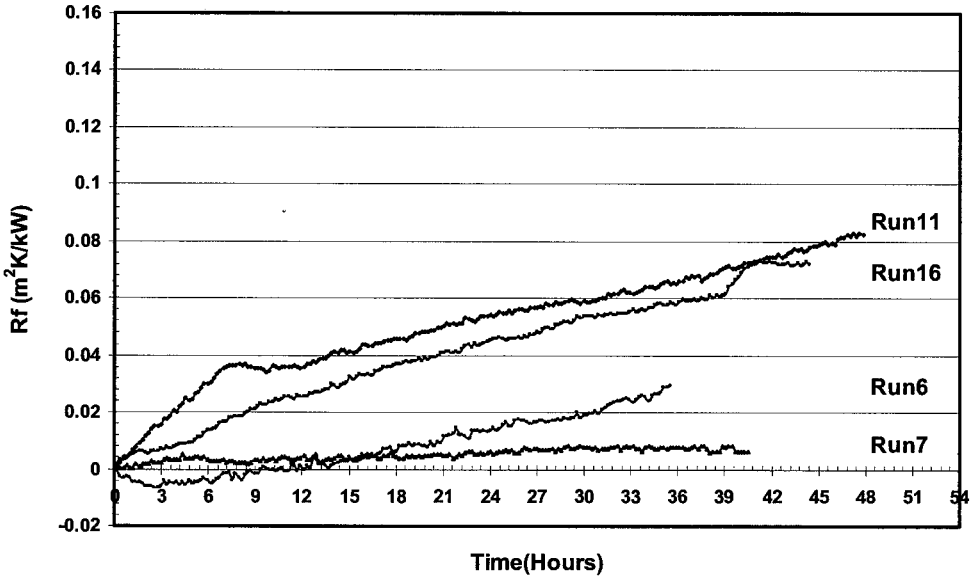

Figure 5.6 Fouling Resistance Vs Time Plot for MDL Crude Oil Runs

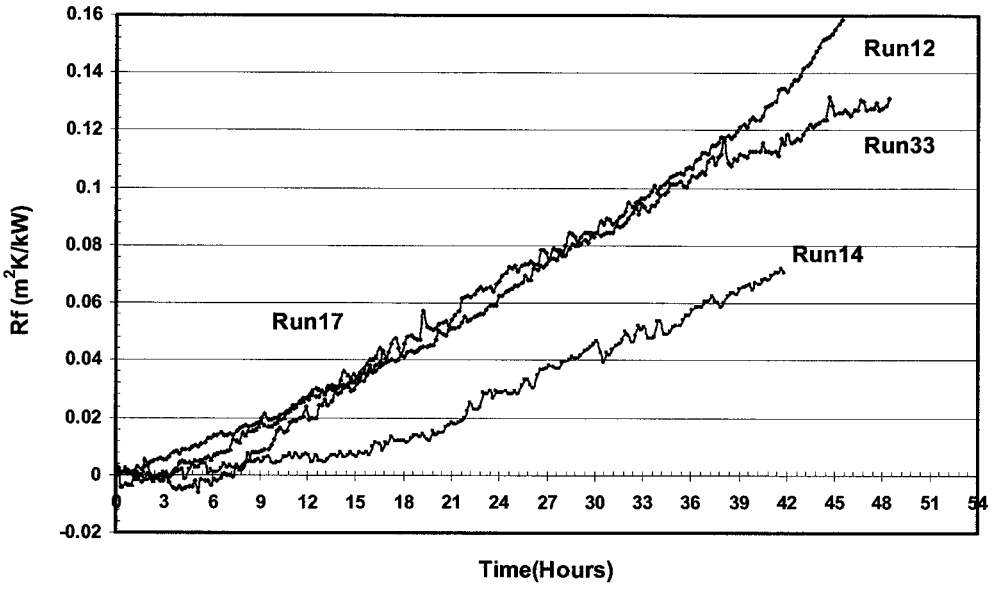

Figure 5.7 Fouling Resistance Vs Time Plot for CLK Crude Oil Runs

5.5 Fouling Rate versus Film Temperature for Various Crude Oil Samples

Figure 5.10 shows a linear plot of fouling rate versus film temperature. Results appear more consistent than when plotting with surface temperature, no doubt in part because the change in both surface and bulk temperatures are reflected in the film temperature values. There seems a clear ordering of the oils at the highest film temperatures (~320°C) in terms of decreasing fouling rates in the ranking **Cold Lake>LSB>Midale**.

Examining the semi-log plot (Figure 5.11), again the clear ranking is evident. Based upon LSB, on an average, the fouling rate increases by a factor of 4.6, with a 70°C increase in the film temperature from 250°C to 320°C. Another way to express this is that the fouling rate doubles for an increase in film temperature of 32°C. To summarize this part of the study, three different oil samples have been characterized for fouling rates over a range of temperatures in a re-circulation loop in which oils were heated for 48-hour periods. The velocity was about 0.75m/s, and film temperatures (average of

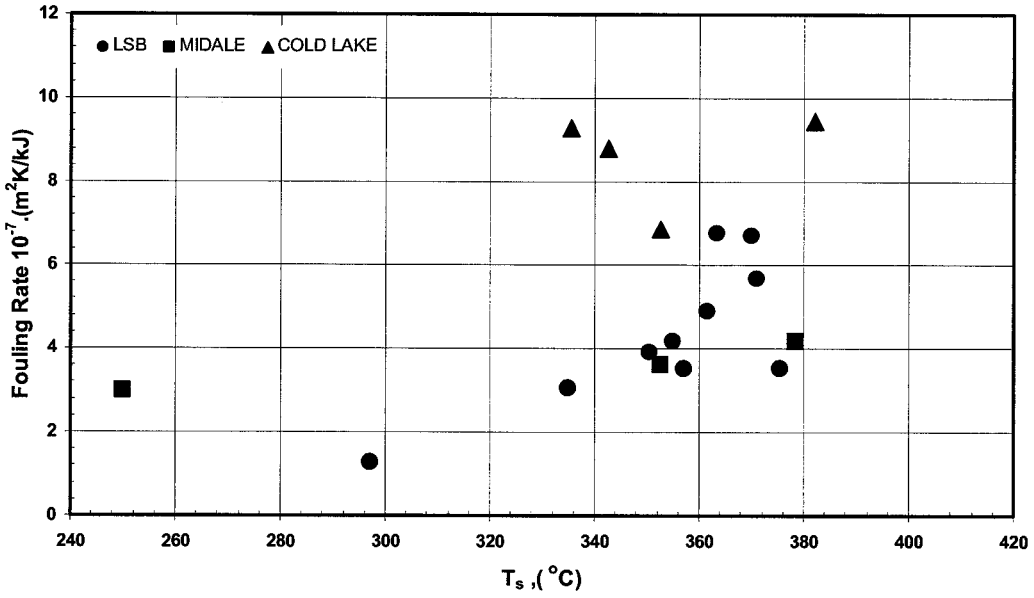

Figure 5.8 **Fouling Rate Vs Surface Temperature for LSB, CLK, and MDL Crudes Oils (Bulk Temperature 146°C to 286°C, Velocity 0.75 m/s)**

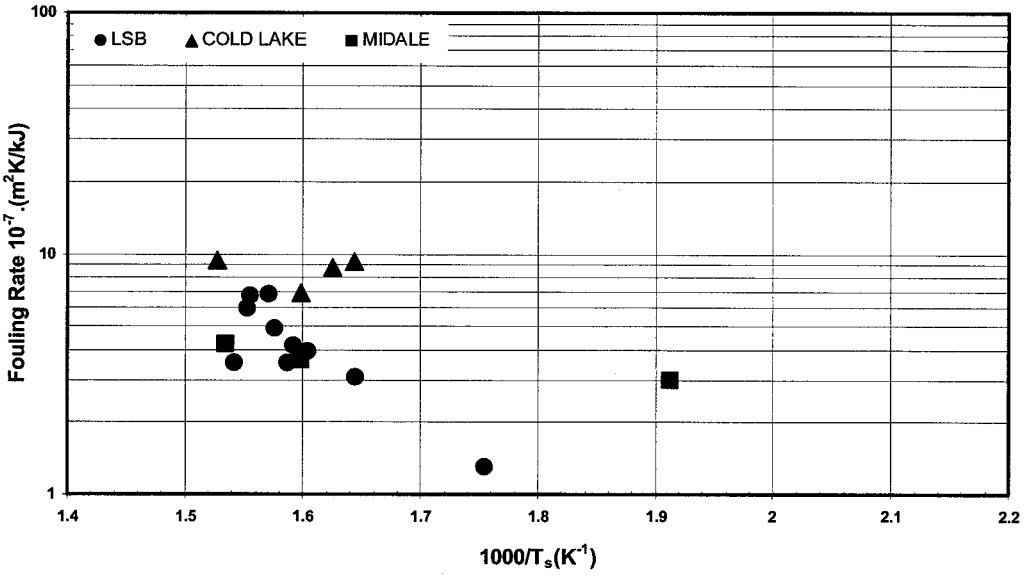

Figure 5.9 **Semi Log Plot of Fouling Rate Vs $1000/T_{surface}$ for LSB, CLK, and MDL Crude Oils**

fluid and surface temperatures) covered the range of about 280 to 330°C. Generally, the heat flux was high, with wall temperatures about 100°C above that of the bulk fluid, and in the range 330 to 380°C.

Over the 48 hour typical run time, the overall heat transfer coefficient decreased by between 5% and 60%, more typically in the range 10-32%. The fouling rate was determined from the slope of the inverse of the overall heat transfer coefficient versus time. Results were most reproducible where larger sample sizes of 4.5 kg of fluid were used. To confirm the ability of the apparatus to run with small samples, a comparision of the effect of feed sample size on fouling rate was made using LSB. Three Runs (7, 15, 18), were carried out with smaller sample sizes of 3.25 kg, 3.5 kg and 2.5 kg respectively. Two different shipments of LSB had been received from Shell Canada Limited. Run 5, which used 4.5 kg of the original LSB shipment was repeated as Run 18, with 2.5 kg of oil from the third shipment. The fouling rate of Run 18, appeared about 3 times higher than that of the original fouling Run 5. To confirm if this was due to the composition of the new shipment, Run 5 was repeated again as Run 19, with the usual sample size of 4.5 kg. The fouling rate of Run 19 was similar to that of Run 5. This suggested that the original and subsequent shipments of LSB were essentially the same as far as the fouling rate was concerned, and that the high fouling rate results of Run 18 were associated with the sample size used in that experiment. For all oils, the fouling rate increased strongly with film and surface temperatures. At any given temperature, the difference in rate between the most severely fouling oil and the least severely fouling oil was no more than a factor of about 4. At the highest surface temperatures (370°C), fouling was greatest for Cold Lake. Cold Lake maintained the highest fouling rate even at lower temperatures of 350°C and below, followed by Light Sour Blend and Midale at the lowest temperature tested.

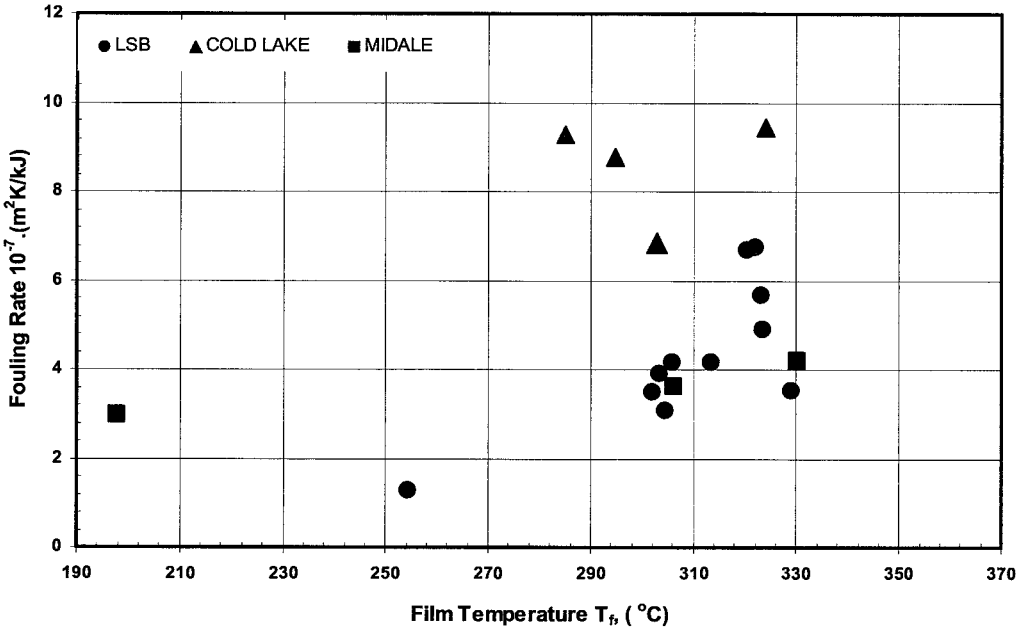

Figure 5.10 Fouling Rate Vs FilmTemperature for LSB, CLK, and MDL Crude Oils

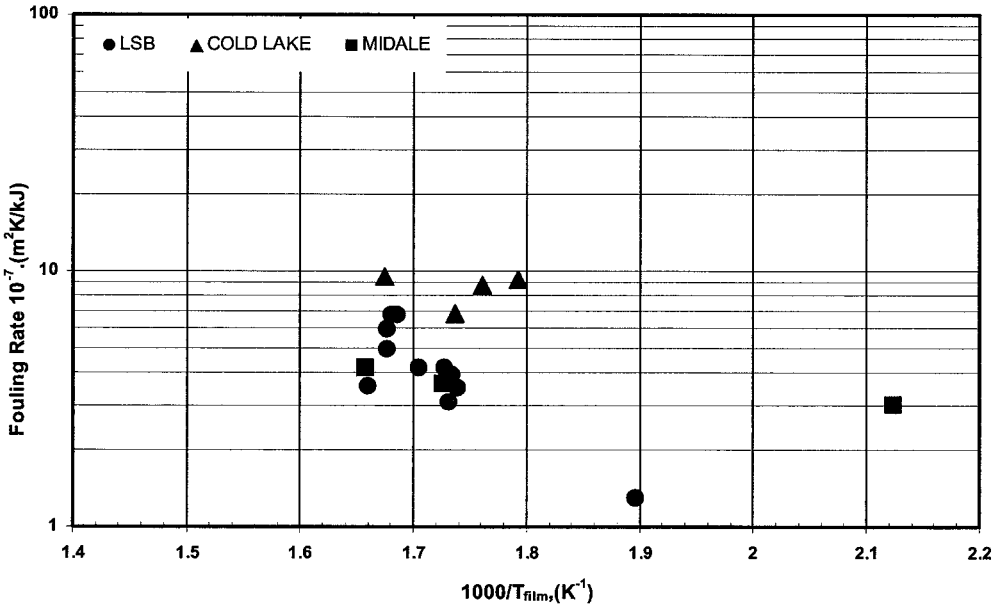

Figure 5.11 Semi Log Plot of Fouling Rate Vs 1000/T_{film} for LSB, CLK, and MDL Crude Oils

5.6 Detailed Study on LSB Crude Oil.

LSB crude oil was selected for a more detailed study of temperature and velocity effects.

5.6.1 Effects of Surface Temperature on Fouling

The scope of this study was limited due to various bottlenecks in the apparatus. The main constraint was the limitation of the heat flux. The HTRI probe is designed for a maximum of 1920 W @ 240 V. It was operated no more than 90% of its rated value as a safety precaution to take into account the power surges in the incoming line, inspite of the power stabilizers and transformer in the secondary circuit.

Considering these constraints the conditions for the surface temperature effects were determined and the runs executed.

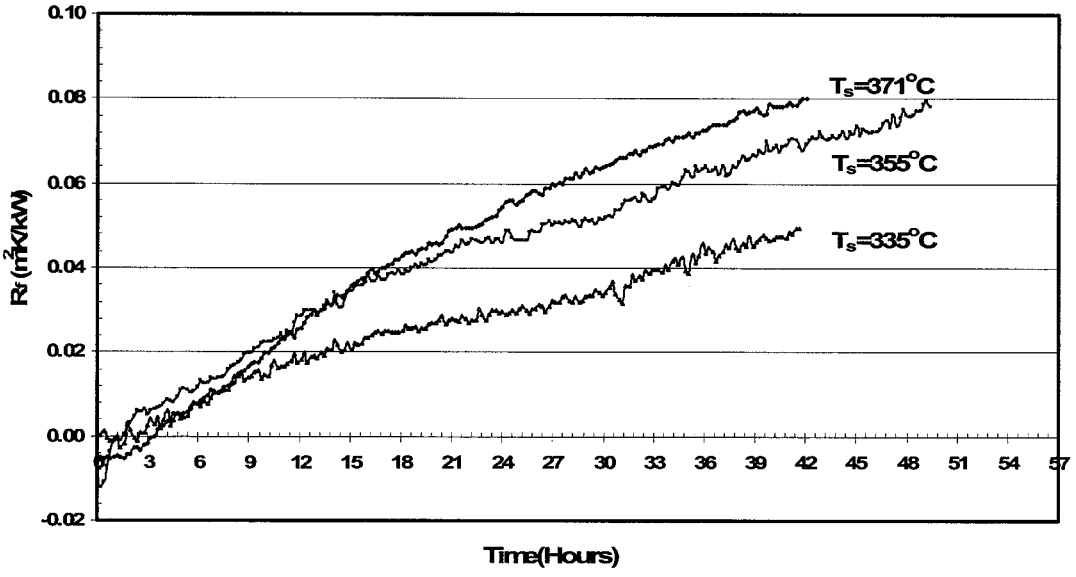

Figure 5.12 Fouling Resistance Vs Time Plot for LSB Crude Oil – Surface Temperature Effects at Constant Bulk Temperature of 275°C

Three runs were carried out at a constant bulk temperature of 275.5°C and initial surface temperatures of 371°C, 355°C and 335°C. Figure 5.12 shows the fouling trend. Table 5.2

summarizes the results for the three runs. Larger induction times were observed for lower surface temperatures. As can been seen higher surface temperatures yielded higher fouling rates comparatively. All the runs were conducted at a constant annular velocity of 0.75 m/s. A global activation energy can be arrived at based on the Arrhenius type equation as below.

Table 5.2 Surface Temperature Effects on LSB Crude Oil Fouling Rate
$T_b \sim 275.5^{\circ}C$, V=0.75 m/s

Run No.	T_s (°C)	T_{film} (°C)	q kW/m^2	U_o kW/m^2K	R_f final (m^2K/kW)	Period (Hours)	Fouling Rate (m^2K/kJ)
4	371.00	323.20	421.00	4.4869	0.0801	4.5-42.0	5.67 E-07
21	355.00	313.50	342.70	4.1969	0.0751	0.6-47.9	4.16 E-07
23	335.00	304.50	251.50	4.1779	0.0471	12.9-51.8	3.06 E-07

5.6.2 Effects of Bulk Temperature on LSB Crude Oil Fouling Rates

Four runs were performed to study the effect of bulk temperatures on the fouling of LSB crudes. Larger induction times are observed with a decrease in bulk temperature. A very minimal increase in the fouling rates can be seen with an increase in bulk temperatures. Table 5.3 summarizes the results for the four runs.

Table 5.3 Bulk Temperature Effects on LSB Crude Oil Fouling
$T_s \sim 360^{\circ}C$, V=0.75 m/s

Run No.	T_b (°C)	T_{film} (°C)	q kW/m^2	U_o kW/m^2K	R_f final (m^2K/kW)	Period (Hours)	Fouling Rate (m^2K/kJ)
27	247.50	302.20	484.40	4.4378	0.0486	12.3-48.2	3.50 E-07
19	256.50	305.80	422.20	4.3000	0.0648	17.3-47.6	4.16 E-07
21	272.00	313.50	342.70	4.1969	0.0751	0.6-47.9	4.16 E-07
32	280.40	321.90	260.80	3.3454	0.0876	12.3-48.2	6.75 E-07

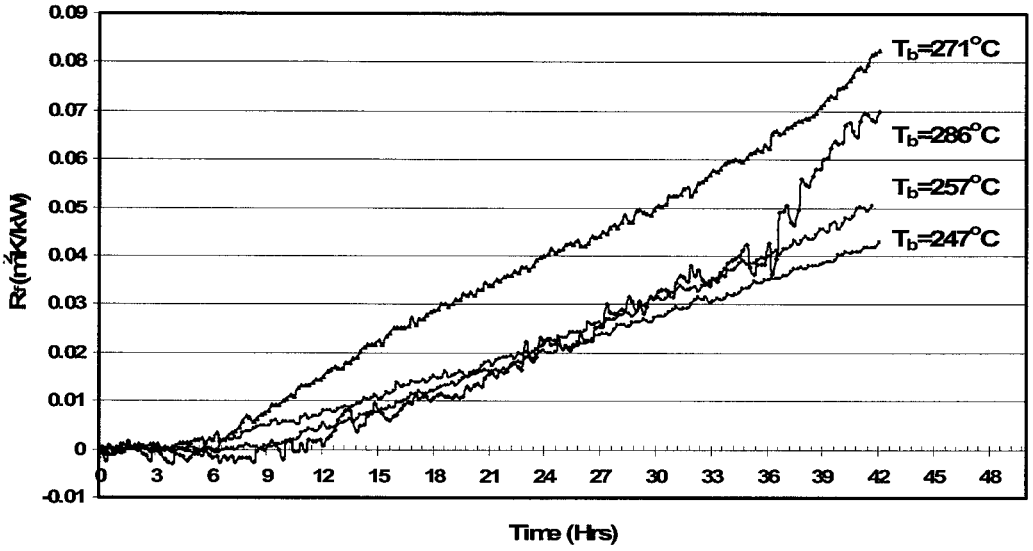

Figure 5.13 Bulk Temperature Effects on LSB Crude Oil Fouling $T_s \sim 360^{\circ}C$, V=0.75 m/s

5.6.3 Determination of Activation Energies on LSB Crude Oil Fouling

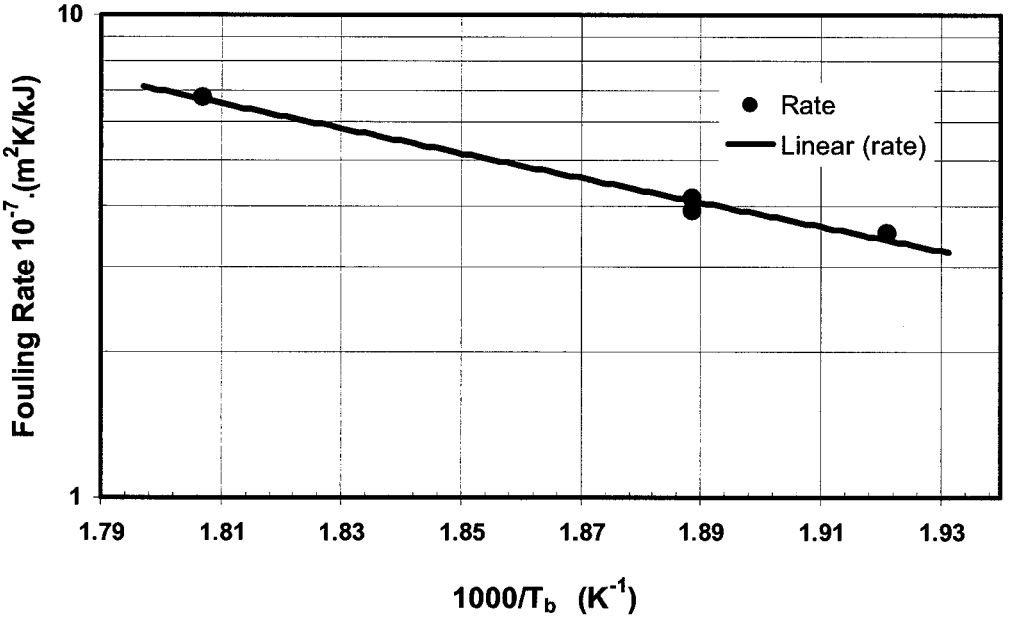

Figure 5.14 Arrhenius Type Plot for LSB Crude Fouling Runs – Constant Initial Surface Temperature and Varying Bulk Temperatures

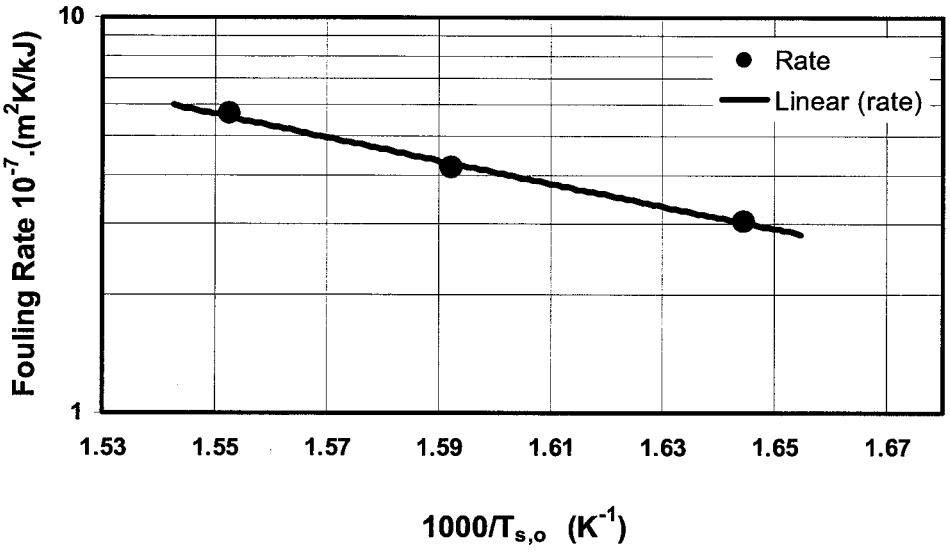

Figure 5.15 Arrhenius Type Plot for LSB Crude Fouling Runs – Constant Bulk Temperature and Varying Initial Surface Temperatures

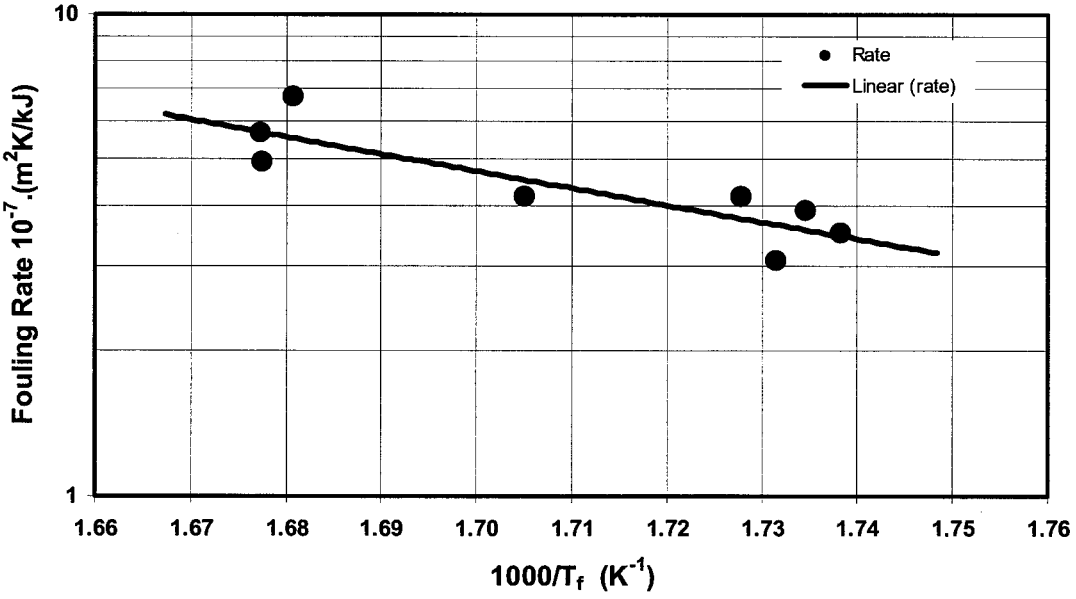

Figure 5.16 Arrhenius Type Plot for LSB Crude Fouling Runs – Based on Conventional Film Temperature $(T_b+T_{s,o})/2$

5.6.4 Re-defining Film Temperature T_{film}, Based on the Characteristics of LSB Crude Oil Fouling.

In the range studied, interactions were observed on the fouling rates of LSB at varying bulk temperatures at almost normal surface temperatures. In the previous work, activation energies have been reported in the fouling studies either based on the surface temperatures or based on the film temperatures. Conventionally film temperatures have been defined as:

$$T_{film} = 0.5\ T_b + 0.5\ T_s \qquad 5.1$$

In the present work, the activation energies based on the varying surface temperatures and varying bulk temperatures seem to fall almost in a very close range. Based on this finding, an attempt was made to re-define a film temperature, which would give an improved fit to the fouling rate data. Accordingly, T_{film} was re-defined as:

$$T_{film,\ modified} = (\alpha\ T_b + (1-\alpha)\ T_s) \qquad 5.2$$

All the data points used for plotting varying surface and varying bulk temperatures have been used for the following plot. On solving a non-linear equation using Matlab and by using a program that does brute force optimization, (Appendix VI) reasonable values were determined for α and $(1-\alpha)$ as shown in Table 5.4.

Table 5.4 Constants for Re-Defining New Film Temperature (T_f')

Constant	Value
α	0.30
$(1-\alpha)$	0.70

This implies the emphasis of a higher magnitude of influence of surface temperature on arriving at the film temperature as against the equal contribution of surface and bulk temperatures as used in previous work. G.T. Polley et al.(2002), in a critique of the

threshold fouling model of Ebert-Panchal, state that the use of film temperature based on some form of linearization is suspect in the use of the Arrhenius –like relationship to

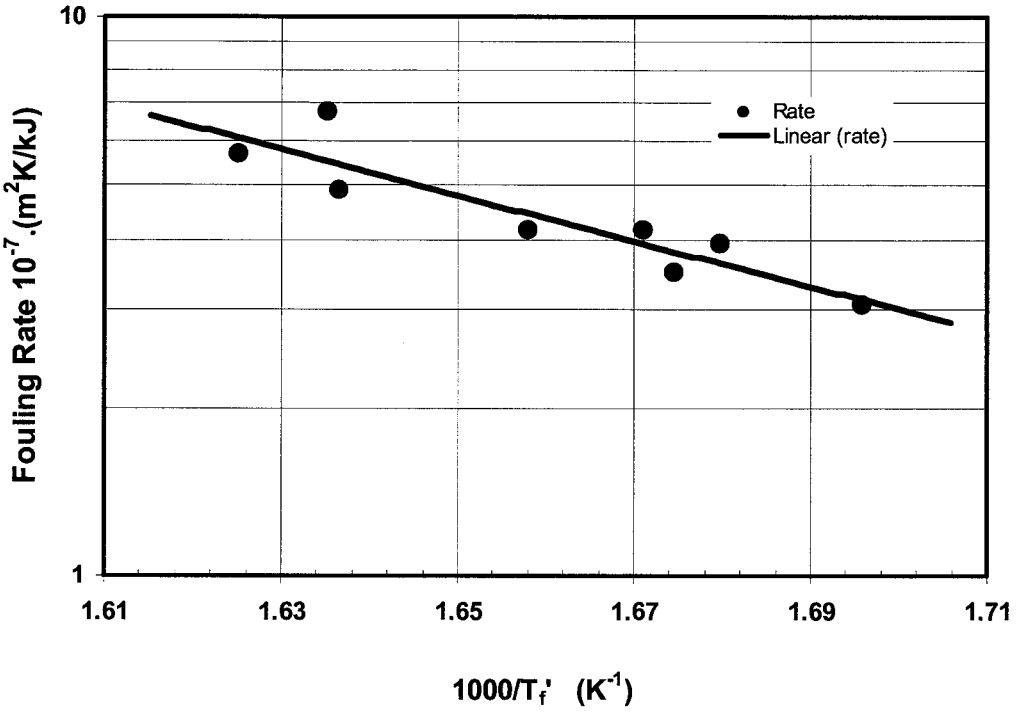

Figure 5.17 Arrhenius Type Plot for LSB Crude Fouling Runs – Based on Modified Film Temperature (T_f')

Table 5.5 Summary of Activation Energies and Pre-exponential Constants for LSB Crude Oil Fouling Runs– Varying Conditions

S.No	Condition*	Corresponding Figure	Activation Energy, kJ/mol	Pre-exponential Constant (A_o) (m^2K/kJ)
1	Constant $T_{s,o}$ and varying T_b	Figure 5.14	48.62	0.028
2	Constant T_b and varying $T_{s,o}$	Figure 5.15	54.20	0.015
3	Varying conventional film temperature $(T_b+ T_{s,o})/2$	Figure 5.16	67.10	0.493
4	Varying new modified film temperature T_f', $(0.3.T_b+ 0.7.T_{s,o})$	Figure 5.17	77.20	2.53

relate the reaction rate and temperature. They suggest that the exponential term be based on the wall temperature instead, which is consistent with the chemical reaction fouling model of Paterson and Fryer (1988). The values for the activation energies and the pre-exponential constant for the LSB Crude Oil Fouling runs based on varying conditions of bulk, surface and film temperatures (conventional and modified) are summarized in Table 5.5. If the conventional film temperature is the realistic approach, then the activation energies obtained for the same crude oil under similar velocity conditions and similar conventional film temperature (either by varying the bulk temperature or the surface temperature) should be similar if not the same. The activation energies (Table 5.5) are varying and the new modified film temperature bridges the gap between the bulk temperature effect and surface temperature effect for the same conventional film temperature. However, the new modified film temperature needs to be validated in future studies for a crude oil with the "threshold fouling" mapped. This finding (Equation 5.2), may be limited to this particular range of study and can be applied to verify on similar ranges of fouling studies for crude oils. Also the activation energy determined applying the new film temperature is fairly close to the values reported in the literature (Chapter II -Table 2.7).

Figure 5.18 Threshold Fouling Loci from EXPRESS^{TM}– Based on Originally Proposed Ebert - Panchal Model*

Figure 5.18 has been removed because of copyright restrictions.
Figure 5.18 shows the Threshold Fouling Loci from EXPRESS^{TM}– Based on Originally Proposed Ebert - Panchal Model*
Figure 5.18 was taken from G.T.Polley et al. (2005).

One of the significant uses of the Ebert-Panchal Model (Chapter 2- Equation (2.3)) is the identification of the velocity at which fouling is suppressed. G.T.Polley et al. (2005) show in Figure 5.18, a range of loci ("fouling thresholds') relating the film temperature at which crude oil fouling is initiated as a function of velocity. Each locus relates to a different value of "activation energy" E, the other parameters being fixed. The sensitivity of the threshold line to the activation energy is very evident. Figure 5.18 is based on the parameters obtained from the reconciliation of monitoring data for different activation energies given in the legend. Uppermost locus, 44 kJ/mol; lowest locus, 35 kJ/mol. Upper hatched region shows fouling region for E= 40 kJ/mol, locus indicated by solid black line. Hatched region on t right shows prohibited region for design, as velocities > 3m/s are not permitted. Circle indicates exchanger design conditions. Also shown on the plot is the point representing the conditions at the exit of the heat exchanger. In this case the unit would not foul if the activation energy is around 42 kJ/mol. With the increasing number of models and software simulations being generated to combat the crude oil fouling, it will be very useful for the researchers and industry experts to work with a common understanding for the definition of film temperature. This could be a suggestion to COFTF (C.A Bennett et al. (2006)), who are working towards a principal endeavor of standardizing crude oil fouling research and making it relevant to the industry.

5.6.5 Effects of Velocity on LSB Crude Oil Fouling Rates

Figure 5.19 shows the plots of the three runs conducted at different annular velocities. As explained before, due to the limitations on the PFRU wattage, the range of the study was constrained to a maximum annular velocity of 0.75 m/s and hence the Reynolds number was in the range 1100-5900. As is evident from the plot and Table 5.6, the change in the fouling rates with velocity was small. But there appears a trend in favor of previous research work (Panchal et al. (1997), Watkinson (2005)). For a 5-fold reduction in the annular bulk velocity an increase of 75% was observed in the fouling rates. The Panchal et al. (1997) study was conducted in the velocity ranges of 0.9 - 3.2 m/s. The Reynolds number in their work was in the range of 8,800 - 119,000. The crude oil bulk

temperature was in the range of 204°C and 363°C, while the surface temperature was in the range of 232°C and 467°C.

Table 5.6 and Figure 5.20 show a decrease in fouling rate with an increase in velocity. The results presented below were for a bulk velocity of 0.75 m/s, 0.35 m/s and 0.15 m/s. Experiments were carried out at these three velocities; initial surface and bulk temperatures were held constant. Fouling rate is seen to vary as velocity to the – 0.35 power. Panchal et al. (1997), report a velocity dependence of –0.66 for the threshold model for flow conditions that were turbulent. The low velocity exponent in the current work is no doubt influenced by the flow regime.

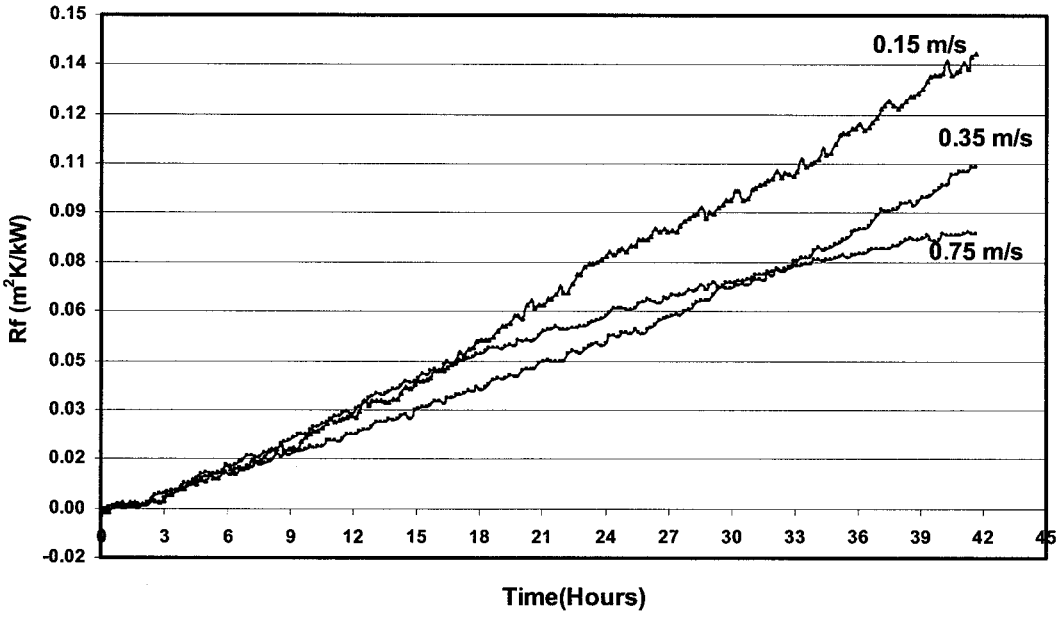

Figure 5.19 Velocity Effects on LSB Crude Oil Fouling Runs

Table 5.6 Velocity Effects on LSB Crude Oil Fouling Rate $T_b \sim 275.5^{\circ}C$, $T_s \sim 375.0^{\circ}C$

Run No.	U (m/s)	T_{film} (°C)	q kW/m²	U_o kW/m²K	$R_{f,final}$ (m²K/kW)	Period (Hours)	Fouling Rate (m²K/kJ)
4	0.75	323.20	421.00	4.4889	0.0801	5.1-46.2	5.67 E-07
29	0.35	325.30	420.62	3.9960	0.1041	0.6-49.2	6.98 E-07
30	0.15	325.70	353.81	3.5877	0.1468	7.5-43.6	9.91 E-07

The relationship between fouling rate and annular velocities can be expressed in terms of power law as:

$$\dot{R}_f = 5.03 * 10^{-7} / V^{0.348} \qquad 5.3$$

(at $T_b \sim 275.5^{\circ}C$ and $T_s \sim 375.0^{\circ}C$)

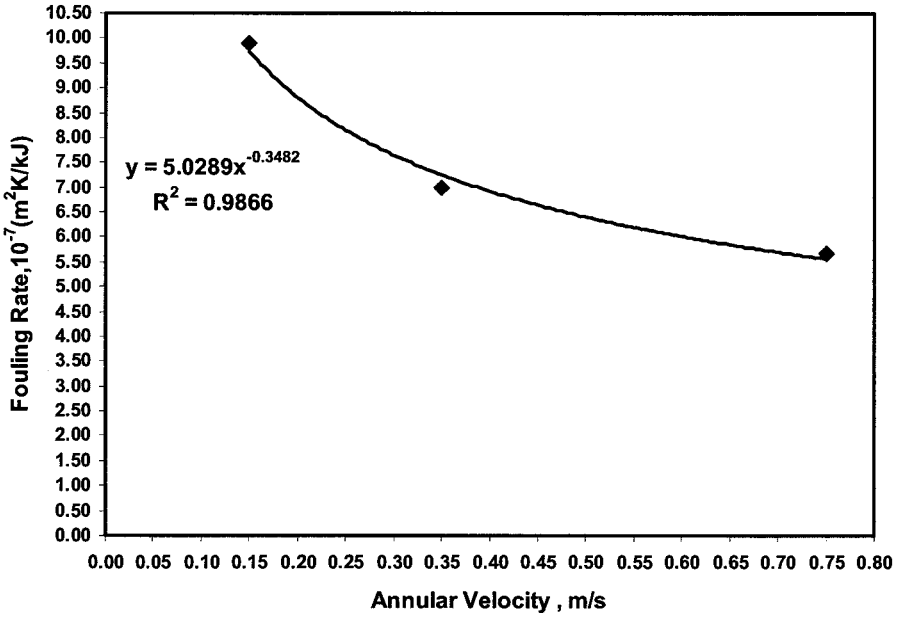

Figure 5.20 Velocity Effects on LSB Crude Oil Fouling Rate $T_b \sim 275.5^{\circ}C$, $T_s \sim 375.0^{\circ}C$

One important observation on the deposit morphology in this study of the effect of velocity was that the deposits were adhered very strongly to the heated test section for runs at lower velocities. Also the deposits were more concentrated at the inlet rather than the outlet of the test sections. The scraped deposit particles from the heated section of PFRU exhibited a very silvery and luminous metallic finish. The ash content measurement of the deposit by TGA analysis (Appendix VII) indicate a higher percentage fixed carbon content (FC) with a reduction in the annular velocity which suggests an increase in the fouling magnitude.

5.6.6 Correlation of Results

Using the form of empirical equation shown below, results for the LSB fouling rate could be fitted as shown in Figure 5.21.

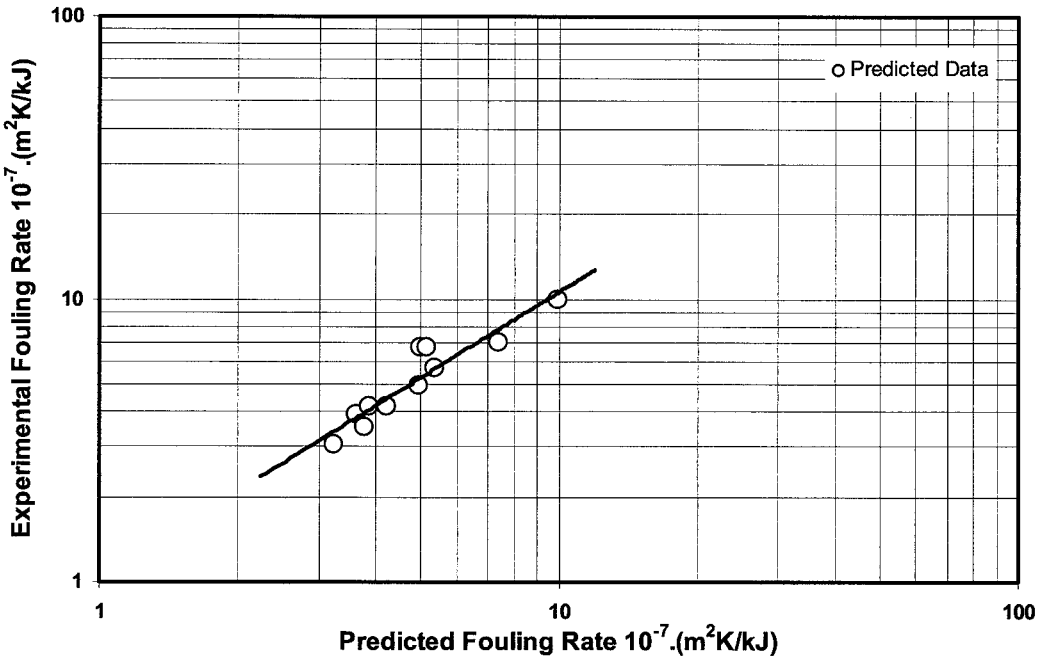

Figure 5.21 Log – Log Plot of Experimental Vs Predicted Fouling Rates for LSB Crude Oil (Based on Equation 5.4)

$$dR_f / dt = a. V^{-0.35}. \exp(- E_f / RT_f^{'}) \quad 5.4$$

The results of this study for LSB oil can be summarized in equation (5.4), which was found to fit the rate data within ± 8 %. The plot as shown in Figure 5.21 incorporates ten runs for LSB crude oil and yielded an activation energy of 59.3 kJ/mol with the constant a = 0.05.

5.6.7 Effects of Contaminants (rust) on LSB Crude Oil Fouling Rates

Samples of crude oils to be tested at U.B.C were received in 5 gallons metallic containers from Shell Canada Limited, Calgary. One of the samples was identified as contaminated with rust. Two runs were executed with the contaminated oil. The first run was normal and no indication of the contamination was observed. However the observation of the fouling trend of the second run indicated abnormality. As could be seen from Figure 5.22 and Table 5.7, there was absolutely no induction time. Also the initial fouling rate was approximately 8 to 9 times the normal fouling rate. This supports results of a previous study (Chapter II – Figure 2.19) on a synthetic oil blend (SSB), where the fouling rates increased by an order of magnitude when iron oxide was added at 250 ppm to simulate the presence of suspended corrosion products.

The presence of iron rust and other contaminants in the present sample exhibited a rapid initiation of the fouling mechanism leading to the absence of induction time, which was present in other similar experimental conditions. During the first 6 hours, the fouling rate accelerated to the highest value of 36.2 E-07 m^2K/kJ and then tapered off to the normal value. If the rate is calculated as an average of the initial high fouling rate and the second phase of normal fouling rate, the rate is of the magnitude of 20.0 E-07 m^2K/kJ. The maximum fouling rate in this study of LSB crude even for runs at highly reduced annular velocities was less than half of this value, which gives a strong suggestion that the increase is due to the presence of iron and or other metallic oxide contaminants.

The deposit morphology indicated a strong adhesion of the deposit to the hot surface. The deposits were of uniform thickness along the test section and adhered strongly. Deposit chemical analysis was also affected, as will be shown in Appendix V.

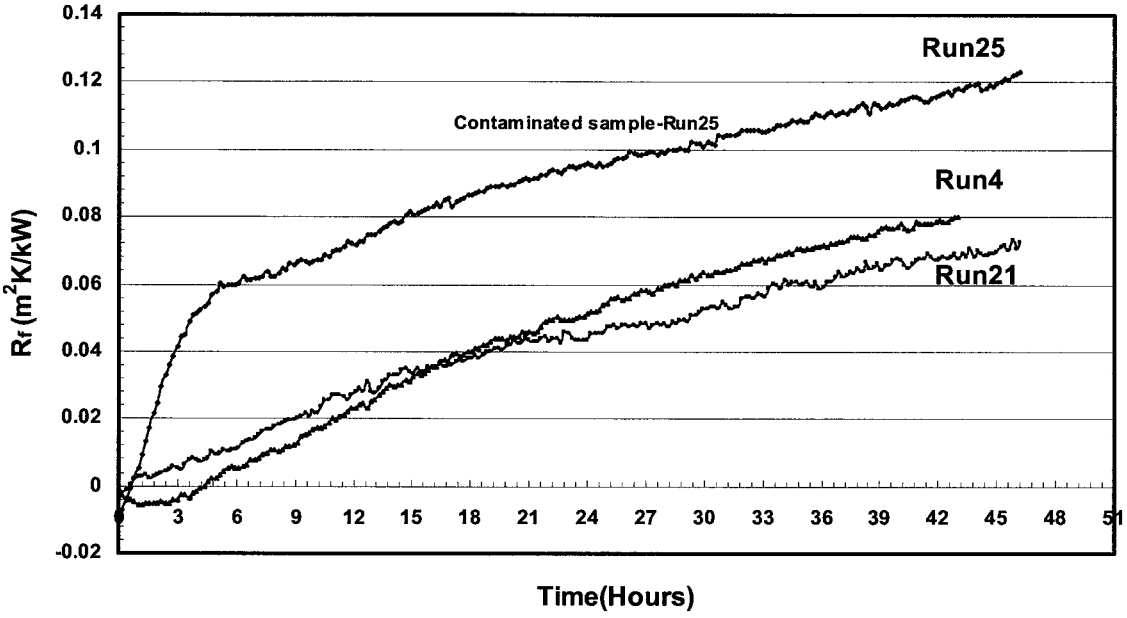

Figure 5.22 Effects of Contaminants on LSB Crude Oil Fouling Rate - Annular Velocity of 0.75m/s.

Table 5.7 Effects of Contaminants on LSB Crude Oil Fouling Rate – Annular Velocity 0.75m/s.

Run No.	T_s (°C)	T_b (°C)	T_{film} (°C)	q kW/m²	U_o kW/m²K	R_{fo} final (m²K/kW)	Period (Hours)	Fouling Rate (m²K/kJ)
4	371.0	275.4	323.20	421.00	4.4889	0.0801	4.5-42.0	5.67 E-07
21	355.0	272.0	313.50	342.70	4.1969	0.0751	0.6-47.9	4.16 E-07
25*	362.5	272.8	304.50	395.78	4.4837	0.0591	0.6-5.3	36.2 E-07
25*						0.1281	10.3-48.0	3.87 E-07

* Contaminated sample (iron rust).

5.6.8 Reproducibility of Fouling Runs - LSB Crude Oil

The reliability of the data generated by the high temperature fouling apparatus was confirmed by carrying out two runs under similar conditions. Subject to the fact that there were minor variations in the sample quality tested (each run was executed with a different sample lot) and test conditions, the results and trends are similar as shown in Figure 5.23 and Table 5.8. The variation of 10% on the absolute values of the fouling rates is slightly higher side than desired and could be reduced to a greater extent by implementing the recommendations for upgrading the fouling apparatus, incorporating the storage/sampling system and relevant procedures, as given in section 6.2. Table 5.9 provides the mean and standard deviation for the LSB runs 5, 19 and 27.

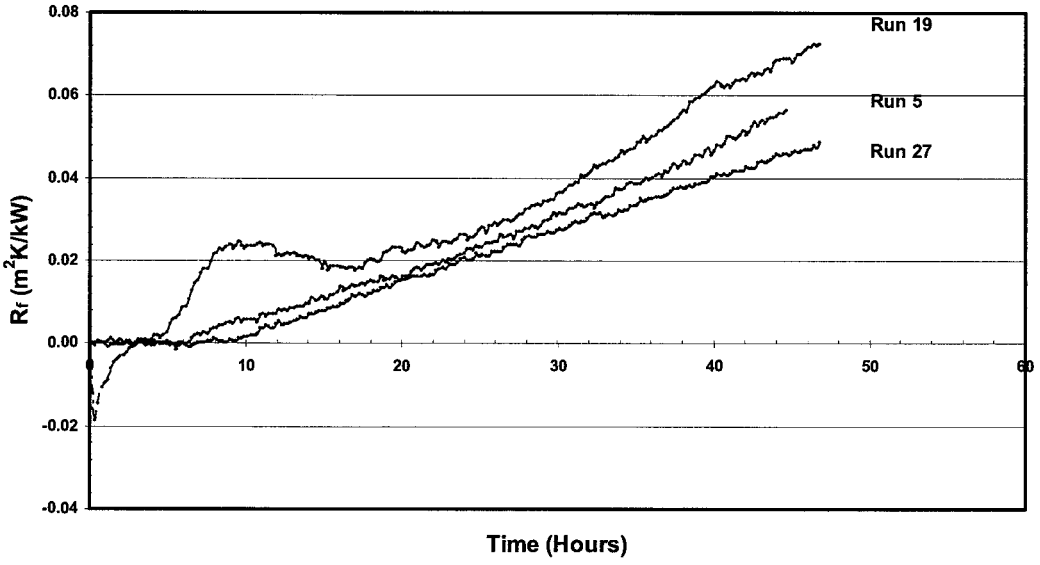

Figure 5.23 Reproducibility of LSB Crude Oil Fouling Runs - Annular Velocity of 0.75m/s.

Table 5.8 Reproducibility of LSB Crude Oil Fouling Runs - Annular Velocity 0.75m/s.

Run No.	T_o (°C)	T_b (°C)	T_f' (°C)	q kW/m^2	U_o kW/m^2K	R_{fo} final (m^2K/kW)	Period (Hours)	Fouling Rate (m^2K/kJ)
5	350.5	256.5	322.3	423.3	4.5619	0.0562	9.7-47.8	3.91 E-07
19	355.0	256.5	325.5	422.2	4.3000	0.0723	17.3-47.6	4.16 E-07
27	357.0	247.5	324.2	484.4	4.4378	0.0486	12.3-48.2	3.50 E-07

Table 5.9 Reproducibility of LSB Crude Oil Fouling Runs - Mean & Standard Deviation (Based on Table 5.8)

Parameters	Mean	Standard Deviation
T_f' (°C)	324	1.58
Fouling Rate $10^{-7}.(m^2K/kJ)$	3.86	0.33

5.6.9 Influence of Fluid Physical Properties on Heat Transfer Coefficient

Due to the severity of the operating conditions, changes in viscosity with time were anticipated. The extent of change would depend on the severity of conditions and system leaks as well. As mentioned earlier, some amount of volatiles escaped from the system through some leaky joints and flanges. This would cause an increase in the viscosity of the fluid over 40-50 hrs of the run-time. This change in the fluid property would create a change in the overall heat transfer coefficient.

In the procedure used for the fouling tests, the oil sample was subjected to volatile loss and possibly thermal degradation during the continuous recirculation for about 50 hours. The resulting change in the physical properties can affect heat transfer. A run was conducted to determine if the properties had changed sufficiently to affect the clean heat transfer coefficient. The spent oil from Run#19 was used, in a short duration test with the probe freshly cleaned. A decrease of ~5 % in the clean heat transfer coefficient was observed in the repeat run. This test indicates that a small portion of the decrease in heat transfer coefficient with time could be attributed to slight changes in fluid properties,

rather than fouling as such. The viscosity measurements and summary of the results are given in Appendix V.

5.7 Compatibility Tests for Crude Oils

The phase behavior of petroleum is complex because of the large mixture of diverse molecules and because petroleum has some properties of a colloidal dispersion and some properties of a solution.

The simplified physical model of petroleum (Wiehe et al.(1999)) has the largest aromatic molecules, the asphaltenes (A) which are actually submicroscopic solids dispersed in the oil by resins(R), the next largest, most aromatic group of molecules. This asphaltene resin dispersion is dissolved into petroleum by small ring aromatics (a) that are solvents but opposed by saturates (s) that are non-solvents. Thus asphaltenes are held in petroleum in a delicate balance, and this balance can be easily upset by adding saturates or by removing resins or aromatics. Assuming the resins and asphaltenes are always associated with each other, the phase behavior is then considered to be based upon solubility and upon the aromatics-saturates balance.

5.7.1 Heithaus Titration

The Heithaus titration test uses a solution of the crude oil or bitumen, or residua sample in an aromatic solvent, which is then titrated with n-heptane until the asphaltenes and resins precipitate. Heithaus referred to the method as "flocculation ratio" and used a microscope for determination of the flocculation point. The method was later developed by Pauli (1996) to a semi-automatic turbidimetric titration test. He also changed the precipitant or titrant from n-heptane to iso-octane to increase the versatility of the method. But in this study n-heptane was used as the titrant.

The principle of the method is to make a solution of crude oil sample in toluene. Three to five samples of test crude are weighed into 30 mL vials with Teflon sealed caps in

Figure 5.24 Schematic Drawing of the Automated Flocculation Titration Apparatus (AFT)

Figure 5.24 has been removed because of copyright restrictions.
Figure 5.24 is the Schematic Drawing of the Automated Flocculation Titration Apparatus (AFT)
Figure 5.24 was taken from Pauli (1996).

amounts of 0.5000 g to 1.2500g ± 0.0005g. Toluene (HPLC-grade) is added to each vial in 3.000 mL ± 0.005 mL aliquots and the vials are capped and the crude oil sample which contains asphaltenes, is allowed to dissolve. The vials are kept at room temperature for 24-36 hours.

The vials containing the crude solutions are loaded into a reaction vessel and maintained at 25°C with a temperature-controlled bath and allowed to attain a steady state temperature (for about 10 minutes). The titrant, either iso-octane or n-heptane (HPLC-grade) which is also maintained at 25°C is introduced into the vial at a known flow rate. The change in the percent transmittance (%T) at an absorbance wavelength of 740 nm is plotted versus time t, during which titrant is added to the reaction vessel. The curves exhibit first an increase, since (% T) increases as a result of dilution with the titrant. At the flocculation onset point, the formation of asphaltene particles causes an immediate decrease in (% T) due to light scattering effects. The time required to reach the maximum (% T) from the onset of titration of a sample is defined as the flocculation time, t_f. The

titrant volume V_T, required to cause the onset of flocculation for each sample is obtained by multiplying the value t_f for each sample by the titrant flow rate.

The Heithaus parameters Pa, Po and P are calculated from the flocculation ratio and concentrations, respectively. The flocculation ratio (FR) and the concentration (C) are calculated as:

$$FR = \frac{Vs}{Vs + VT} \qquad 5.5$$

$$C = \frac{Ws}{Vs + VT} \qquad 5.6$$

where V_S is the volume of the solvent, V_T is the volume of the titrant (n-heptane in this case) required to initiate flocculation and W_A is the weight of the crude sample. The x and y intercept values FR_{max} and $C^{-1}{}_{min}$ extrapolated from the FR Vs C line are used to calculate Heithaus parameters Pa, Po and P:

$$Pa = 1\text{-}FR_{max} \qquad 5.7$$

$$Po = FR_{max}(C^{-1}{}_{min}+1) \qquad 5.8$$

Pa	:	The peptizabilty of asphaltenes
Po	:	The peptizing power of maltenes
P	:	The state of peptization of the crude

The solubility parameter of the mixture of oil (oil), toluene (To), and n-heptane (H) at the flocculation point is the flocculation solubility parameter δ_f, determined with the volumetric mixing rule:

$$\delta_f = \left(\frac{V_T \partial T + V_H \partial H + V_{oil} \partial_{oil}}{V_T + V_H + V_{oil}} \right) \qquad 5.9$$

Since asphaltenes are defined as toluene soluble and n-heptane insoluble, the solubility parameter can be stretched out on a reduced n-heptane-toluene scale as two solubility parameters, the insolubility blending number I_N, and the solubility blending number, S_{BN} , defined as:

$$I_N = 100\frac{(\delta_f - \delta_H)}{(\delta_T - \delta_H)} \qquad 5.10$$

$$S_{BN} = 100\frac{(\delta_{oil} - \delta_H)}{(\delta_T - \delta_H)} \qquad 5.11$$

Where

δ_f = the flocculation solubility parameter

δ_T = the solubility parameter of Toluene

δ_H = the solubility parameter of n-heptane

δ_{oil} = the solubility parameter of the oil

AUTOMATED FLOCCULATION TEST RESULTS

Table 5.10 Table of Compatability Test Results (Using Automated Flocculation Test (AFT))

Crude	C_5 Asphaltenes Shell Method * (wt%)	Pa	Po	P	I_N	S_{BN}	δ_{oil} (Mpa$^{0.5}$)	δ_f (Mpa$^{0.5}$)
MDL	6.44	0.6102	0.8442	2.1655	38.5	75.0	17.53	16.40
LSB	3.13	0.6420	0.6523	1.8219	36.1	64.2	17.19	16.32
CLK	13.2	0.6817	0.7105	2.2324	31.4	64.3	17.19	16.17

Four samples were run for each crude sample. Only three of them were used in the flocculation peak plots.

* Data as supplied by Shell Canada Limited

The solubility parameter (δ_Φ) values for toluene and n-heptane were taken from literature (Z.Yang et al. (1999)).

$\delta_{Toluene} = 18.3\ MPa^{0.5}$

$\delta_{N\text{-}Heptane} = 15.2\ MPa^{0.5}$

If the oil is completely soluble in n-heptane and thus contains no asphaltenes the insolubility number is 0, but if the asphaltene-resin dispersion is barely soluble in toluene the insolubility number is 100. Likewise, an oil that is as poor a solvent as n-heptane has a solubility blending number of 0, and an oil that is as good a solvent as toluene has a solubility blending number 100.

Of the three crude oils tested, Midale (MDL) has a slightly higher insolubility number (I_N) and solubility blending number (S_{BN}) compared to the other two crude oils.

Once the insolubility and the solubility blending numbers of a number of crude oils have been measured, the set of potentially incompatible pairs of crude can be predicted and compared with experimentally blending a number of pairs of crudes in a number of proportions. However, this is beyond the scope of this study and can be extended for future work.

A standard test method for measuring n-heptane induced phase separation of asphaltene containing heavy fuel oils, as separability number is available in ASTM D 7061-04(2004). This test method covers the quantitative measurement of how easily asphaltene containing heavy fuel oils diluted in toluene phase separate upon addition of heptane. This is measured as a separability number (%) by the use of an optical scanning device. This ASTM test method is one of the standard techniques recommended by COFTF (Chapter II - Table 2.4) for asphaltene flocculation propensity.

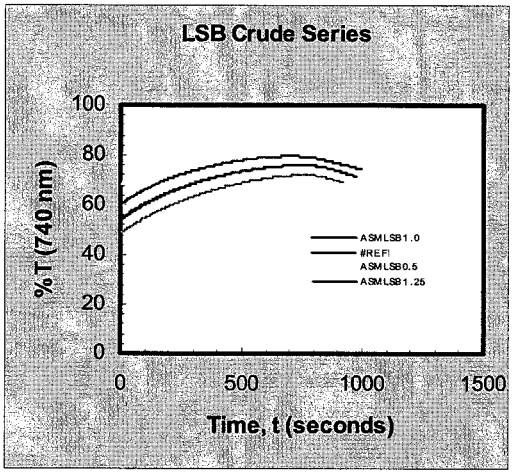

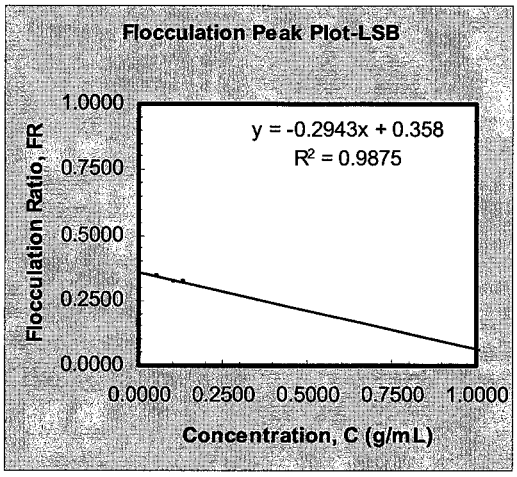

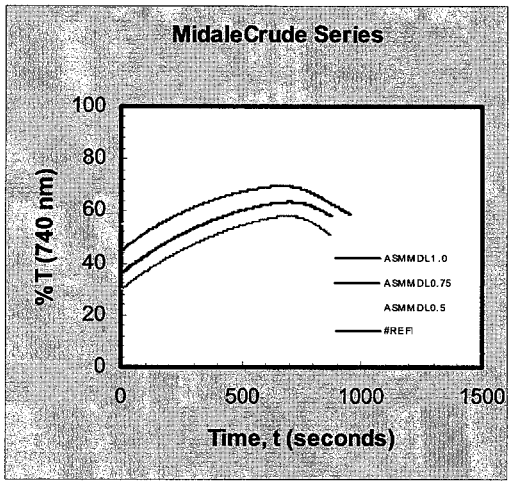

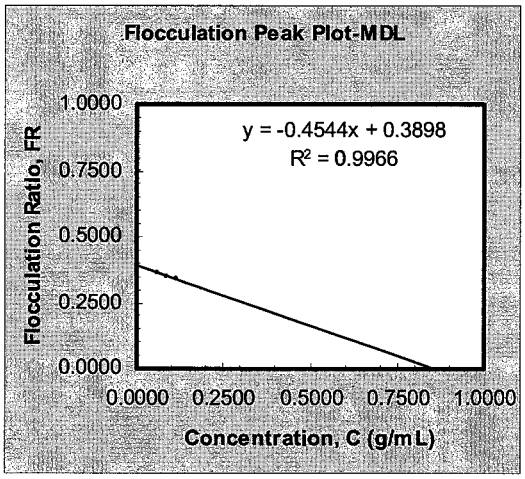

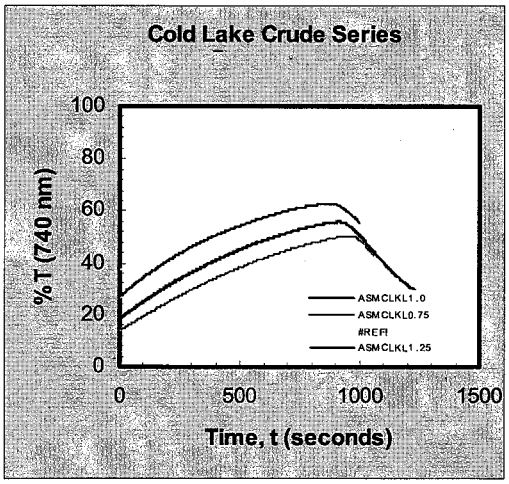

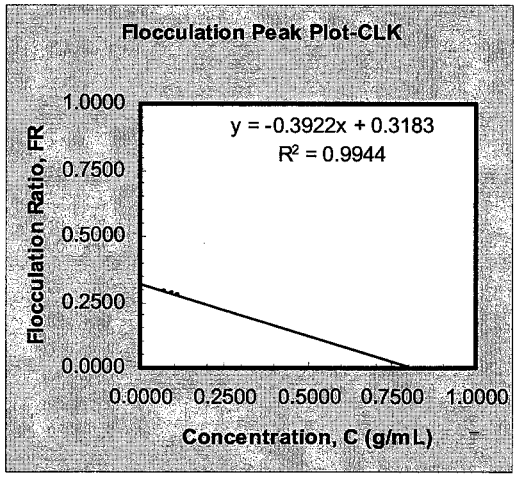

Figure 5.25 (a-f) Flocculation Tests for LSB, MDL, and CLK Crude Oils

5.8 Post Fouling Studies

5.8.1 Deposit Morphology – TGA Studies

The recovered deposit samples were subjected to analysis using the in-house Thermo-Gravimeteric Analyzer and the results tabulated in Appendix V.

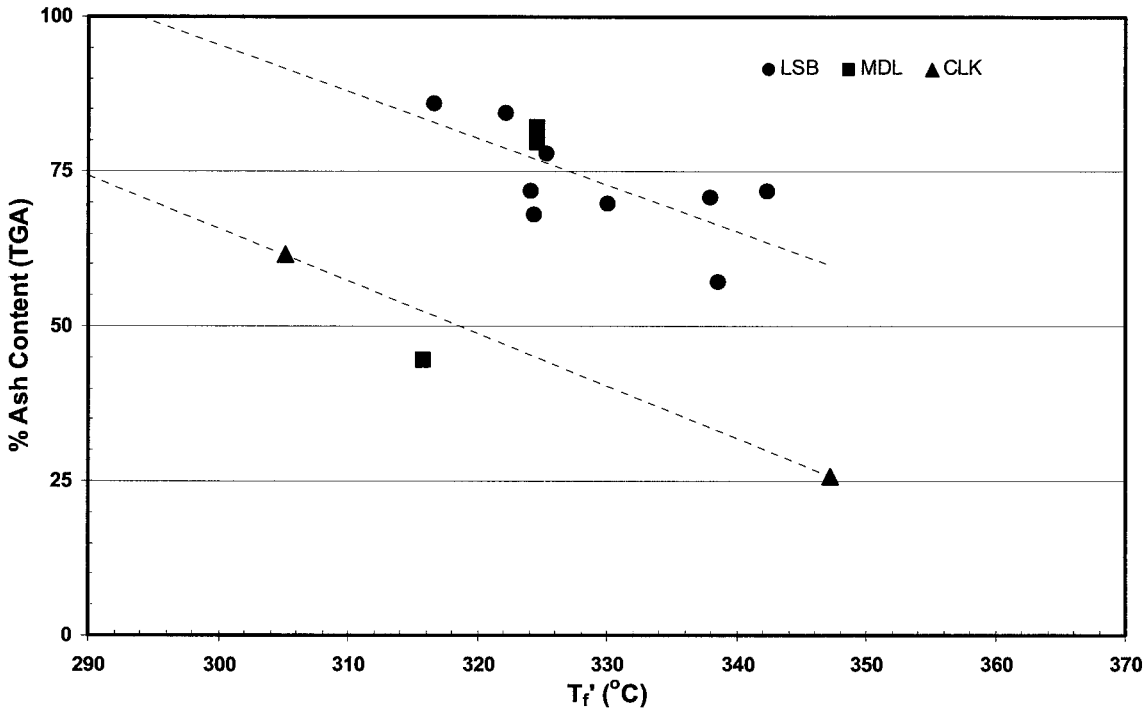

Figure 5.26 TGA Results for LSB, MDL, and CLK Crude Oils

5.8.2 Deposit Morphology – Elemental Analysis

Deposits were analyzed using energy dispersive x-ray, giving point analyses on the deposit surface, and by micro-elemental analysis for bulk content of C, H, S and N. The latter analyses were done at Canadian Microanalytical Service Limited (Delta, B.C). Thermogravimetry was used to determine bulk ash content. Figure 5.26 is a plot of

modified film temperature T_f' and % ash content for the three crude oils namely LSB, MDL and CLK. Results are shown in Table 5.11.

Deposits were very high in inorganic matter, and very high in sulfur content. Sulfur can be present in either organic or inorganic forms, and hence a portion of the sulfur content appears in the ash analysis. For LSB, ash content varied from 58-84%, and averaged 67 %.

The organic portion of the deposit had an average H/C atomic ratio of 0.8. Sulfur content averaged 18.4 %, and appeared from the EDX data to be linked to iron content. On a carbon- free basis, all deposits were about 52-66% Fe, and 25-37% S.

Table 5.11 Analyses of Deposits from the Three Crudes Oils

Oil	% Ash	% C	% H	% N	% S	% Fe* (C-f)	% S* (C-f)	Fe/S* (wt/wt)
LSB	71.6	17.0	1.2	0.34	17.8	56.5	25.3	2.2
LSB	84.3	4.5	0.7	0.30	22.1	N/A	N/A	N/A
LSB	57.2	35.2	1.5	0.53	12.6	66.2	26.0	2.5
MDL	44.4	22.8	1.2	1.80	24.3	58.5	37.3	1.6
MDL	80.9	9.4	0.9	0.30	23.6	65.2	32.1	2.0
CLK	25.7	66.4	3.1	1.32	7.1	51.6	26.1	2.0
CLK	61.5	26.0	2.4	0.31	17.2	58.5	29.3	2.0

* EDX surface analysis; carbon free basis

FeS has a Fe/S mass ratio of 1.745. On average for LSB deposits, Fe/S mass ratios were higher at ratios of 2.2-2.5. For MDL, the two deposits analyzed had ash content of 44 and 80%, with corresponding C contents of 9.4 and 23 %. H/C atomic ratio was 0.9. From EDX measurements, the Fe/S mass ratio is 1.6-1.8. For CLK, deposits ranged from 18-61 % ash, with H/C 0.83, and S content of 6-18 %. Fe/S by EDX was 1.97-2.0.

Deposits from Midale oil have Fe/S ratios consistent with FeS. All other deposits appear iron-rich, with Fe/S ratios greater than that of FeS. A rough correlation of decreasing ash

content in the deposits with increasing film temperature was obtained, indicating the tendency for greater contributions from organic fouling at higher temperatures. Lambourn and Durrieu (1983) reported iron salts of 20-35 % in deposits from medium crudes, and 75-90% for light (°API >40) crudes. Panchal et al. (1999) investigated iron sulfide fouling in gas oils. By adding soluble iron and sulfur as thiophenols at Fe/S ratios of 0.18 to 0.33, their deposits showed Fe/S ratios of 1.8 to 2.2, which are in the range of the current work.

5.8.3 Deposit Morphology – SEM Studies

Scanning Electron Microscopy was done for one deposit sample from each crude oil. The photomicrographs are shown in Figure 5.27, Figure5.28, and Figure 5.29. The SEM looks distinct for three crudes tested. CLK is the heaviest crude of the three and comparatively richer in the metal and sulfur contents. The LSB and MDL deposits resemble a honey comb structure with varying porosity (LSB is more porous) indicating that the deposits are more susceptible nucleate sites for further fouling. Such deposits might be rather weak and tend to get washed off in the bulk if the experiments are carried out under different conditions due to the strength of attachment.

CLK deposits, in spite of their lower ash content, appear to be crystalline in nature and were typically harder deposits compared to the other two. Also they do not exhibit porosity similar to those from the other crude oils tested. One possible explanation for the fracture of CLK deposits, (this was noticed during the examination of the deposits) would be due to the differential thermal expansion of the deposit on the metal surface of the tube and or when the organic compound on the inside of the deposit harden to the extent due to aging of the deposit. The close observation of the deposits on the probe gave an indication that the deposits could be imagined to be formed as layers with the strength of adhesion decreasing from the immediate layer on the metal probe to outermost layer. There was no indication of entrapped crude oil at the very firm layer immediately on the

metal. However in some cases, due to the fracture of the deposit, crude oil was trapped between the reasonably fouled probe and the fractured deposit layers.

5.9 Probable Fouling Mechanism and Discussions

In section 3.1, the properties and characteristics of the three crude oils LSB, MDL, and CLK were reviewed. Based on their total sulfur content, MCR, sediments and salt, metal content, asphaltene content, residue ($565^{o}C^{+}$), the fouling tendency or the fouling potential of the crude oils were ranked as follows: **CLK>MDL>LSB**. This assumption was based on the available crude oil characterization. As mentioned earlier, to characterize the fouling of a given crude oil, one generally requires over nine experiments. Three levels of each of the following variables should be explored: velocity, surface temperature, and bulk or film temperature. In this project, due to experimental set-up limitations, velocity was generally held constant, and 3-5 experiments at different temperatures were done to characterize fouling of each of the crude oils.

For CLK, four fouling runs were carried out at a constant velocity of 0.75 m/s. As given in Table 5.1, the bulk temperatures were in the range of $234^{o}C$ -$266^{o}C$ and the surface temperatures were in the range of $335^{o}C$ -$382^{o}C$. The fouling rates were in the range of 6.84 E-07 m^2K/kJ to 9.44 E-07 m^2K/kJ. CLK was high in asphaltene content and organic sulphur compared to the other two crude oils. Also, CLK had substantially higher viscosity compared to the other two crude oils. Hence for the same velocity of 0.75 m/s, the Reynolds numbers (at film temperatures) for CLK were between 1273 and 1475. The lower Reynolds number for CLK may contribute to its higher fouling rate compared to the other two crude oils as can be seen in Figure 5.11. The viscosity of the spent fluid of post run had a 250-300% change (increase in viscosity) from the initial sample viscosity. Hot filtration results are summarized in Appendix A.3. The hot filtration of the fresh sample for CLK was 4.35 wt% which is possibly due to the asphaltene precipitation. The reduction in the insoluble contents on the post run test fluid for CLK could be due to the increased solubility of asphaltenes at higher bulk temperatures. Also, the spent test fluid

sample from the fouling loop was withdrawn when the fluid temperature was around 65-85°C. As summarized in Appendix V (Table A.5.1 and A.5.2), the deposits for CLK had, ash content ranging 18-61%, H/C of 0.83 and S content of 6-18%. Fe/S by EDX was 1.97-2.0. A rough correlation of decreasing ash content in the CLK deposits with increasing film temperatures is evident from Figure 5.26. This suggests the tendency for greater contributions from organic fouling at higher temperatures. Overall, based on a comparision at the fixed velocity, CLK exhibited the highest fouling rate, amongst the three crude oils tested.

For MDL, four fouling runs were carried out at a constant velocity of 0.75 m/s. As given in Table 5.1, the bulk temperatures were in the range of 146°C -282°C and the surface temperatures were in the range of 250°C -379°C. The fouling rates were in the range of 0.43 E-07 m^2K/kJ to 4.18 E-07 m^2K/kJ. MDL ranked next to CLK in terms of asphaltene content and organic sulphur. MDL ranked next to CLK with respect to viscosity and density. For the same velocity of 0.75 m/s, the Reynolds number (at film temperatures), for MDL were between 2213-3941. The viscosity of the spent fluid of post run had a 200-255% change (increase in viscosity) from the initial sample viscosity. Hot filtration results are summarized in Appendix III. The hot filtration of the fresh sample for MDL was 0.21 wt% with a very marginal increase (0.24-0.36 wt%) in the insoluble contents on the post run test fluid indicating that the gum formation due to autooxidation, or asphaltene precipitation were not occurring in the bulk fluid. As summarized in Appendix V (Table A.5.1 and A.5.2), the deposits for MDL had, ash content of 44% and 80% for the two samples tested with a corresponding C content of 9.4% and 23%. The H/C atomic ratio was 0.9. Fe/S by EDX was 1.6-1.8. The deposits from MDL have Fe/S ratios consistent with FeS. Overall, based on a comparision at the fixed velocity, MDL exhibited the least fouling rate, amongst the three crude oils tested.

LSB was the selected crude oil to carry out a detailed investigation on fouling. Sixteen fouling runs were carried out. Thirteen runs were at a constant velocity of 0.75 m/s. Three runs were at 0.30 m/s, 0.35 m/s and 0.15 m/s As given in Table 5.1, the bulk temperatures were in the range of 134-286°C and the surface temperatures were in the range of 250-

378°C. The fouling rates were in the range of 1.29 E-07 m^2K/kJ to 20 E-07 m^2K/kJ. LSB had the minimum of asphaltene content and organic sulphur. LSB was the lightest crude oil amongst the crude oils tested. For the same velocity of 0.75 m/s, the Reynolds number (at film temperatures), for LSB were between 4750-5800. The viscosity of the spent fluid of post run had a 55-1000% change (increase in viscosity) from the initial sample viscosity, for the samples tested. Hot filtration results are summarized in Appendix III. The hot filtration of the fresh sample for LSB was 0.13 wt% with a very marginal increase (0.14-0.25 wt%) in the insoluble contents on the post run test fluid indicating that the gum formation due to auto-oxidation, or asphaltene precipitation were not occurring in the bulk fluid. As summarized in Appendix V (Table A.5.1 and A.5.2), the deposits for LSB had, ash content varying in the range of 50-84% and averaged 67%. The organic portion of the deposit had an average H/C atomic ratio of 0.8. Sulfur content averaged 18.4% and appeared from the EDX data to be linked to iron content. On average for LSB deposits, Fe/S ratio were 2.2-2.5, which is significantly higher than the Fe/S mass ratio of 1.745 for pure FeS. A rough correlation of decreasing ash content in the LSB deposits with increasing film temperatures is evident from Figure 5.24. This suggests the tendency for greater contributions from organic fouling at higher temperatures. The deposits were rich in mineral matter and in sulfur, indicating the formation of iron sulfide in the deposits. For LSB, fouling increased strongly with bulk temperature (constant surface temperature), yielding a fouling activation energy of 48.6 kJ/mol, which corresponded to a doubling of fouling rate and a 30°C increase in bulk temperature. The fouling activation energy can reflect transport, chemical reactions, and adhesion steps that may contribute to the overall process of fouling. Fouling rates increased sharply with initial surface temperature (constant bulk temperature), doubling over an increase in surface temperature of approximately 40°C, with a fouling activation energy of 54.2 kJ/mol. Also, fouling rate decreased as the velocity was increased to the power -0.35. Overall, based on a comparision at the fixed velocity, LSB ranked second in the fouling potential amongst the three crude oils tested.

The ranking of crude oils in terms of fouling propensity (fouling rates) is **CLK>LSB>MDL**.

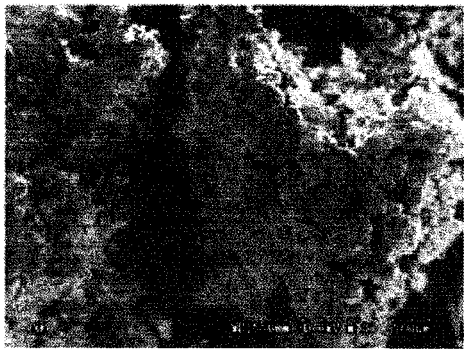

Figure 5.27 SEM Analysis for LSB Crude Oil Deposit - Run 32

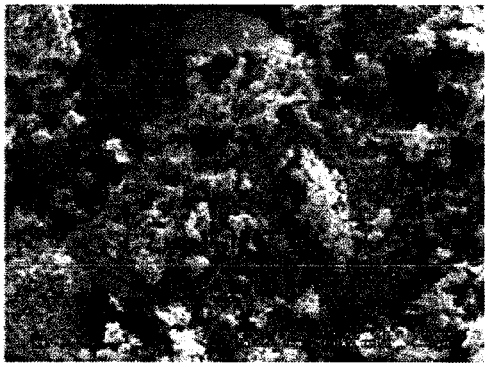

Figure 5.28 SEM Analysis for MDL Crude Oil Deposit - Run 11

Figure 5.29 SEM Analysis for CLK Crude Oil Deposit - Run 17

CONCLUSIONS AND RECOMMENDATIONS

6.1 Conclusions

Three different sour crude oils have been characterized for fouling rates over a range of temperatures in a re-circulation loop in which the oils were heated for 48- hour periods. The velocity was about 0.75 m/s, and film temperatures (average of fluid and surface temperatures) covered the range of about 280 to 330°C. Generally the heat flux was high, with wall temperatures about 100°C above that of the bulk fluid and in the range of 330-390°C. One of the three crude oils, tested in the first phase of study, Light Sour Blend (LSB), was used to investigate the effects of bulk temperatures, surface temperatures, film temperatures, and annular bulk velocity on the fouling rate. The results are highlighted below:

- Over the 48 hour typical run time, the overall heat transfer coefficient decreased by between 5 % and 60%, more typically by 10-32%. Reproducibility of the results was achieved, with a variation close to approximately 10% on the absolute values (for runs 5 and 27) of fouling rates.

- The changes in the physical properties of the fluid due to the severity in temperature and longer re-circulation times in the fouling loop over the entire duration of a fouling run, contributed to approximately 5% decline in the heat transfer. The distribution of this 5% decline over the entire run time cannot be determined. However this result suggests that a small portion of the decrease in heat transfer coefficient is associated with the physical property changes related to vapor loss from the system and thermal degradation of the oil.

- For all the crudes, the fouling rate increased strongly with the film and surface temperature. At any given temperatures fouling rates of all the crude oils were well within an order of magnitude; the difference between the highest fouling rate and the

lowest fouling rate was less than a factor of four. Cold Lake maintained the highest fouling rate over the range of temperatures.

- Three runs were conducted at a constant bulk temperature and constant annular bulk velocity to investigate the influence of surface temperature on fouling rate. A fouling activation energy of 54.2 kJ/mol was determined. The fouling rate increased with an increase in the surface temperature. The probe deposits from the runs at higher surface temperatures were much firmer, harder and more uniformly distributed than the deposits from the runs at lower surface temperatures.

- Four runs were conducted at constant surface temperatures to study the influence of bulk temperatures on the fouling rate. Fouling rate increased with bulk temperature, yielding a fouling activation energy of 48.6 kJ/mol. This indicates that there is no or little difference between the activation energies of bulk and surface temperature effects. The conditions for the runs performed for the surface temperature effect and bulk temperature effects were set in such a way that the film temperatures $(T_{s,o}+T_b)/2$ were similar for the set of runs in both the cases mentioned above. The probe deposits from the runs were generally very loose rather than firm but evenly distributed. They exhibited a multi-layer soft deposit. The innermost layer was very hard and sometimes had very light oil entrapped in the deposit.

- The average Reynolds number was in the range of 1500-7500. Based on the experimental findings a new $T_{film,}$ modified is defined as follows:

$$T_f^{'} = (\alpha\, T_b + (1-\alpha)\, T_s)$$

Instead of the simple averaging of T_b and T_s, more weight is added to the surface temperature. The linear regression was done for the Arrhenius type plot for all the runs which yielded the more appropriate activation energy of 77 kJ/mol. The value of the constants α and $(1-\alpha)$ are 0.30 and 0.70 respectively.

- The hot filtration studies indicate that there is no or minimal increase in the filterable solids in the bulk. This indicates two things: (1). The deposit formation occurs totally on the hot surface of the probe. (2). Even in case the foulants are formed in the bulk, the entire foulants adhere to the hot surface and do not remain in the bulk fluid.

- One experiment (Run 25) was conducted with a sample contaminated with an undetermined amount of iron –rust (from the container). It appears that the presence of iron- rusts (iron oxides) accelerated the chemical reaction fouling in a manner similar to particulate fouling. This is evident from the absence of induction time and a higher initial fouling rate to the order of nine times the actual rate (even though the overall rate was almost the same as in the case of the normal sample).

- Increases in bulk velocity decreased the fouling rates. The absence of induction time and higher fouling rates at lower bulk annular velocities indicate that the fouling mechanism is chemical reaction based (laminar sub-layer). This is in agreement with the findings of other researchers in this field of study.

The results of this study for LSB crude oil can be summarized in the equation below which was found to fit the experimental fouling rate data from eleven runs for the LSB crude oil, within ± 8 %. An Arrhenius type plot yielded an activation energy of 77.2 kJ/mol and the constant a = 0.05.

$dR_f / dt = a. V^{-0.35}. \exp(- E_f / RT_f^{'})$ where $T_f^{'}$ is the modified film temperature

- The probe deposits were very hard and more concentrated at the entrance of the heated section of the probe at lower bulk annular velocities. Also the TGA gave higher fixed carbon content (FC) and lower ash content at lower bulk annular velocities. In general the deposits were rich in mineral matter and in sulphur, indicating the formation of iron sulphide in the deposits. As the film temperature was raised, the organic fraction of the deposits increased. The implication with respect to the impact of these crude oils in the refining units would be that, the processing of LSB and MDL crude oils can have

longer run lengths between maintenance schedules for heat exchanger cleaning, compared to processing CLK crude oil. Also the efforts and methods involved in cleaning the exchangers while processing CLK crude oil could potentially be slightly more expensive and elaborate compared to the other two crude oils namely LSB and MDL crude oils. However, the correlation of laboratory data to the industry is complex and needs to be evaluated closely.

- Compatibility tests were carried out in house using the Automated Flocculation Titrimeter (AFT) for LSB, MDL and CLK. The ranking based on the insolubility number (I_N) and solubility blending number (S_{BN}) is MDL>LSB>CLK. The solubility blending number is typically the same for LSB and CLK. Of the three crudes, MDL is the most compatible crude, followed by LSB and CLK.

6.2 Recommendations

The present study was limited to the fouling behavior of just three crudes. This could be extended to some other crude oils and synthetic crudes as well.

- The system limitations (Chapter III) have to be eliminated in order to extend the study to higher and wider ranges of film and surface temperatures. The main things that require de-bottlenecking are:

1. Higher power on the HTRI probe – to the order of 10 kW.
2. High capacity, balanced -dual mechanical seal fitted, high suction/discharge pressure rated centrifugal pump with API plans for seal flushing and cooling.
3. Reliable controls for regulating the system pressure connected to data acquisition

- The validation of film temperature definition to be confirmed with more sets of runs at wider range of bulk and surface temperatures.

- The effect of iron-oxide on crude fouling at higher film temperature would be an interesting study for major furnace related fouling issues in refineries and upgraders.

- A very reliable power system is required. The incoming line has great power surges. This causes lot of noise in the data acquired. This could be eliminated by regulating the incoming power through a high rated automatic voltage transformer (60 kVA) cum stabilizer with provision of taking 60V, 115 V and 240 V outlets.

- The power drawn by the motor should be measured and logged. This can be useful in confirming the flow variations, if any, or trouble shooting maintenance issues for the pump and motor.

- The flow metering setup should be relocated to a horizontal position rather than the vertical position, as per good engineering practice.

- The PFRU design can be modified to accommodate a detachable sleeve (similar to the corrosion coupons used in cooling water studies) to the heated section. This would allow us to determine the exact weight of the deposit adhering to the probe.

- A sampling system needs to be built. Oil samples are received at U.B.C in metallic containers or drums ranging from 5-45 gallons. The samples are not a representative homogeneous sample of a particular sample date to be back traced in order to confirm certain specifications with the industry supplying the samples. This is of great importance in case of spectacular findings from the pilot studies conducted. A 250 litre metallic tank with a nitrogen blanketing, provided with a circulation pump, could be the ultimate solution to this problem and will support the ongoing research in the case of crude oils and/ or any other hydrocarbons.

- A final visual inspection of the fouling unit at the end of a fouling study may be important to assess the integrity of the components in the unit and at the same time see if there are any signs of corrosion or erosion in the feed tank and associated piping/tubing.

This will be helpful during reporting the findings and at the same time stand as a means of confirmation for the cleanliness of the fouling unit prior to starting another fouling study.

REFERENCES

Asomaning, S., "*Heat Exchanger Fouling by Asphaltenes*", Ph.D Thesis, The University of British Columbia, 1997.

Asomaning, S., and Watkinson, A.P., "*Petroleum Stability and Heteroatom Species Effects in Fouling of Heat Exchangers by Asphaltenes*", Heat Transfer Engineering, vol.21, no.3, pp. 10-16, 2000.

Asomaning, S., Panchal, C.B., and Liao, C.F., "*Correlating Field and Laboratory Data for Crude Oil Fouling*", Heat Transfer Engineering, vol.21, no.3, pp. 17-23, 2000.

Beg, S.A., Amin, M.B., and Hussain, I., "*Generalized Kinematic Viscosity-Temperature Correlation for Undefined Petroleum Fractions*". The Chemical Engineering Journal, vol.38, pp.123-136, 1988.

Bennett, C.A., Appleyard, S., Gough, M., Hohmann, R.P., Joshi, H.M., King, D.C., Lam, T.Y., Rudy, T.M., Stomierowski, S.E., "*Industry- Recommended Procedures for Experimental Crude Oil Preheat Fouling Research*", Heat Transfer Engineering, vol.27, no.9, pp. 28-35, 2006.

Bennison, T., "*Prediction of Heavy Oil Viscosity*", IBC Heavy Oil Field Development Conference, London, December 1998.

Crittenden, B.D., Hout, S.A., and Alderman, N.J., "*Model Experiments of Chemical Reaction Fouling*",vol.65, pp.165-170, March 1987.

Crittenden, B.D., Kolaczkowski, S.T., and Downey, I.L., "*Fouling of Crude Oil Preheat Exchangers*", Trans IChemE, Part A, vol.70, pp.547-557, 1992.

Crittenden, B.D., Kolaczkowski, S.T., and Hout, S.A., "*Modelling Hydrocarbon Fouling*", IChemE, Chemical Engineering Research and Design,vol.65, pp.171-179, March 1987.

Crittenden, B.D., Kolaczkowski, S.T., and Takemoto, T., "*Use of In-Tube Inserts to Reduce Fouling from Crude Oils*", AIChE, Symp. Ser., vol.89(295), pp.300-307, 1993.

Dickakian, G., and Seay, S., "*Asphaltene Precipitation Primary Crude Exchanger Fouling Mechanism*", Oil and Gas Journal, vol.86, pp.47-50, 1988.

Eaton, P., and Lux, R., "*Laboratory Fouling Test Apparatus for Hydrocarbon Feedstocks*", ASME HTD, vol.35, pp.33-42, 1984.

Ebert, W.A., and Panchal, C.B., "*Analysis of Exxon Crude Oil Slip-Stream Coking Data*" in Fouling Mitigation of Industrial Heat-Exchange Equipment, Panchal, Bott, Sommerscales and Toyama (eds.), Begell House, New York, pp.451-460, 1997.

Epstein, N., "*A model of the Initial Chemical Reaction Fouling Rate for Flow Within a Heated Tube and its Verification*", Proceedings, Tenth International Heat Transfer Conference, IChemE., Brighton, UK, Vol.4, pp.225-229, 1994.

Epstein, N., "*Thinking about Heat Transfer Fouling: A 5X5 Matrix*", Heat Transfer Engineering, vol.4, pp.43-56, 1983.

Fetissoff, P.E., Watkinson, A.P., and Epstein, N., "*Comparison of Two Heat Transfer Fouling Probes*", Proc. 7th International Heat Transfer Conference, vol.6, pp.391-396, 1982.

Gentzis, T., Parker, R.J., and McFarlane, R.A., "*Microscopy of Fouling Deposits in Bitumen Furnaces*", Fuel 79, pp.1173-1184, 2000.

Hays, G.F., Beardwood, E.S., and Colby, S.J., "*Enhanced Heat Exchanger Tubes: Their Fouling Tendency and Potential Cleanup*", ECI Symposium Series, Volume RP2: Proceedings of 6th International Conference on Heat Exchanger Fouling and Cleaning – Challenges and Opportunities, Germany, June 2005.

Juliet McClatchey Allan, and Amyn, S.Teja, "*Correlation and Prediction of the Viscosity of Defined and Undefined Hydrocarbon Liquids*", The Canadian Journal of Chemical Engineering, vol.69, August 1991.

Klaren, D.G., De Boer, E.F., Sullivan, D.W., "*Zero Fouling Self-Cleaning Heat Exchanger*", Heat Transfer Engineering, vol.28, no.3, pp. 216-221, 2007.

Knudsen, J.G., Lin, D., and Ebert, W.A., "*The Determination of a Threshold Fouling Curve for Crude Oil*", in Understanding Heat Exchanger Fouling and Its Mitigation, ed. T.R.Bott, pp.265-272, Begell House, New York, 1999.

Lambourn, G.A., and Durrieu, M., "*Fouling in Crude Preheat Trains*", in Heat Exchangers – Theory and Practice, eds. Taborek, Hewitt, and Afgan, pp.841-850, Hemisphere Publishing Company, New York, 1983.

Liporace, F.S., and Sergio Gregorio De Oliveira, "*Real Time Fouling Diagnosis and Heat Exchanger Performance*", Heat Transfer Engineering, vol.28, no.3, pp. 193-201, 2007

Navaneetha Sundaram, B., "*The effects of Oxygen on Synthetic Crude Oil Fouling*", M.A.Sc. Thesis, The University of British Columbia, 1998.

Nesta, J., and Bennett, C.A., "*Fouling Mitigation by Design*", ECI Symposium Series, Volume RP2: Proceedings of 6th International Conference on Heat Exchanger Fouling and Cleaning – Challenges and Opportunities, Germany, June 2005.

Panchal, C.B., and EHR-Ping Huangfu, "*Effects of Mitigating Fouling on the Energy Efficiency of Crude-Oil Distillation*", Heat Transfer Engineering, vol.21, no.3, pp. 3-9, 2000.

Panchal, C.B., and Watkinson, A.P., "*Chemical Reaction Fouling Model for Single-Phase Heat Transfer*", AIChE Symp.Ser., vol.89, pp.323-334, 1993.

Panchal, C.B., Halpern, Y., Kuru, W.C., and Miller, G., "*Mechanisms of Iron Sulfide Formation*", in Refinery Processes, in Understanding Heat Exchanger Fouling and Its Mitigation, ed. T.R.Bott, pp.291-298, Begell House, New York, 1999.

Panchal, C.B., Kuru, W.C., Lia, C.F., Ebert, W.A., and Palen, J., "*Threshold Condition for Crude Oil Fouling*", in Understanding Heat Exchanger Fouling and Its Mitigation, ed. T.R.Bott, pp.273-282, Begell House, New York, 1999.

Parker, R.J., and McFarlane R.A., "*Mitigation of Fouling in Bitumen Furnaces by Pigging*", Energy and Fuels, vol.14, pp.11-13, 2000.

Paterson, W.R., and Fryer, P.J., "*A Reaction Engineering Approach to the Analysis of Fouling*", Chemical Engineering Science, vol.43, no.7, pp. 1714-1717, 1988.

Pauli, A., "*Asphalt Compatibility Testing Using the Automated Heithaus Titration*" Test Preprints, Div. Fuel Chem., Am. Chem. Soc. Vol.41, no.4, pp.1276-1281, 1996.

Petrosky, G.E., and Farshad, F.F., "*Viscosity Correlations for Gulf of Mexico Crude Oils*", SPE 29468, Production Operations Symposium, Oklahama City, Oklahama, April 1995.

Polley, G.T., Wilson, D.I., Pugh, S.J., Petitjean, E., "*Extraction of Crude Oil Fouling Parameters from Plant Exchanger Monitoring*", ECI Symposium Series, Volume RP2: Proceedings of 6th International Conference on Heat Exchanger Fouling and Cleaning – Challenges and Opportunities, Germany, June 2005.

Polley, G.T., Wilson, D.I., Yeap, B.L., and Pugh, S.J., "*Evaluation of Laboratory Crude Oil Threshold Fouling Data for Application to Refinery Pre-Heat Trains*", Applied Thermal Engineering, vol.22, pp.777-788, 2002.

Polley, G.T., Wilson, D.I., Yeap, B.L., and Pugh, S.J., "*Use of Crude Oil Fouling Threshold Data in Heat Exchanger Design*", Applied Thermal Engineering, vol.22, pp.763-776, 2002.

Puttagunta, V.R., Miadonye, A., and Singh, B., "*Viscosity-Temperature Correlation for Prediction of Kinematic Viscosity of Conventional Petroleum Liquid*", Trans IChemE, Part A, vol.70, pp.627-631, 1992.

Rodriguez, C., and Smith, R., "*Optimization of Operating Conditions for Mitigating Fouling in Heat Exchanger Networks*", Trans IChemE, Part A, Chemical Engineering Research and Design,vol.85(A6), pp.839-851, 2007.

Saleh, Z.S., and Sheikholeslami, R., "*Fouling Characteristics of a Light Australian Crude Oil*", Heat Transfer Engineering, vol.26, no.1, pp.15-22, 2005.

Saleh, Z.S., Sheikholeslami, R., and Watkinson, A.P., "*Blending Effects on Fouling of Four Crude Oils*", ECI Symposium Series, Volume RP2: Proceedings of 6th International Conference on Heat Exchanger Fouling and Cleaning – Challenges and Opportunities, Germany, June 2005.

Simard, M., "*Analysis of A High Temperature Fouling Unit for Heavy Hydrocarbon Fractions*", M.A.Sc. Thesis, The University of British Columbia, 2000.

Smaili, F., Vassiliadis, V.S., and Wilson, D.I., "*Mitigation of Fouling in Refinery Heat Exchanger Networks by Optimal Management of Cleaning*", Energy and Fuels, vol.15, pp.1038-1056, 2001.

Srinivasan, M., and Watkinson, A.P., "Fouling of Some Canadian Crude Oils", Heat Transfer Engineering, vol.26, no.1, pp.7-14, 2005.

Taborek, J., Aoki, T., Ritter, R.B., Palen, J.W., and Knudsen, J.G., "*Fouling – The Major Unresolved Problem in Heat Transfer*", Chem. Eng. Prog.68, pp.59-67, 69-78, 1972.

Watkinson, A.P., "*Chemical Reaction Fouling of Organic Fluids*", Chem. Eng. Technology, vol.15, pp.82-90, 1992.

Watkinson, A.P., "*Critical Review of Organic Fluid Fouling*", final report, ANL/CNSV-TM-208, Argonne National Laboratory, II, 1988.

Watkinson, A.P., "*Deposition from Crude Oils in Heat Exchangers*", ECI Symposium Series, Volume RP2: Proceedings of 6th International Conference on Heat Exchanger Fouling and Cleaning – Challenges and Opportunities, Germany, June 2005.

Watkinson, A.P., and Wilson, D.I., "*Chemical Reaction Fouling: A Review*", Experimental Thermal and Fluid Science, vol.14, pp.361-374, 1997.

Watkinson, A.P., Sundaram, N.S., and Posarac, D., "*Fouling of a Sweet Crude Oil under Inert and Oxygenated Conditions*", Energy and Fuels, vol.14, pp.64-69, 2000.

Wiehe, I., and Kennedy, R., "*The Oil Compatibility Model and Crude Oil Incompatibility*", Energy and Fuels, vol.14, pp.56-59, 2000.

Wiehe, I., Kennedy, R., "*Application of the Oil Compatibility Model to Refinery Streams*", Energy and Fuels, vol.14, pp.60-63, 2000.

Wiehe, I., Kennedy, R., Dickakian, G., "*Fouling of Nearly Incompatible Oils*", Energy and Fuels, vol.15, pp.1057-1058, 2001.

Wilson, D.I., Polley, G.T., and Pugh, S.J., "*Mitigation of Crude Oil Fouling Preheat Train Fouling by Design*", Heat Transfer Engineering, vol.23, no.1, pp. 24-37, 2002.

Wilson, D.I., Polley, G.T., and Pugh, S.J., "*Ten Years of Ebert, Panchal and The "Threshold Fouling" concept*", ECI Symposium Series, Volume RP2: Proceedings of 6th International Conference on Heat Exchanger Fouling and Cleaning – Challenges and Opportunities, Germany, June 2005.

Yeap, B.L., Wilson, D.I., Polley, G.T., and Pugh, S.J., "*Mitigation of Crude Oil Refinery Heat Exchanger Fouling Through Retrofits Based On Thermo-Hydraulic Fouling Models*", Trans IChemE, Part A, Chemical Engineering Research and Design, vol.82 (A1), pp.53-71, January 2004.

Yeap, B.L., Wilson, D.I., Polley, G.T., and Pugh, S.J., "*Retrofitting Crude Oil Refinery Heat Exchanger Networks to Minimize Fouling While Maximizing Heat Recovery*", Heat Transfer Engineering, vol.26, no.1, pp. 23-34, 2005.

APPENDIX I

Sample Calculation for Fouling Run – LSB Run 4

Calculation of Annular Velocity

The volumetric flow rates are calculated as follows, using the equation below:

$$Q = C_d * A_{or} * \sqrt{[2*\Delta P/\rho*(1-\beta^4)]} \quad \text{A.1.1}$$

Where

Q is the volumetric flow rate m^3/s

C_d is the orifice coefficient of discharge, 0.62

A_{or} is the orifice cross-sectional area, m^2

ΔP is the pressure drop in Pa, with dimension of $kg/(m.s^2)$

ρ is the density of the flowing fluid, kg/m^3

β is the ratio of orifice hole diameter (d_1) to the pipe diameter (d_2), constant

d_1 = Orifice hole diameter = 0.0032 m

d_2 = Pipe diameter = 0.0159 m

$A_{or} = \pi * d_1^2/4 = 0.00000792\ m^2$

$\beta = d_1/ d_2 = 0.2$

T_b = Bulk Temperature = 275.4°C

The cross-sectional area of the annulus is given by

$A_{cr} = \pi * (do^2 - di^2)/4 = \pi * (0.0159^2 - 0.0107^2)/4 = 0.000109\ m^2$

$\rho_{Tb} = 699.10\ kg/m^3$ (Appendix II)

$\Delta P = 96537\ kg/(m.s^2)$

$$Q = 0.62*0.00000792 * \sqrt{[2*96537/699.10 *(1-0.2^4)]} = 0.00008167\ m^3/s \quad \text{A.1.2}$$

The Bulk Fluid Annular Velocity is calculated as below,

$V = Q / A_{cr} = 0.00008167/0.000109 = 0.75$ m/s A.1.3

Calculation of Heat Transfer and Fouling Rates (LSB Run 4 - @ time t= 2.78 hrs)

Heat flow to the oil, was directly measured by the power controller which had been previously calibrated with a known resistance, current and voltage measurements and the heat flux (kW/m^2) determined using Q, and A, the heated area of the probe. We define an overall heat transfer coefficient, U, as in equation (A.1.4) below:

$Q = V * I = U A (T_s - T_b)$ A.1.4

$Q_{t=2.78\ hrs} = V * I = 1438$ Watts

$D_{eq} = (0.0159-0.0107) = 0.005225$ m

The surface area A of the heated section of the probe is calculated from $A = \pi * D * L$ where, D is the diameter of the heated probe (0.01065m) and L is the length of the heated section (0.102 m):

$A = \pi * D * L = \pi * (0.01065) * (0.102) = 0.003414\ m^2$

$q = \text{Heat Flux} = Q/A = 1438/1000/0.003414 = 421\ kW/m^2$

T_s is the surface temperature of the heated probe, and T_b the average bulk temperature of the fluid. Average values of T_s are evaluated from three thermocouples located at the same axial position, and different angular positions. The average bulk temperature of the fluid is determined from the average of the inlet and outlet fluid temperature measurements.

The wall temperatures were converted to the surface temperatures using the formula:

$T_{s1} = T_{wi} - s/\lambda * q$ A.1.5

where, s/λ was determined by Wilson method (Asomaning, 1997). The value of s/λ has been used from previous work due to the identical construction of the heater probes and due to non-availability of the information from supplier.

$s_1/\lambda = 8.333*10^{-3}$ m^2K/kW

$s_2/\lambda = 7.692*10^{-3}$ m^2K/kW

$s_3/\lambda = 1.667*10^{-2}$ m^2K/Kw

For probe thermocouple number 1,

$T_{s1} = 370-8.333*10^{-3}*421 = 366.8°C$

$T_{s2} = 365-7.692*10^{-3}*421 = 361.8°C$

$T_{s3} = 365-1.667*10^{-2}*421 = 364.6°C$

The average surface temperature:

$T_{s,\,avg.} = (T_{s1}+ T_{s2}+ T_{s3})/3 = (366.8+361.8+364.6)/3 = 364.40°C$

The bulk fluid temperature is evaluated as the average of the entry and the exit bulk fluid temperatures

$T_{b,\,avg.} = (T_b\ in+ T_b\ out)/2 = (264+275)/2 = 269.5°C$

The overall heat transfer coefficient is calculated at any time (t), from

$$U_{(t)} = q_{(t)} / (T_{s\,(t)} - T_{b\,(t)}) \qquad \text{A.1.6}$$

$$U_{(2.78\ hrs)} = q_{(2.78\ hrs)}/((T_{s\,(2.78\ hrs)} - T_{b\,(2.78\ hrs)})$$

$U_{(2.78\ hrs)} = 421/(364.4-269.5) = 4.4345\ \ kW/m^2K$

Generally the unit is operated at constant q, and with constant Tb, with time, hence the decline in U due to fouling, is determined by the increase in Ts with time. There is a short period (2.5-3.5 hrs) of unsteady state heat transfer at the beginning of the runs and in

some cases, an induction period before fouling begins. The value of $U_{(t=0)}$ was calculated from averaging data points for U(t) between 2.58-3.58 hours.

$U_{(t=0)} = 4.4869$ kW/m^{2}K

The initial thermal resistance or the reciprocal of the initial heat transfer coefficient is calculated from:

$R_{t,0} = 1/U_{t,0} = 0.2229$ m^{2}K/ kW

The thermal fouling resistance is calculated as the diffence between the reciprocals of overall heat treansfer coefficients under clean and fouled conditions.

$$R_f = [1/U(t) - 1/U_{(t=0)}] \qquad \text{A.1.7}$$

$R_{t,2.78\ hrs} = [1/U_{t,2.78\ hrs} - 1/ U_{t,0}\ ] = [0.2255\text{-}0.2229] = 0.0026$ m^{2}K/ kW

The initial fouling rates were evaluated as the slope (linear regression) of the fouling resistance versus time plot, wherever the profile was linear. Since $1/U_{(t=0)}$ is a constant, the fouling rate can be determined from the slope of the curve $1/U_{(t)}$ versus time, t.

$$\text{Fouling rate} \qquad d R_f/ dt = d [1/U_{(t)}] / dt \qquad \text{A.1.8}$$

Rates were determined by curve fitting the linear part of the 1/U vs t curve. The section of the curve over which the rate was measured, was indicated, since the fouling rate changes with time in some cases.

Figure A.1.1 shows the fouling resistance versus time plot. The slope of the curve was estimated between the following data points: t =7.74 hrs and t= 46.21 hrs.

$d R_f/ dt = 2.04$ E-03 m^2.K/kW.hr = 2.04 E-03/3600 m^2.K/kJ = 5.67 E-07 m^2.K/kJ

The detail summary of LSB run 4 data is provided in Appendix VII.

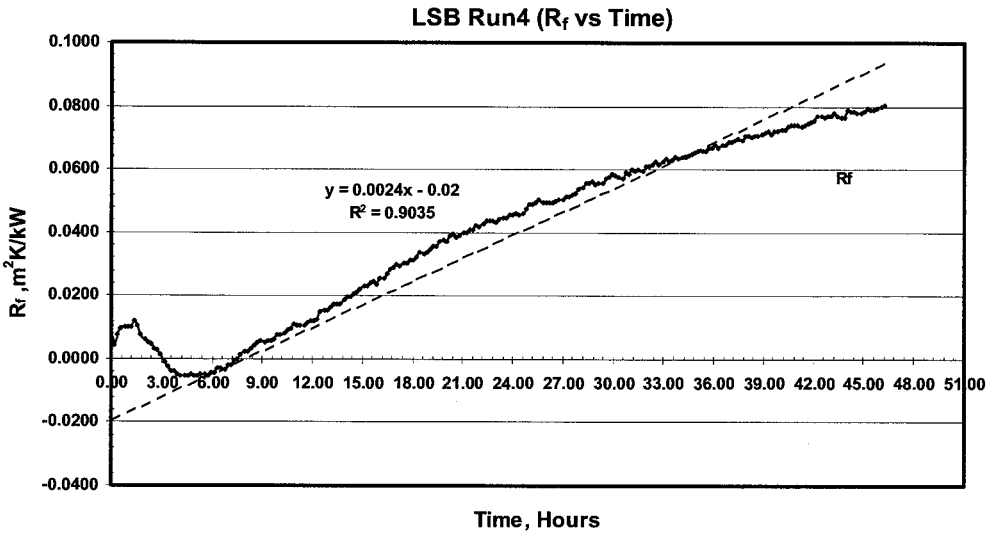

Figure A.1.1 Fouling Resistance Vs Time Plot for LSB Crude Oil – Run 4

APPENDIX II

Estimation of Reynolds Number for Crude Oils (LSB, MDL,CLK) at Bulk Temperatures (T_b) and Film Temperatures (T_f)

The density of the crude oils – LSB, MDL and CLK were extrapolated by using a modified version of the correlation provided by Polley et al. (2002), as shown in Table A.2.1

Table A.2.1 Density Correlation for LSB, MDL, and CLK Crude Oils - Density Estimation at Bulk Temperatures (T_b) and Film Temperatures (T_f)

Crude Oil	Correlation (T°C) for T < 250°C	Correlation (T°C) for T > 250°C
LSB	865.5-0.833T	928.5-0.833T
MDL	911.5-0.833T	974.5-0.833T
CLK	970.5-0.833T	1033.5-0.833T

The viscosity correlations summarized in Bennison (1998) were checked for the three crude oils. The correlation provided by Petrosky and Farshad (1995) yielded a comparatively better fit.

$$\mu = 2.3511*10^{7}*T^{-2.10255}*(\text{Log }^{\circ}\text{API})^{(4.59388*(\text{LogT})-22.82792)}$$

T is in °F, °API is the gravity of oil at 60°F and μ is the viscosity of the crude oil in centipoise. °API for LSB, MDL and CLK are taken from Table 3.1.

Sample Calculations:

For LSB Run 4

$\rho_{Tb} = 928.5 - 0.833\ (275.4) = 699.10\ kg/m^3$

$\rho_{Tf} = 928.5 - 0.833\ (323.2) = 659.30\ kg/m^3$

$\mu_{Tb} = 2.3511*10^{7}*(527.6)^{-2.10255}*(Log^{o}34.142)^{(4.59388*(Log527.6)-22.82792)} = 0.5388$ cp

$\mu_{Tf} = 2.3511*10^{7}*(613.7)^{-2.10255}*(Log^{o}34.142)^{(4.59388*(Log613.7)-22.82792)} = 0.4461$ cp

$D_{eq} = 0.005225$ m

$V = 0.75$ m/s

$$Nre_{(Tb)} = \frac{D_{eq}* V* \rho_{Tb}}{\mu_{Tb}} = (0.005225*0.75*699.1)/0.5388 = 5085$$

$$Nre_{(Tf)} = \frac{D_{eq}* V* \rho_{Tf}}{\mu_{Tf}} = (0.005225*0.75*659.3)/0.4461 = 5792$$

Tables A.2.2, A.2.3, and A.2.4 summarize the Reynolds number for LSB, MDL, CLK crude oils at T_b and T_f. Tables A.2.5 provides a better comparision for the three crude oils at the same film temperatures. (6°C, 25°C & 310°C)

Table A.2.2 Summary of Reynolds Number for Crude Oil – LSB at Bulk Temperatures (T_b) and Film Temperatures (T_f)

Crude	Run No.	Vel (m/s)	Tb avg °C	Ts @t=0,°C	Tfilm °C	$\rho_{Tb\ avg}$	ρ_{Tf}	$\mu_{Tb\ avg}$	μ_{Tf}	$Nre(T_b\ avg)$	$Nre(T_f)$
LSB	1A	**0.30**	134.4	250.0	192.2	753.5	705.4	1.2222	0.8175	**966**	**1353**
	3A	0.75	211.8	297.0	254.4	689.1	716.6	0.7312	0.5911	**3693**	**4750**
	4	0.75	275.4	371.0	323.2	699.1	659.3	0.5388	0.4461	**5085**	**5792**
	5	0.75	256.5	350.5	303.5	714.8	675.7	0.5854	0.4805	**4785**	**5511**
	10	0.75	270.6	370.0	320.3	703.1	661.7	0.5498	0.4508	**5011**	**5752**
	15	0.75	282.7	375.5	329.1	693.0	654.4	0.5224	0.4366	**5199**	**5874**
	18	0.75	255.5	354.0	304.8	715.7	674.6	0.5882	0.4782	**4768**	**5529**
	19	0.75	256.5	355.0	305.8	714.8	673.8	0.5855	0.4763	**4784**	**5544**
	21	0.75	272.0	355.0	313.5	701.9	667.4	0.5467	0.4624	**5032**	**5655**
	23	0.75	274.0	335.0	304.5	700.2	674.8	0.5419	0.4786	**5064**	**5526**
	24	0.75	285.7	360.5	323.1	690.5	659.3	0.5159	0.4462	**5245**	**5791**
	25*	0.75	272.8	362.5	317.7	701.2	663.9	0.5447	0.4552	**5045**	**5715**
	27	0.75	247.5	357.0	302.2	659.4	676.7	0.6105	0.4829	**4232**	**5492**
	29	**0.35**	275.6	375.0	325.3	698.9	657.5	0.5383	0.4426	**2375**	**2717**
	30	**0.15**	276.3	375.0	325.7	698.3	657.2	0.5366	0.4420	**1020**	**1165**
	32	0.75	280.4	363.5	322.0	694.9	660.3	0.5274	0.4481	**5163**	**5775**

Table A.2.3 Summary of Reynolds Number for Crude Oil – MDL at Bulk Temperatures (T_b) and Film Temperatures (T_f)

Crude	Run No.	Vel (m/s)	Tb avg °C	Ts @t=0,°C	Tfilm °C	$\rho_{Tb\ avg}$	ρ_{Tf}	$\mu_{Tb\ avg}$	μ_{Tf}	$Nre(T_b\ avg)$	$Nre(T_f)$
MDL	6A	0.75	145.9	250.0	**198.0**	790.0	746.6	1.9154	1.3218	**1616**	**2213**
	7	0.75	247.7	345.0	**296.3**	768.2	727.7	1.0004	0.7979	**3009**	**3574**
	11	0.75	259.7	352.5	**306.1**	758.2	719.5	0.9427	0.7658	**3152**	**3682**
	16	0.75	281.7	378.5	**330.1**	739.9	699.5	0.8507	0.6956	**3408**	**3941**

Table A.2.4 Summary of Reynolds Number for Crude Oil – CLK at Bulk Temperatures (T_b) and Film Temperatures (T_f)

Crude	Run No.	Vel (m/s)	Tb avg °C	Ts @t=0,°C	Tfilm °C	$\rho_{Tb\ avg}$	ρ_{Tf}	$\mu_{Tb\ avg}$	μ_{Tf}	$Nre(T_b\ avg)$	$Nre(T_f)$
CLK	12	0.75	266.2	382.0	324.1	811.8	763.5	2.7063	2.0287	**1175**	**1475**
	14	0.75	252.9	352.5	302.7	822.8	781.3	2.9145	2.2426	**1106**	**1365**
	17	0.75	234.3	335.5	284.9	775.3	796.2	3.2547	2.4505	**933**	**1273**
	33	0.75	247.2	342.5	294.8	764.6	787.9	3.0129	2.3307	**994**	**1325**

Table A.2.5 Comparision of Reynolds Number for Crude Oils – LSB, MDL, CLK at a constant Film Temperature (T_f) of 6°C, 25°C & 310°C

CRUDE	°C	$Nre(T_f)$
LSB	6	271
	25	554
	310	5605
MDL	6	139
	25	300
	310	3725
CLK	6	30
	25	73
	310	1403

Table A.2.6 Comparision of Reynolds Number for Crude Oil – LSB at a Constant Film Temperature (T_f) of 310°C and Varying Velocities of 0.15 m/s, 0.35 m/s and 0.75 m/s.

CRUDE	V (m/s)	Nre(T_f)
LSB 310°C(Film)	0.15	1121
	0.35	2616
	0.75	5605

Table A.2.7 Comparision of Reynolds Number for Crude Oil – LSB at a Constant Bulk Temperature (T_b) of 275°C and Varying Velocities of 0.15 m/s, 0.35 m/s and 0.75 m/s.

CRUDE	V (m/s)	Nre(T_b)
LSB 275°C (Bulk)	0.15	1016
	0.35	2370
	0.75	5079

APPENDIX III

Hot Filtration of Pre and Post Fouled Crude Oil Samples

A clean glass liner was weighed and then about 1.5 g of the crude oil sample was placed in the glass liner. Then the glass liner was placed in a sealed flask with 100 ml n-heptane without agitation for 16 hours. The resulting suspension was filtered through a 1μm, 47 mm Gelman Science Teflon filter at 85°C and by using vacuum provided by a water aspirator. After filtering all the suspension in the flask, the glass liner and the flask container were flushed with 50 ml n-heptane and put in the ultrasonic bath for 2 minutes, in order to remove any possible adhering insolubles from the wall of the glass liner and the flask. This suspension was also filtered through the same filter. A constant filtration temperature was achieved by wrapping a heating pad on the entire filtration assembly. The wall of the glass funnel was also flushed with n-heptane and the residue on the filter was washed with toluene until the filtrate became clear. Then the filter and its residue were removed from the filtration system using a forceps into a watch glass, which were then dried for 16 hours at 90°C in air at atmospheric pressure before weighing. Also after removing the filter from the filtration system, any possible residue stuck to the glass funnel was scraped and collected with the residue on the filter in the watch glass prior to drying. The difference in weight of the filter paper is reported as wt% of insolubles.

Hot Filtration Tests on Fresh and Spent Crude Oils

Individual results for most of the runs are listed in Table A.3.1. Table A.3.2 lists average hot filtration results for fresh and spent oils. All results are quite different than given in the typical benchmark oil specifications of Table 3.1 provided by Shell Canada Limited. This could possibly be due to differences in measurement techniques, or to contamination of oil in sample pails for example with wax or rust. For LSB and for MDL, which have respectively 0.13 and 0.21 wt% insolubles in the feed samples, there were increases as shown in Table A.3.2 over the 48-hour runs. For CLK, the initial oil samples were much higher in insolubles at 4.35%. However at the end of the run, the insolubles were similar to the other crude oils, i.e., 0.35 wt%. For CLK crude oil the high insoluble content was

possibly due to the asphaltene precipitation. The reduction in the insoluble contents on the post run test fluid in the case of CLK could be due to the increased solubility of asphaltenes at higher bulk temperatures. Also, the spent test fluid sample from the fouling loop was withdrawn when the fluid temperature was around 65-85°C. The absence of large increases in hot filtration insolubles indicates that gum formation due to autoxidation, or asphaltene precipitation were not occurring in the bulk fluid during the fouling experiments.

Table A.3.1 Summary of Hot Filtration Tests on Some Fouling Runs

S.No	Sample	Run No.	Wt (%)	% Change
1	**LSB-Fresh**	-	**0.13**	
2	LSB	1&2	0.15	17
3	LSB	3	0.15	21
4	LSB	4	0.16	26
5	LSB	5	0.14	14
6	LSB	10	0.11	-9
7	LSB	15	0.23	82
8	LSB	18	0.23	84
9	LSB	19	0.25	96
10	**MDL-Fresh**	-	**0.21**	
11	MDL	6	0.24	14
12	MDL	7	0.36	76
13	MDL	11	0.31	49
14	MDL	16	0.36	71
15	**CLK-Fresh**	-	**4.35**	
16	CLK	14	2.74	-37
17	CLK	17	0.36	-92
18	CLK	11	0.31	-93

Table A.3.2 Average Fresh and Spent Oil Hot Filtration Solids Concentrations

Oil	Fresh Oil Insolubles (% wt) (Average)	Spent Oil Insolubles (% wt) (Average)	% Change	Runs Used (for average)
CLK	4.35	0.34	-92	11, 17
LSB	0.13	0.23	77	15, 18, 19
MDL	0.21	0.33	57	7, 11, 16

APPENDIX IV

Viscosity Measurements

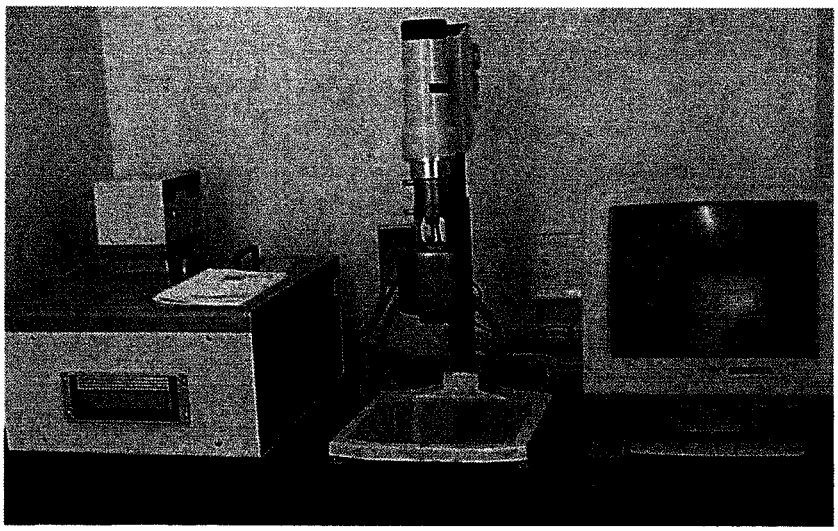

Figure A.4.1 Photograph of Roto-Viscometer

Figure A.4.1 shows the Haake Roto-Visco Meter VT500. The viscosity is measured from the measured torque and rotational speed as well as the dimension of the measuring geometry. In this model, the measuring geometry used was coaxial cylinders called the rotor and the cup with a temperature control through as temperature controlled circulating fluid. For a Newtonian fluid in the absence of turbulence, the rate of shear D (s^{-1}) is directly proportional to the shear stress τ (mPa) and the viscosity is defined by the Newton equation:

$$\mu = \tau / D$$

The viscometer was calibrated using a Brookfield standard. The results are tabulated in Table A.4.1. For LSB and MDL crude oils, the measurement was carried out at 25°C. For CLK crude oil, the measurements were carried out at 85°C. The viscosity for the post fouling run fluid increased several folds due to the loss of volatiles from the system due to some leaks. The viscosity change for LSB spent oil was higher in magnitude compared

to MDL and CLK spent oils. This is due to the fact that the weight percent of the lighter components in the LSB is relatively higher than MDL and CLK. Due to the system leaks (fouling loop) volatile losses were observed from the system. This led to the increase in viscosity in all the three crude oils relative to their lighter component content. (Chapter III - Table 3.1)

Table A.4.1 Table of Viscosity Results for Crude Oil Fouling Runs - LSB, MDL, and CLK

S.No	Sample	Temperature,°C	Viscosity(mPa-s)	% Change
1	Brookfield standard	25	483.00	
2	Brookfield standard (test)	25	413.47	14.40
	LSB SAMPLE-FRESH OIL			
3	**LSB-INITIAL SAMPLE**	25	12.74	
4	**LSB-INITIAL SAMPLE-Repeat**	25	10.05	
	LSB SAMPLES-SPENT OIL			
5	LSB-Run # 1,2 final	25	21.62	69.70
6	LSB-Run # 3 final	25	31.69	148.70
7	LSB-Run # 4 final	25	21.45	68.33
8	LSB-Run # 5 final	25	22.25	74.65
9	LSB-Run # 10 final	25	22.00	72.68
10	LSB-Run # 15 final	25	24.50	92.31
11	LSB-Run # 18 final	25	19.80	55.42
12	LSB-Run # 19 final	25	22.80	78.96
13	LSB-Run # 21 final	25	38.40	201.41
14	LSB-Run # 23 final	25	40.00	213.97
15	LSB-Run # 24 final	25	36.20	184.14
16	LSB-Run # 25 final	25	25.26	98.27
17	LSB-Run # 26 final	25	180.50	1316.80
18	LSB-Run # 27 final	25	54.00	323.86
19	LSB-Run # 28 final	25	220.30	1629.20
20	LSB-Run # 29 final	25	142.37	1017.50
21	LSB-Run # 32 final	25	141.00	1006.75
	MDL SAMPLE -FRESH OIL			
22	**MIDALE INITIAL SAMPLE**	25	19.58	
	MDL SAMPLE -SPENT OIL			
23	MIDALE-Run # 6 final	25	65.01	232.08
24	MIDALE-Run # 7 final	25	58.70	199.87
25	MIDALE-Run # 11 final	25	71.20	263.73
26	MIDALE-Run # 16 final	25	69.50	255.04
	CLK SAMPLE -FRESH OIL			
27	**CLK-INITIAL SAMPLE**	85	150.00	
	CLK SAMPLE -SPENT OIL			
28	CLK-Run # 12 final	85	520.00	246.67
29	CLK-Run # 14 final	85	585.00	290.00
30	CLK-Run # 17 final	85	550.00	266.67
31	CLK-Run # 33 final	85	497.00	231.33

APPENDIX V

Deposit Characterization

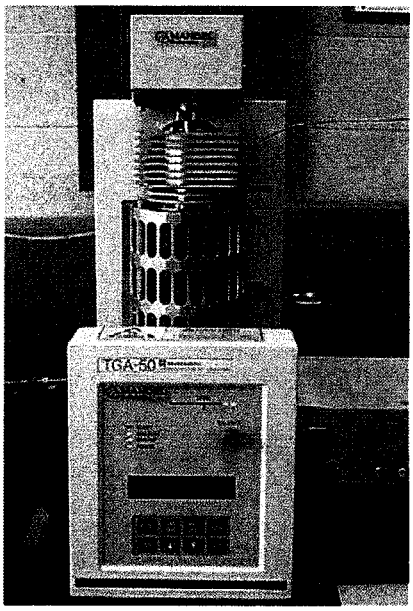

Figure A.5.1 **Photograph of Thermo Gravimetric Analyzer (TGA)**

The thermal analysis of the fouling deposits were done to determine their thermal behaviour at elevated temperatures, and to determine their Moisture Content (MC), Volatile Content (VC), Fixed Carbon (FC), and Ash Content (ASH Experimental). The thermal analysis was done on a TGA-50 (Shimadzu) Thermo Gravimetric Analyzer (Figure A.5.1). The temperature program was setup with a minimum of 50°C, and a maximum of 900°C and a heating ramp up as shown in the Figure A.5.2, A.5.3, and A.5.4,

Figures A.5.2, A.5.3 and A.5.4 show the TGA curves for LSB (run 4), MDL (run 11) and CLK (run 17) respectively. There was a period of gradual weight loss, followed by a period of constant weight in a nitrogen purge atmosphere. When oxygen supply was turned on, a further weight loss was observed when the

fixed carbon was burnt leaving a residue of ash. Table A.5.1 shows the results for the thermal analysis of samples from the fouling runs.

Table A.5.1 **Table of TGA Results for Crude Oil Deposits - LSB, MDL, and CLK**

TGA ANALYSIS				
Sample	MC	VC	FC	ASH.exp
LSB-3A	0.24	12.942	25.778	**61.04**
LSB-4	0.20	10.50	17.71	**71.59**
LSB-5	0.04	6.02	9.68	**84.26**
LSB-5 repeat	0.05	6.19	9.52	**84.25**
LSB-18	0.14	30.55	1.28	**68.03**
LSB-19	0.28	16.90	5.15	**77.67**
LSB-21	0.30	24.50	5.56	**69.64**
LSB-23	0.35	6.32	7.50	**85.83**
LSB-24	0.20	22.31	6.83	**70.66**
LSB-25	0.43	27.60	32.06	**39.91**
LSB-27	0.23	25.62	2.31	**71.83**
LSB-29	0.81	23.96	24.28	**50.95**
LSB-30	0.17	27.77	4.97	**67.08**
LSB-32	0.62	25.78	16.45	**57.15**
MID-7	4.51	2.70	48.35	**44.44**
MID-11	0.03	12.47	5.42	**82.08**
MID-11repeat	0.03	11.83	8.49	**79.65**
CLK-12	0.46	12.43	61.37	**25.74**
CLK-17	0.99	27.03	10.49	**61.49**

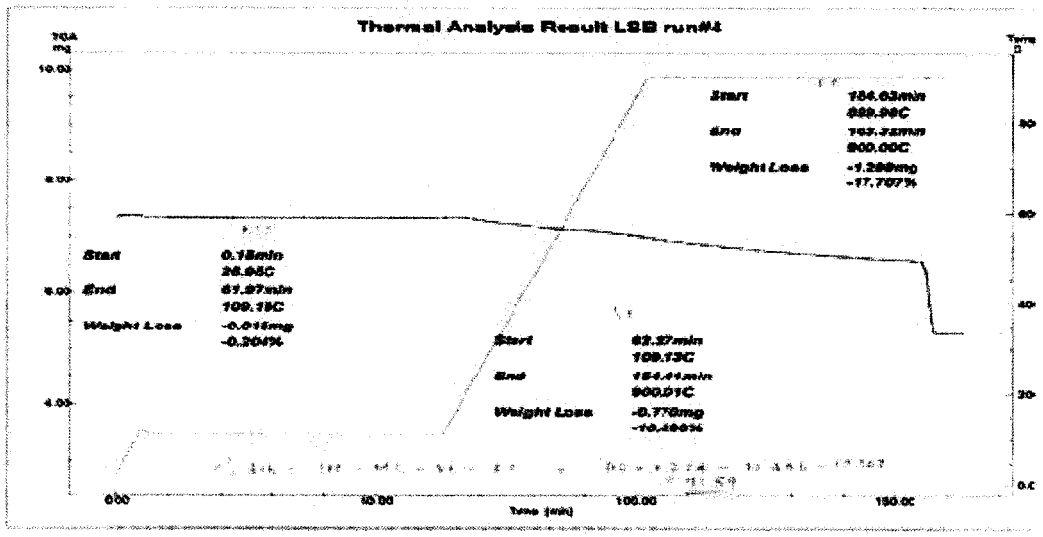

Figure A.5.2 **Thermo Gravimetric Analysis – LSB Run 4**

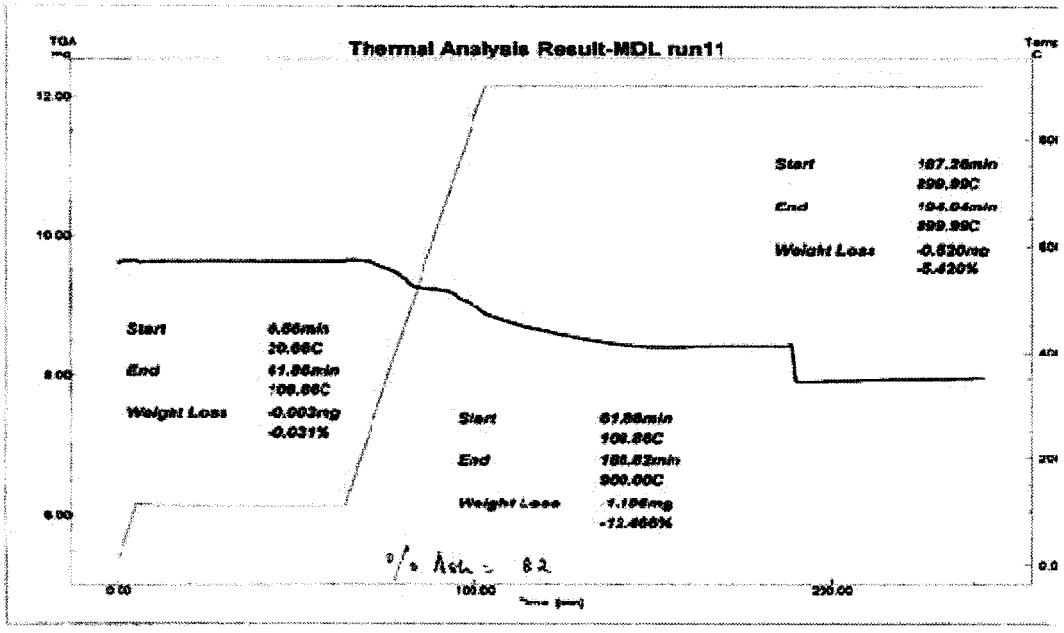

Figure A.5.3 Thermo Gravimetric Analysis – MDL Run 11

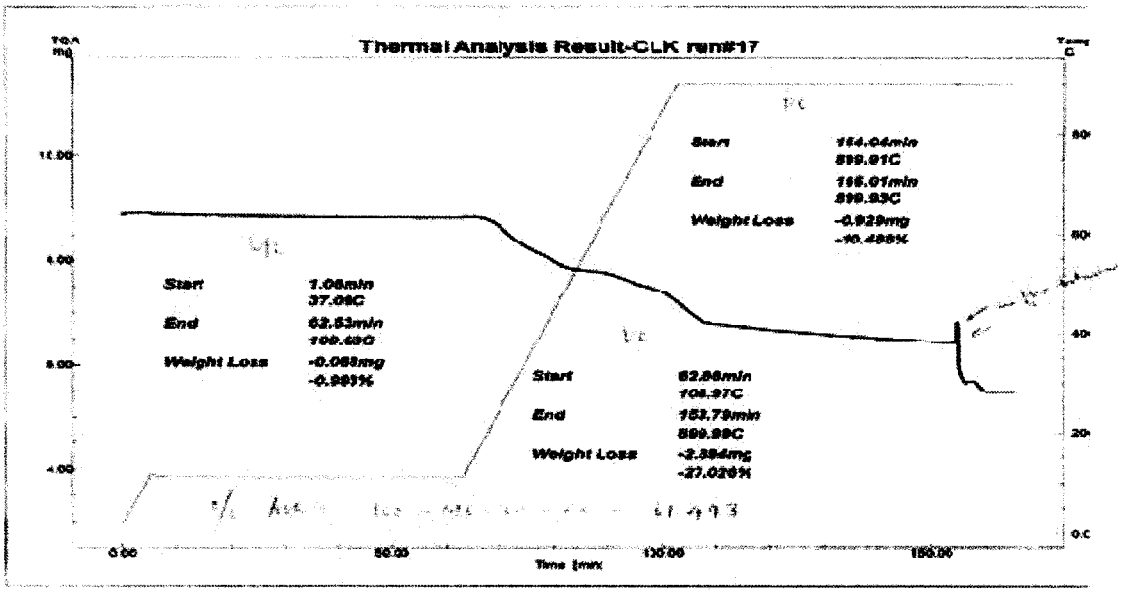

Figure A.5.4 Thermo Gravimetric Analysis – CLK Run 17

The deposits were analyzed using Energy Dispersive X-ray (EDX), giving point analyses on the deposit surface and a micro-elemental analysis for the bulk content of C, H, S and N. The results are tabulated in Table A.5.2. For LSB deposits, the ash content varied from 50-85% and averaged at 67%. The organic portion of the deposit had an average H/C atomic ratio of 0.8. Sulfur content averaged 18.4% and appeared from the EDX data to be linked to iron content. On average for LSB deposits Fe/S mass ratios were 2.2-2.5, which is significantly higher than the Fe/S mass ration of 1.745 for pure FeS.

For CLK deposits, the ash content ranged from 18-61%, with H/C of 0.83 and sulfur content of 6-18%. Fe/S by EDX was 1.9-2.0.

For MDL, the two deposits analyzed had ash content of 44 and 80%, with corresponding carbon contents of 9.4 and 23%. The H/C atomic ratio was 0.9. From EDX measurements, the Fe/S mass ratio is 1.6-1.8. Thus deposits from MDL crude oil have Fe/S ratios consistent with FeS, whereas deposits from other crude oils appear iron-rich, with Fe/S ratios greater than that of FeS.

Table A.5.2 Table of TGA/EDX/Micro-Elemental Analysis for Crude Oil Deposits - LSB, MDL, and CLK

Oil	% Ash	% C	% H	% N	% S	% Fe* (C-f)	% S* (C-f)	Fe/S* (wt/wt)
LSB	71.6	17.0	1.2	0.34	17.8	56.5	25.3	2.2
LSB	84.3	4.5	0.7	0.30	22.1	N/A	N/A	N/A
LSB	57.2	35.2	1.5	0.53	12.6	66.2	26.0	2.5
MDL	44.4	22.8	1.2	1.80	24.3	58.5	37.3	1.6
MDL	80.9	9.4	0.9	0.30	23.6	65.2	32.1	2.0
CLK	25.7	66.4	3.1	1.32	7.1	51.6	26.1	2.0
CLK	61.5	26.0	2.4	0.31	17.2	58.5	29.3	2.0

* EDX surface analysis; carbon free basis

APPENDIX VI

Modified Film Temperature

The following is the matlab code for determining modified film temperature based on the experimental findings:

```
Tb=[275.4
272.0
274.0
256.5
256.5
247.5
285.7
280.4];

Tb=Tb+273;  % Tb in Kelvin

Ts=[371
355
335
350.5
355
357
360.5
363.5];

Ts=Ts+273;  %Ts in Kelvin

RATE=[5.67E-07
4.16E-07
3.06E-07
3.91E-07
4.16E-07
3.50E-07
4.90E-07
6.75E-07];

lnRf=log(RATE);

T=(Tb+Ts)/2;

Y= lnRf.*Tb;
x0= lnRf.*Ts;
```

```
X=[ones(8,1)*2 Tb Ts -1*x0];

B=inv(X'*X)*(X'*Y);

Tcalc = (Tb + B(4)*Ts)/2;

ycalc = B(2) + B(1)*(1./Tcalc);

%Tcalc = (Tb - 0.7641*Ts)/2;

%lnRfcalc = -14.8001 - 12.8358 * (1./Tcalc);

X2=[ones(8,1) 1./T];

B2=inv(X2'*X2)*(X2'*lnRf);


%figure(1);

%plot(1./T,lnRf,'*');

%figure(2);

plot(1./T,lnRf,'*',1./Tcalc,lnRfcalc,'o');

%plot(1./T(1),lnRf(1),'*',1./Tcalc(1),lnRfcalc(1),'o');
```

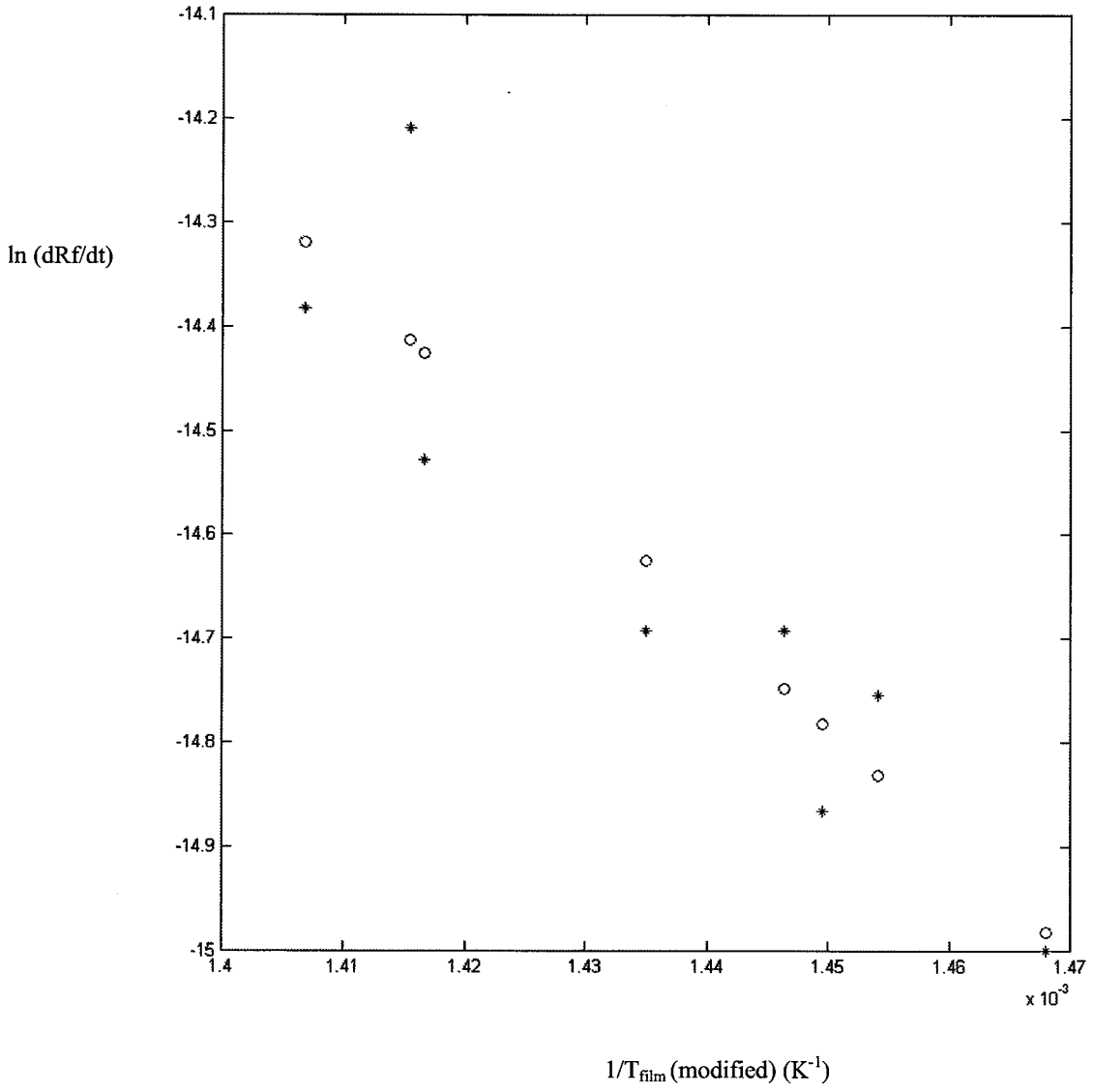

Figure A.6.1 Determination of Modified Film Temperature (T_f')

APPENDIX VII

Summary of Raw Data from Fouling Run (LSB Run 4)

Table A.7.1 Summary of Raw Data from Fouling Run – LSB Run 4

Time (Hours)	t1	t2	t3	t4	tin	tout	Power (watts)	T_b,avg °C	T_s,avg °C	q, kW/m^2	1/U, m^{2}K/kW	U, kW/m^{2}K	R_f(4), m^{2}K/kW
0.00	290	287	287	281	204	213	1137	208.65	286.30	333	0.2334	4.2852	0.0105
0.20	317	312	312	305	210	222	1437	216.10	311.55	421	0.2270	4.4059	0.0041
0.40	311	305	305	298	201	213	1449	206.95	304.78	424	0.2307	4.3348	0.0078
0.60	319	314	314	307	210	221	1445	215.05	313.43	423	0.2326	4.2987	0.0098
0.79	345	339	339	332	234	246	1442	240.10	338.43	422	0.2330	4.2920	0.0101
0.99	358	352	351	345	247	258	1445	252.75	351.18	423	0.2327	4.2965	0.0099
1.19	349	343	342	335	238	250	1444	243.75	342.23	423	0.2330	4.2914	0.0102
1.39	350	344	344	336	239	250	1446	244.10	343.48	423	0.2348	4.2584	0.0120
1.59	357	351	351	344	246	257	1451	251.60	350.63	425	0.2332	4.2882	0.0103
1.79	360	355	355	347	251	262	1448	256.25	354.03	424	0.2307	4.3341	0.0079
1.98	362	356	356	349	253	264	1450	258.60	355.85	424	0.2292	4.3635	0.0063
2.18	363	358	358	350	255	266	1449	260.60	357.28	424	0.2280	4.3864	0.0051
2.38	364	359	359	351	256	268	1443	261.90	358.08	422	0.2277	4.3910	0.0049
2.58	367	362	362	354	260	271	1447	265.40	361.18	423	0.2262	4.4215	0.0033
2.78	370	365	365	357	264	275	1438	269.50	364.40	421	0.2255	4.4345	0.0026
2.98	372	367	367	360	266	277	1445	271.55	366.43	423	0.2244	4.4573	0.0015
3.17	372	367	368	360	267	278	1448	272.70	366.78	424	0.2220	4.5045	-0.0009
3.37	374	369	369	361	269	280	1451	274.90	368.50	425	0.2204	4.5368	-0.0024
3.57	375	370	370	362	271	282	1447	276.65	369.38	423	0.2190	4.5670	-0.0039
3.77	376	371	372	364	272	284	1447	277.95	370.68	423	0.2190	4.5670	-0.0039
3.97	377	372	372	364	273	284	1448	278.45	370.90	424	0.2182	4.5837	-0.0047
4.17	377	372	372	364	273	284	1453	278.75	371.23	425	0.2175	4.5983	-0.0054
4.36	377	372	372	364	273	284	1453	278.75	371.15	425	0.2173	4.6020	-0.0056
4.56	377	372	372	364	274	284	1448	278.85	371.08	424	0.2176	4.5949	-0.0052
4.76	378	372	373	365	274	285	1448	279.55	371.85	424	0.2178	4.5912	-0.0051
4.96	378	373	373	366	275	286	1447	280.35	372.53	423	0.2177	4.5942	-0.0052
5.16	378	373	373	366	275	286	1441	280.75	372.58	422	0.2177	4.5926	-0.0051
5.36	378	374	374	366	276	286	1440	280.90	372.80	421	0.2181	4.5857	-0.0048
5.55	379	374	375	366	276	287	1444	281.35	373.43	423	0.2179	4.5897	-0.0050
5.75	380	375	375	367	277	287	1449	282.00	374.30	424	0.2177	4.5943	-0.0052
5.95	380	375	376	368	277	288	1445	282.25	374.65	423	0.2185	4.5767	-0.0044
6.15	381	376	376	368	277	287	1454	281.85	374.83	426	0.2185	4.5767	-0.0044
6.35	380	375	375	367	276	286	1443	281.35	374.28	422	0.2200	4.5445	-0.0028
6.55	381	376	376	368	277	287	1443	282.00	374.93	422	0.2200	4.5445	-0.0028
6.74	381	376	376	368	277	287	1450	281.95	375.05	424	0.2194	4.5580	-0.0035
6.94	380	375	375	366	275	285	1446	280.20	373.68	423	0.2209	4.5272	-0.0020
7.14	379	374	374	365	274	285	1449	279.20	372.95	424	0.2211	4.5233	-0.0018
7.34	379	373	374	365	273	284	1448	278.70	372.90	424	0.2223	4.4986	-0.0006
7.54	379	373	373	365	272	284	1453	277.90	372.65	425	0.2228	4.4879	0.0000
7.74	377	372	372	364	271	282	1445	276.55	371.38	423	0.2242	4.4596	0.0014
7.93	377	371	372	364	270	281	1445	275.50	370.80	423	0.2254	4.4374	0.0025
8.13	377	372	372	364	270	281	1452	275.15	370.90	425	0.2253	4.4380	0.0025
8.33	376	371	371	363	269	280	1451	274.30	370.38	425	0.2262	4.4199	0.0034

Appendix VII

Time (Hours)	t1	t2	t3	t4	tin	tout	Power (watts)	T_b,avg °C	T_s,avg °C	q, kW/m^2	1/U, m^{2}K/kW	U, kW/m^{2}K	R_f(4), m^{2}K/kW
8.53	377	371	371	363	269	280	1448	274.15	370.33	424	0.2270	4.4062	0.0041
8.73	376	371	371	362	269	279	1439	273.70	369.83	421	0.2283	4.3811	0.0054
8.92	377	371	372	363	268	280	1447	273.95	370.68	423	0.2284	4.3781	0.0055
9.12	378	372	372	363	269	280	1449	274.75	371.48	424	0.2281	4.3841	0.0052
9.32	378	373	373	366	270	281	1454	275.30	372.48	426	0.2284	4.3789	0.0055
9.52	378	372	373	365	270	281	1444	275.25	371.83	423	0.2285	4.3758	0.0057
9.72	378	372	373	364	269	280	1443	274.80	371.58	422	0.2292	4.3637	0.0063
9.92	377	372	372	364	269	280	1438	274.05	371.15	421	0.2307	4.3341	0.0079
10.12	377	372	372	364	268	279	1443	273.75	371.18	422	0.2307	4.3346	0.0078
10.31	378	372	372	364	268	279	1443	273.70	371.30	422	0.2311	4.3268	0.0082
10.51	378	372	373	364	268	279	1445	273.80	371.88	423	0.2319	4.3119	0.0090
10.71	378	373	373	365	269	279	1445	273.95	372.25	423	0.2325	4.3020	0.0096
10.91	379	373	373	366	268	279	1445	273.85	372.70	423	0.2338	4.2781	0.0109
11.11	379	373	374	366	269	280	1446	274.05	372.88	423	0.2335	4.2821	0.0107
11.31	380	375	375	366	270	280	1447	274.95	373.75	423	0.2333	4.2861	0.0104
11.50	381	375	375	367	270	281	1446	275.70	374.48	423	0.2334	4.2843	0.0105
11.70	381	375	376	368	270	281	1446	275.70	374.93	423	0.2345	4.2648	0.0116
11.90	381	375	376	368	270	281	1448	275.40	374.90	424	0.2348	4.2589	0.0119
12.10	382	376	376	368	270	281	1448	275.55	375.15	424	0.2350	4.2547	0.0122
12.30	382	376	377	368	271	281	1445	275.95	375.50	423	0.2354	4.2480	0.0125
12.50	382	376	377	368	270	281	1444	275.05	375.48	423	0.2376	4.2080	0.0148
12.69	382	376	377	368	269	281	1443	274.95	375.50	422	0.2381	4.1999	0.0152
12.89	382	376	377	368	270	281	1441	275.35	375.90	422	0.2384	4.1941	0.0156
13.09	382	376	376	368	269	280	1437	274.80	375.48	421	0.2394	4.1772	0.0165
13.29	383	377	377	370	270	281	1438	275.60	376.65	421	0.2401	4.1646	0.0172
13.49	383	378	377	370	270	281	1441	275.65	376.95	422	0.2402	4.1630	0.0173
13.69	384	378	378	370	271	281	1443	276.00	377.50	422	0.2404	4.1606	0.0175
13.88	384	378	379	370	271	281	1439	276.00	377.68	421	0.2414	4.1419	0.0186
14.08	384	378	378	370	270	281	1435	275.40	377.35	420	0.2428	4.1193	0.0199
14.28	384	378	378	369	270	281	1439	275.30	377.48	421	0.2426	4.1217	0.0198
14.48	384	378	379	370	270	281	1435	275.20	377.50	420	0.2436	4.1052	0.0207
14.68	385	378	379	370	270	281	1440	275.20	377.98	421	0.2439	4.1004	0.0210
14.88	385	379	379	370	270	281	1435	275.05	377.93	420	0.2450	4.0822	0.0221
15.07	385	378	379	370	269	281	1432	275.00	378.05	419	0.2459	4.0668	0.0230
15.27	385	379	380	371	270	281	1436	275.20	378.55	420	0.2459	4.0663	0.0231
15.47	385	379	380	372	270	281	1436	275.20	378.90	420	0.2468	4.0526	0.0239
15.67	386	380	380	372	270	281	1434	275.45	379.25	420	0.2473	4.0430	0.0245
15.87	386	380	380	371	270	281	1443	275.20	379.18	422	0.2462	4.0616	0.0233
16.07	387	380	380	372	269	280	1443	274.80	379.60	422	0.2482	4.0296	0.0253
16.26	386	380	380	372	269	280	1443	274.65	379.58	422	0.2485	4.0248	0.0256
16.46	387	380	380	372	269	280	1441	274.30	379.70	422	0.2499	4.0011	0.0271
16.66	386	379	380	372	269	279	1434	273.90	379.30	420	0.2512	3.9817	0.0283
16.86	386	380	380	372	269	279	1434	273.85	379.53	420	0.2518	3.9713	0.0289
17.06	388	381	381	373	269	280	1437	274.35	380.65	421	0.2528	3.9562	0.0299
17.26	388	382	382	374	270	281	1437	275.30	381.35	421	0.2522	3.9655	0.0293
17.45	389	382	383	374	270	281	1440	275.55	382.13	421	0.2529	3.9542	0.0300
17.65	389	383	383	375	271	282	1435	276.05	382.35	420	0.2531	3.9507	0.0303
17.85	390	383	383	375	270	281	1439	275.60	382.68	421	0.2543	3.9330	0.0314
18.05	389	382	383	375	270	280	1442	275.10	382.25	422	0.2539	3.9385	0.0310
18.25	390	383	384	376	270	281	1445	275.20	383.10	423	0.2552	3.9192	0.0323
18.45	390	384	384	376	270	281	1441	275.25	383.35	422	0.2563	3.9012	0.0335
18.64	390	384	384	376	270	281	1440	275.45	383.33	421	0.2560	3.9066	0.0331

Appendix VII

Time (Hours)	t1	t2	t3	t4	tin	tout	Power (watts)	T_b,avg °C	T_s,avg °C	q, kW/m^2	1/U, m^{2}K/kW	U, kW/m^{2}K	R_f(4), m^{2}K/kW
18.84	390	384	384	376	270	281	1439	275.45	383.40	421	0.2563	3.9012	0.0335
19.04	390	383	384	376	270	280	1437	274.95	383.18	421	0.2573	3.8858	0.0345
19.24	390	383	384	376	269	280	1440	274.30	383.28	421	0.2586	3.8671	0.0357
19.44	390	384	384	376	269	280	1439	274.50	383.38	421	0.2585	3.8680	0.0357
19.64	390	384	384	376	269	280	1432	274.55	383.38	419	0.2597	3.8510	0.0368
19.83	390	383	384	376	268	280	1435	274.00	383.30	420	0.2603	3.8423	0.0374
20.03	391	384	384	376	268	279	1448	273.55	383.63	424	0.2598	3.8498	0.0369
20.23	390	383	384	376	268	279	1439	273.25	383.43	421	0.2616	3.8224	0.0387
20.43	390	384	384	376	268	279	1433	273.25	383.33	419	0.2625	3.8099	0.0396
20.63	391	384	385	376	269	279	1438	274.05	384.08	421	0.2614	3.8249	0.0386
20.83	392	385	386	377	269	280	1444	274.50	385.13	423	0.2618	3.8200	0.0389
21.02	392	385	386	378	269	280	1440	274.40	385.20	421	0.2629	3.8035	0.0400
21.22	393	386	386	378	269	280	1441	274.80	385.63	422	0.2628	3.8052	0.0399
21.42	392	385	386	377	269	280	1431	274.65	385.03	419	0.2636	3.7942	0.0407
21.62	392	385	385	377	269	280	1433	274.35	385.03	419	0.2639	3.7892	0.0410
21.82	392	386	386	378	269	280	1434	274.20	385.38	420	0.2649	3.7748	0.0420
22.02	393	386	387	378	269	280	1439	274.45	385.93	421	0.2647	3.7778	0.0418
22.21	394	387	387	379	269	280	1434	274.75	386.30	420	0.2658	3.7621	0.0429
22.41	394	387	387	379	269	280	1436	274.75	386.78	420	0.2666	3.7514	0.0437
22.61	395	387	388	380	270	280	1438	275.20	387.38	421	0.2666	3.7516	0.0437
22.81	395	388	389	380	270	280	1446	275.05	387.90	423	0.2667	3.7499	0.0438
23.01	396	388	389	380	270	281	1443	275.75	388.10	422	0.2660	3.7588	0.0432
23.21	396	388	389	380	270	281	1439	275.45	387.98	421	0.2672	3.7425	0.0443
23.40	396	389	390	381	271	281	1446	275.75	388.93	423	0.2674	3.7391	0.0446
23.60	397	390	390	381	271	282	1444	276.45	389.43	423	0.2673	3.7406	0.0445
23.80	397	390	390	382	271	282	1440	276.25	389.50	421	0.2687	3.7212	0.0459
24.00	396	390	389	382	271	282	1435	276.45	389.20	420	0.2685	3.7247	0.0456
24.20	397	390	390	382	272	282	1431	277.05	389.63	419	0.2688	3.7201	0.0459
24.40	398	391	391	381	272	282	1442	276.70	390.00	422	0.2685	3.7247	0.0456
24.59	398	391	391	382	271	282	1442	276.70	390.18	422	0.2689	3.7189	0.0460
24.79	397	390	390	382	270	281	1440	275.70	389.60	421	0.2703	3.6999	0.0474
24.99	396	389	389	381	270	280	1434	274.75	388.75	420	0.2716	3.6813	0.0488
25.19	396	388	388	380	269	279	1436	273.80	388.15	420	0.2721	3.6751	0.0492
25.39	396	389	389	381	269	279	1438	274.05	388.68	421	0.2724	3.6714	0.0495
25.59	397	390	390	381	269	280	1438	274.80	389.73	421	0.2731	3.6618	0.0502
25.78	398	390	391	381	270	281	1439	275.35	390.03	421	0.2723	3.6724	0.0494
25.98	399	392	392	383	271	282	1442	276.70	391.65	422	0.2724	3.6712	0.0495
26.18	400	393	393	384	272	283	1441	277.75	392.55	422	0.2722	3.6735	0.0494
26.38	400	393	393	385	273	284	1437	278.20	392.78	421	0.2724	3.6705	0.0496
26.58	400	393	393	384	272	283	1438	277.50	392.30	421	0.2728	3.6658	0.0499
26.78	400	392	393	384	272	282	1439	276.95	391.98	421	0.2731	3.6612	0.0503
26.97	400	391	393	384	271	282	1440	276.65	391.83	421	0.2733	3.6590	0.0504
27.17	399	392	392	384	271	282	1439	276.30	391.78	421	0.2742	3.6469	0.0513
27.37	400	392	393	384	271	281	1444	276.10	392.10	423	0.2745	3.6430	0.0516
27.57	400	393	393	384	271	281	1445	276.05	392.30	423	0.2749	3.6377	0.0520
27.77	400	392	392	384	271	281	1441	275.85	391.98	422	0.2754	3.6316	0.0525
27.97	399	392	392	384	270	281	1435	275.40	391.55	420	0.2766	3.6157	0.0537
28.16	399	392	392	384	270	280	1438	275.15	391.80	421	0.2772	3.6077	0.0543
28.36	399	391	392	384	270	280	1432	274.60	391.35	419	0.2786	3.5896	0.0557
28.56	399	392	392	384	269	280	1432	274.70	391.53	419	0.2788	3.5873	0.0559
28.76	400	393	393	384	270	281	1434	275.30	392.35	420	0.2789	3.5854	0.0560
28.96	401	393	394	385	271	282	1438	276.15	393.15	421	0.2780	3.5969	0.0551

Appendix VII

Time (Hours)	t1	t2	t3	t4	tin	tout	Power (watts)	T_b,avg °C	T_s,avg °C	q, kW/m^2	1/U, m^{2}K/kW	U, kW/m^{2}K	R_f(4), m^{2}K/kW
29.16	401	393	393	386	270	281	1442	275.70	393.20	422	0.2784	3.5916	0.0556
29.35	400	393	393	385	270	281	1443	275.25	393.00	422	0.2788	3.5864	0.0560
29.55	400	393	393	385	269	280	1440	274.65	392.70	421	0.2801	3.5699	0.0573
29.75	400	392	393	384	269	280	1435	274.45	392.18	420	0.2803	3.5673	0.0575
29.95	401	393	394	385	270	280	1436	274.95	393.15	420	0.2813	3.5554	0.0584
30.15	402	394	395	386	270	281	1440	275.60	394.08	421	0.2811	3.5571	0.0583
30.35	402	395	395	385	271	282	1434	276.45	394.20	420	0.2806	3.5640	0.0577
30.54	403	395	395	386	271	282	1445	276.55	394.98	423	0.2800	3.5709	0.0572
30.74	403	395	395	386	271	281	1437	276.30	394.83	421	0.2818	3.5481	0.0590
30.94	403	395	395	387	271	282	1435	276.70	394.98	420	0.2816	3.5507	0.0588
31.14	403	395	396	387	271	282	1432	276.70	395.20	419	0.2828	3.5365	0.0599
31.34	403	396	396	387	271	282	1436	276.65	395.38	420	0.2825	3.5397	0.0596
31.54	404	396	397	388	271	282	1440	276.80	396.08	421	0.2830	3.5332	0.0602
31.73	404	396	397	387	271	282	1443	276.65	396.03	422	0.2827	3.5376	0.0598
31.93	403	396	396	388	271	282	1434	276.55	395.75	420	0.2840	3.5207	0.0612
32.13	403	396	396	388	271	282	1435	276.45	395.73	420	0.2840	3.5209	0.0611
32.33	403	396	396	388	271	282	1437	276.15	395.68	421	0.2842	3.5185	0.0613
32.53	403	396	396	387	271	281	1432	275.90	395.55	419	0.2855	3.5026	0.0626
32.73	404	396	397	387	271	282	1440	276.05	395.90	421	0.2844	3.5162	0.0615
32.92	403	396	396	388	271	281	1435	276.00	395.90	420	0.2855	3.5026	0.0626
33.12	403	395	396	387	270	280	1432	275.15	395.18	419	0.2864	3.4916	0.0635
33.32	404	397	397	388	271	281	1442	276.05	396.48	422	0.2854	3.5043	0.0625
33.52	405	397	397	389	271	282	1443	276.30	397.00	422	0.2858	3.4988	0.0629
33.72	405	398	398	390	271	282	1443	276.45	397.55	422	0.2868	3.4872	0.0639
33.91	405	398	398	390	271	282	1445	276.40	397.55	423	0.2865	3.4906	0.0636
34.11	405	398	398	390	271	282	1445	276.30	397.55	423	0.2867	3.4877	0.0639
34.31	406	398	398	390	272	282	1444	276.85	398.10	423	0.2869	3.4853	0.0640
34.51	405	397	398	388	272	282	1432	276.75	397.13	419	0.2872	3.4815	0.0644
34.71	405	397	397	388	271	282	1432	276.50	397.05	419	0.2877	3.4764	0.0648
34.91	405	397	397	388	271	281	1432	276.00	396.78	419	0.2882	3.4699	0.0653
35.10	405	397	397	388	271	281	1430	275.85	396.73	418	0.2888	3.4622	0.0660
35.30	406	398	398	390	271	282	1434	276.35	397.60	420	0.2889	3.4612	0.0661
35.50	406	398	398	390	271	282	1440	276.35	398.08	421	0.2888	3.4621	0.0660
35.70	406	398	398	390	271	281	1439	275.90	397.95	421	0.2898	3.4505	0.0669
35.90	405	397	398	389	270	281	1435	275.45	397.18	420	0.2898	3.4501	0.0670
36.10	405	397	398	389	270	281	1432	275.40	397.13	419	0.2905	3.4429	0.0676
36.29	405	397	397	389	271	281	1429	275.95	397.10	418	0.2897	3.4519	0.0668
36.49	406	398	397	389	271	281	1431	275.80	397.48	419	0.2905	3.4419	0.0677
36.69	406	399	399	389	271	281	1436	276.15	398.28	420	0.2906	3.4412	0.0677
36.89	406	398	399	390	271	281	1435	275.70	398.15	420	0.2916	3.4296	0.0687
37.09	406	397	398	390	270	281	1432	275.40	397.65	419	0.2917	3.4281	0.0688
37.29	405	397	397	388	270	280	1432	274.65	396.98	419	0.2919	3.4260	0.0690
37.48	405	397	398	389	269	280	1435	274.55	397.33	420	0.2923	3.4206	0.0695
37.68	406	398	398	390	269	280	1440	274.55	397.70	421	0.2922	3.4220	0.0694
37.88	406	397	398	390	269	280	1436	274.45	397.73	420	0.2933	3.4091	0.0705
38.08	405	397	397	388	269	280	1430	274.10	396.93	418	0.2935	3.4073	0.0706
38.28	406	398	398	389	269	280	1436	274.40	397.50	420	0.2929	3.4139	0.0701
38.48	406	398	398	389	269	279	1432	274.25	397.35	419	0.2937	3.4044	0.0709
38.67	406	398	398	389	269	279	1436	274.00	397.45	420	0.2938	3.4042	0.0709
38.87	406	397	397	389	269	279	1435	273.80	397.23	420	0.2939	3.4025	0.0710
39.07	406	398	398	389	269	279	1437	273.80	397.55	421	0.2943	3.3983	0.0714
39.27	406	398	398	390	269	279	1437	273.95	397.90	421	0.2947	3.3929	0.0719

Appendix VII

Time (Hours)	t1	t2	t3	t4	tin	tout	Power (watts)	T_b,avg °C	T_s,avg °C	q, kW/m^2	1/U, m^{2}K/kW	U, kW/m^{2}K	R_f(4), m^{2}K/kW
39.47	405	397	397	388	268	279	1434	273.50	396.80	420	0.2938	3.4036	0.0709
39.67	405	397	397	388	268	279	1433	273.40	397.05	419	0.2948	3.3916	0.0720
39.86	405	397	397	388	268	279	1433	273.30	396.95	419	0.2948	3.3916	0.0720
40.06	405	397	397	389	268	278	1434	272.85	396.85	420	0.2955	3.3844	0.0726
40.26	405	397	397	387	267	278	1435	272.60	396.68	420	0.2954	3.3847	0.0726
40.46	405	397	397	388	267	278	1431	272.55	396.60	419	0.2962	3.3760	0.0733
40.66	405	397	397	388	267	278	1428	272.55	396.63	418	0.2969	3.3682	0.0740
40.86	405	397	397	388	267	278	1430	272.45	396.65	418	0.2968	3.3695	0.0739
41.05	405	397	396	388	267	278	1430	272.40	396.63	418	0.2968	3.3689	0.0740
41.25	407	398	398	389	268	278	1441	272.95	398.05	422	0.2966	3.3710	0.0738
41.45	407	399	399	390	269	279	1439	273.80	398.75	421	0.2967	3.3704	0.0738
41.65	407	399	399	390	268	279	1436	273.70	398.75	420	0.2976	3.3607	0.0747
41.85	407	399	399	389	268	279	1434	273.50	398.43	420	0.2977	3.3593	0.0748
42.05	407	398	398	390	268	279	1430	273.25	398.15	418	0.2984	3.3506	0.0756
42.24	406	398	398	389	268	278	1428	272.65	397.85	418	0.2996	3.3379	0.0767
42.44	406	398	398	390	267	278	1429	272.70	398.13	418	0.2999	3.3343	0.0770
42.64	407	398	398	390	267	278	1432	272.75	398.28	419	0.2995	3.3386	0.0767
42.84	407	398	398	390	268	278	1432	272.80	398.38	419	0.2996	3.3373	0.0768
43.04	407	398	398	389	267	278	1430	272.60	398.10	418	0.2999	3.3346	0.0770
43.24	407	399	398	390	267	278	1430	272.50	398.35	418	0.3007	3.3254	0.0779
43.43	408	399	399	390	268	278	1439	272.90	399.10	421	0.2997	3.3370	0.0768
43.63	408	400	399	390	268	279	1438	273.25	399.13	421	0.2991	3.3433	0.0762
43.83	407	399	399	390	268	279	1434	273.20	398.88	420	0.2995	3.3393	0.0766
44.03	408	399	399	390	268	278	1430	272.75	398.95	418	0.3016	3.3161	0.0787
44.23	407	399	399	390	268	278	1429	272.70	398.65	418	0.3012	3.3204	0.0783
44.43	408	399	400	390	268	278	1432	273.05	399.23	419	0.3011	3.3214	0.0782
44.62	409	401	401	392	269	280	1435	274.40	400.75	420	0.3009	3.3238	0.0780
44.82	409	401	401	392	270	280	1430	274.95	400.88	418	0.3009	3.3234	0.0780
45.02	410	401	401	392	269	280	1432	274.75	401.00	419	0.3013	3.3195	0.0784
45.22	410	401	401	392	269	280	1430	274.60	401.00	418	0.3020	3.3109	0.0792
45.42	410	401	401	392	270	280	1431	274.70	400.95	419	0.3015	3.3171	0.0786
45.62	410	401	402	392	270	280	1431	274.90	401.15	419	0.3015	3.3171	0.0786
45.81	410	401	401	392	270	280	1428	274.80	401.13	418	0.3023	3.3082	0.0794
46.01	410	401	401	392	269	280	1430	274.30	401.05	418	0.3029	3.3017	0.0800
46.21	410	401	401	392	269	280	1432	274.25	401.20	419	0.3029	3.3012	0.0801